

**A FEASIBILITY STUDY ON THE
APPLICATION OF POLARIMETRIC
DECOMPOSITION ALGORITHMS TO THE
DETECTION OF CONCEALED WEAPONS**

Dean O'Reilly

A thesis submitted in partial fulfilment of the requirements of the
Manchester Metropolitan University for the degree of
Doctor of Philosophy

School of Engineering
Division of Electrical and Electronic Engineering
Manchester Metropolitan University

2015

ABSTRACT

State of the art security screening technology is not meeting all modern day requirements. There exists a gap in the market for the development of real time systems capable of detecting weapons at standoff ranges. Researchers at the Centre of Sensing and Imaging at Manchester Metropolitan University have developed a radar based screening technology. This technology will offer new security screening capabilities, making it feasible to have portable systems that can detect concealed weapons, with the added advantage of being capable of screening people in a crowd. The next step in the development of this radar system is to investigate the potential of using polarimetric scattering effects to detect concealed weapons, with the aim of improving the robustness and detection capabilities in comparison with the current state-of-the-art systems.

This thesis provides a feasibility study in the application of polarimetric decomposition techniques to Concealed Weapon Detection (CWD) and an experimental radar is developed to provide the measurements required for this study. The major outcome of this work is that polarimetric decompositions including the Pauli, Krogager SDH and $H-\alpha$ decompositions have been demonstrated as a viable means of interpreting data for the detection of concealed weapons. This will allow the next generation of radar based weapon detectors to reduce some of the orientation dependency on detection rates as observed in the current state-of-the-art systems. The work presented in this thesis has resulted in a clear understanding of what is required to implement a fully polarimetric radar based weapon detector. The detection of weapons using the developed fully polarimetric radar with the aid of polarimetric decomposition algorithms combined with calibration and signal-processing algorithms has been demonstrated in this thesis.

TABLE OF CONTENTS

Chapter 1 General Introduction	1
1.1 Problem Statement	4
1.2 Aim & Objectives	5
1.2.1 Objectives.....	5
1.3 Contributions to Knowledge	6
1.4 List of publications.....	7
1.5 Thesis Scope	8
Chapter 2 Literature Survey.....	9
2.1 Introduction.....	9
2.2 Acoustic Detection.....	10
2.3 Magnetic Field Detection.....	12
2.4 Infrared Detection Methods	14
2.5 Terahertz Detection Methods.....	15
2.5.1 Terahertz Spectroscopy	15
2.5.2 Terahertz Imaging	17
2.6 Microwave and Millimetre Wave Detection.....	19
2.6.1 Complex Natural Resonances	19
2.6.2 Imaging Techniques	22
2.6.3 Non-Imaging Radar Techniques	25
2.7 Dielectric Materials in CWD	27
2.8 Literature Survey Summary	30
2.9 Methodology	31
2.9.1 The problem	31
2.9.2 Assumptions and experimental boundaries.....	31
2.9.3 Scope.....	33
2.9.4 Stages of development	34
Chapter 3 Development of a Fully Polarimetric Radar.....	36
3.1 Introduction.....	36
3.2 The Radar.....	38
3.2.1 Sampling	44
3.2.2 Calibration.....	46
3.2.3 Range Gating.....	55
3.2.4 Antenna	58
3.3 Verification Measurements	63
3.4 Summary	70
Chapter 4 Polarimetric Measurements of Weapons and the Body	71
4.1 Introduction.....	71
4.2 Weapons & Concealment.....	72
4.3 Experimental Procedures	74
4.4 Sample Sizes	77

4.5 Results & Discussion	79
4.6 Summary	89
Chapter 5 Polarimetric Decomposition Techniques Applied to CWD	90
5.1 Introduction	90
5.2 Polarimetric Decompositions	92
5.3 Coherent Techniques	93
5.3.1 Pauli Decomposition	94
5.3.2 SDH Decomposition	101
5.4 Incoherent Polarimetric Decomposition	110
5.4.1 H-alpha Decomposition	110
5.5 Classification using Polarimetric Data	119
5.5.1 Experiment	119
5.5.2 Data sets	120
5.5.3 Artificial Neural Network	122
5.5.4 Methodology	124
5.5.5 Results and Discussion	125
5.6 Summary	129
Chapter 6 Conclusion and Further Work	130
6.1 Further Work	134
Chapter 7 References	135

LIST OF FIGURES

Figure 3-1 Interaction of an incident wave with an arbitrary target, resulting in a scattered wave.	37
Figure 3-2 Simplified overview of measurement system using a VNA and two antennas, one with vertical linear polarization and the other with horizontal linear polarization, figure reproduced based on [47].	39
Figure 3-3 FMCW radar chirp (Top) and modulating (Bottom) waveforms.	40
Figure 3-4 Range extraction from a FMCW radar.	41
Figure 3-5 Diagram showing sources of measurement errors in a two-port VNA, produced using diagrams in [47].	49
Figure 3-6 Image showing connection of waveguide adaptors for measurement of a ‘thru’ calibration standard.	50
Figure 3-7 Image showing short calibration standards connected to each port on VNA, close up view (Right).	50
Figure 3-8 Image showing a line calibration standard connecting the two ports of the VNA, close up view on right.	51
Figure 3-9 Plots showing measurements of a ‘thru’ calibration standard, each plot represents the log magnitude of the signal associated with each element of the complex S-matrix.	51
Figure 3-10 Plots showing measurements of a Short calibration standard, each plot represents the log magnitude of the signal associated with each element of the complex S-matrix.	53
Figure 3-11 Plots showing measurements of a Line calibration standard, each plot represents the log magnitude of the signal associated with each element of the complex S-matrix.	54
Figure 3-12 Plot showing a co-polar signal relating to a body that was scanned using the radar. A calibration has been applied, but no range gate has been used.	56
Figure 3-13 Plot showing a co-polar signal relating to a body that was scanned using the radar. A calibration and range gating have been applied.	57
Figure 3-14 Far-field radiation pattern of a horn antenna used in the radar, pattern taken at a frequency of 18 GHz.	59
Figure 3-15 Far-field radiation pattern of horn antenna at multiple frequencies across the bandwidth of the radar (18 to 26 GHz).	60

Figure 3-16 Image showing geometry of the beams from each of the horn antennas, angled such that the beams from both antennas are aligned at 2m range (linear dimensions in mm).	61
Figure 3-17 Plot showing the return loss of the antenna used in the radar.	62
Figure 3-18 Plot showing the transmission characteristics of the horn antenna pair selected for use in the radar.	63
Figure 3-19 Plot showing the measured Radar Cross Section (RCS) of a 65 cm diameter conducting sphere against frequency for each polarization on the radar.	65
Figure 3-20 Plot showing the range resolved signals from a conducting sphere of 65cm diameter for each polarization on the radar.....	66
Figure 3-21 Plot showing the measured Radar Cross Section (RCS) of a 55cm diameter conducting sphere against frequency for each polarization on the radar.	67
Figure 3-22 Plot showing the range resolved signals from a conducting sphere of 55cm diameter for each polarization on the radar.....	68
Figure 3-23 Plot showing the measurement error on the RCS of a conducting sphere of 55cm diameter, for each of the co-polarized RCS parameters.....	69
Figure 4-1 Image showing weapons used in measurements, starting from the left a handgun, a smaller revolver type handgun and a Person Borne Improvised Explosive Device (PBIED).	73
Figure 4-2 Image showing the measurement set-up, with a calibration target (conducting sphere) in place.	74
Figure 4-3 Flowchart showing process of taking measurements.	76
Figure 4-4 An example of a measurement made with no weapon concealed on the body against frequency.	79
Figure 4-5 A plot showing 200 range resolved measurements of a person with no concealed weapon.	80
Figure 4-6 An example of a measurement of a person carrying a concealed gun with the barrel vertically aligned to the torso.....	81
Figure 4-7 A plot showing 200 range resolved measurements of a person with a vertically aligned gun concealed on the torso.	82
Figure 4-8 An example of a measurement of a person carrying a concealed gun with the barrel aligned at 45° to the torso.	83
Figure 4-9 A plot showing 200 range resolved measurements of a person with a concealed gun with the barrel aligned at 45° to the torso.	84

Figure 4-10 An example of a measurement of a person carrying a concealed Person Borne Improvised Explosive Device (PBIED).	85
Figure 4-11 A plot showing 200 range resolved measurements of a person with a concealed Person Borne Improvised Explosive Device (PBIED).	86
Figure 4-12 An example of a measurement of a person carrying a concealed small revolver type handgun.	87
Figure 4-13 A plot showing 200 range resolved measurements of a person with a concealed small revolver type handgun.	88
Figure 5-1 Diagram showing different scattering mechanisms that occur from a person with and without a concealed weapon.	92
Figure 5-2 Plot showing weights associated with the Pauli decomposition of a large conducting sphere.	95
Figure 5-3 Plot showing weights associated with the Pauli decomposition of a person without a concealed weapon.	96
Figure 5-4 Plot showing weights associated with the Pauli decomposition of a person carrying a concealed gun on the torso at an alignment of 45°	97
Figure 5-5 Plot showing weights associated with the Pauli decomposition of a person carrying a vertically aligned gun concealed on the torso.	98
Figure 5-6 Plot showing weights associated with the Pauli decomposition of a person carrying a concealed Person Borne Improvised Explosive Device (PBIED).	99
Figure 5-7 Plot showing weights associated with the Pauli decomposition of a person carrying a small revolver pistol concealed on the torso.	100
Figure 5-8 Plot showing weights associated with the SDH decomposition of a large conducting sphere.	104
Figure 5-9 Plot showing weights associated with the SDH decomposition of a person without a concealed weapon.	105
Figure 5-10 Plot showing weights associated with the SDH decomposition of a person carrying a concealed gun on the torso with an alignment of 45°	106
Figure 5-11 Plot showing weights associated with the SDH decomposition of a person carrying a vertically aligned gun concealed on the torso.	107
Figure 5-12 Plot showing weights associated with the SDH decomposition of a person carrying a concealed Person Borne Improvised Explosive Device (PBIED).	108
Figure 5-13 Plot showing weights associated with the SDH decomposition of a person carrying a small revolver pistol concealed on the torso.	109

Figure 5-14 A scatter plot of the H- α parameters corresponding to a large conductive sphere, at various frequencies (18-26 GHz).....	113
Figure 5-15 A scatter plot of the H- α parameters corresponding to a scan of a person without a concealed weapon, at various frequencies (18-26 GHz).....	114
Figure 5-16 A scatter plot of the H- α parameters corresponding to a scan of a person carrying a concealed gun on the torso at a 45° alignment, at various frequencies (18-26 GHz).....	115
Figure 5-17 A scatter plot of the H- α parameters corresponding to a scan of a person carrying a vertically aligned gun concealed on the torso, at various frequencies (18-26 GHz).....	116
Figure 5-18 A scatter plot of the H- α parameters corresponding to a scan of a person carrying a concealed Person Borne Improvised Explosive Device (PBIED), at various frequencies (18-26 GHz).....	117
Figure 5-19 A scatter plot of the H- α parameters corresponding to a scan of a person carrying a small revolver pistol concealed on the torso, at various frequencies (18-26 GHz).....	118
Figure 5-20 A diagram of the formation of three data sets one for each polarimetric decompositions, all taken from same measured data.	120
Figure 5-21 An example of the structure of a three layer feed forward Artificial Neural Network (ANN).	122
Figure 5-22 Flow chart detailing the methodology used for the proposed experiment.	124
Figure 5-23 A series of plots showing the results from the validation of the developed ANNs post-training.	126
Figure 5-24 A series of plots showing the ANN output values for all of the radar scans used in the proposed experiment.	127
Figure 5-25 A plot showing three ROC curves each one corresponding to a different polarimetric decomposition.....	128
Figure 6-1 Diagram showing possible confocal radar system.	132

LIST OF TABLES

Table 2-1 Optical properties of materials encountered in concealed weapon detection [18].	28
Table 3-1 Calculated RCS values for two different sized conducting spheres.	64
Table 3-2 Mean errors on the co-polarized RCS measurements from a conducting sphere of 65cm diameter.	67
Table 3-3 Mean errors on the co-polarized RCS measurements from a conducting sphere of 55cm diameter.	69
Table 3-4 Summary of key selected radar parameters.	70
Table 4-1: Table of average values of the co and cross-polar reflections from the targets that were measured in this thesis.	89
Table 5-1 Table encapsulating key design parameters used to form the ANNs.	123
Table 5-2 Table encapsulating the key training parameters used for each of the developed ANNs.	123
Table 5-3 A table showing the results of the proposed experiment with the outcome of the hypothesis test applied to each polarimetric decomposition.	128

ACKNOWLEDGEMENTS

I would like to thank my director of studies Professor Nicholas Bowring for giving me the opportunity to complete a PhD. This research would not have been conducted without Professor Bowring's support and encouragement. I would also like to give my thanks to him for all of the career guidance and opportunities he has provided me with, I feel that I am in a much stronger position to start my academic career as a direct result of studying under the supervision of Professor Bowring. I must also acknowledge a number of colleagues within the Centre of Sensing and Imaging for their valued input and guidance. In particular, I would like to offer thanks to Dr David Andrews, Dr Stuart Harmer, Dr Neil Salmon and Dr Nacer Rezgui all of whom have provided encouragement and guidance.

I would also like to thank my wife Nicola for her patience, continuous support and for blessing me with a daughter Isabella. I love you both so very much.

Chapter 1

General Introduction

Concealed weapons detection (CWD) is an important area of research in the defence and security community. This is a result of a number of high profile terrorist attacks, which have resulted in loss of life and damage to public infrastructure [1].

The threat facing security forces is diversifying and current technology is struggling to meet the new requirements. The best examples of screening technologies are found in use at airports and these technologies include metal detection portals, millimetre wave imagers, x-ray scanners and ion mobility spectrometers. These technologies are all designed to detect specific threats and collectively they cover a broad spectrum of threats faced by the aviation industry. The use of multiple technologies at airports contributes to delays in the security screening process and lengthy queues are common. The use of multiple technologies coupled with the large volumes of people passing through airports means that a large amount of infrastructure is consumed in the security screening areas. This model for security screening is only used in airports, owing to the infrastructure requirements and the disruption it causes.

As the threat of terrorism spreads to railway stations, shopping centres and sporting events a new model for security screening is required. This new model must allow for the screening of people in crowds whilst moving, this would significantly reduce the disruption in comparison to airport security screening, but this new model must ensure that the technologies employed are able to reliably detect a broad spectrum of threats including Person Borne Improvised Explosive Devices (PBIED), guns and knives. An important factor in the development of security screening technology is false alarm rates, it is crucial that these are minimised to prevent unnecessary disruption to the

public. There is also a risk that false alarms will affect the confidence that operators of screening technology have in the decisions rendered by the technology. Any lack of confidence in the technology may ultimately result in the technology being unused. The new model must also allow for the evolution of threats facing the security forces and not result in a slow progression/transition towards the model currently used at the airports.

A recent evolution in the threat facing security forces came in the form of the 3D-printed gun, the release of designs for the 'Liberator pistol' on the internet captured the attention of security forces and the media [2]. The availability of 3D printed plastic weapons on the internet initially caused concern regarding the effectiveness of current screening technology to detect this specific threat. However, a demonstrator named Millimetre Threat Level Evaluation (MiRTLE) that is capable of detecting this threat was showcased by scientists at Manchester Metropolitan University (MMU) in conjunction with Radio Physics Solutions and the National Ballistic and Intelligence Service [3]. The device is an emerging radar based technology that uses millimetre waves to interrogate a person at standoff range and render a decision as to whether the person under investigation is carrying a concealed threat, without ever having formed an image in the millimetre wave spectrum. The development of this technology is well documented in the literature [4], [5] and [6]. One of the key aspects of this technology is that it can be deployed anywhere to screen crowds of people on the move for threats such as PBIEDs and guns (including 3D printed guns).

The MiRTLE system developed by MMU does have significant scope for improvement. One area for improvement with this device is that the cross-polarized reflection from a weapon, which is a key detection feature within this device, is dependent on the aspect of the weapon including the rotation of the weapon around the radar line of sight. The use of radar that analyses the immediate reflection from a weapon will always have an aspect dependency; however, the effects of the rotation of the weapon around the radar line of sight can potentially be removed. This

may be done by measuring additional information about the target (phase) and using techniques currently used in the field of Polarimetric Synthetic Aperture Radar (PolSAR) for Earth Observation. For the polarimetric techniques to be applied a different radar architecture must be used to measure the target. This radar architecture must be able to record a target's Sinclair scattering matrix, which contains all the available polarimetric information from a target. The architecture of a Vector Network Analyzer (VNA) is ideal for making such measurements. The MiRTLE system for comparison is classified as a direct detection system as it only records the power in co and cross polarizations and it obtains the target range via an independent homodyne receiver. The successful use of cross-polarization as a detection feature on the current state-of-the-art weapon detecting radar and the ability to reduce aspect dependency using polarimetric techniques warrants a comprehensive investigation on the full exploitation of polarization in the detection of weapons.

1.1 Problem Statement

State of the art security screening technology is not meeting all modern day requirements. There exists a gap in the market for the development of real time systems capable of detecting weapons at standoff ranges. A portable (i.e. handheld) screening technology would open avenues to providing increased security to urban soft targets. These targets include shopping centres, coffee shops, sporting events and parks. More generally, an urban soft target is defined as urban area into which large numbers of citizens are freely admitted or special events. Therefore, screening of people in crowds is of particular interest as it is undesirable to individually screen people in the majority of urban soft target scenarios. It is of critical importance that low false alarm rates are achieved; this will result in the operator having confidence in the system and will ensure minimum disruption. Another key performance goal is high throughput or fast screening times.

The next step in the development of this radar system is to investigate the potential of using polarimetric scattering effects to detect concealed weapons, with the aim of improving the robustness and detection capabilities. This thesis provides a feasibility study in the application of polarimetric decomposition techniques to CWD and appropriate instrumentation is developed to provide the measurements required for this study.

1.2 Aim & Objectives

The aim of this research was to investigate whether it is possible to apply polarimetric decomposition techniques to concealed weapon detection via a fully polarimetric radar based standoff weapon detector.

1.2.1 Objectives

The research objectives of this project are:

- Develop an instrument capable of making full polarimetric measurements, i.e. Sinclair scattering matrix.
- Determine a strategy for validating the performance of the developed instrument and assess any measurement uncertainties.
- Make measurements of the polarimetric scattering of a representative set of weapons concealed upon a person.
- Apply a selected set of polarimetric decompositions to data obtained from the measurements.
- Investigate the optimum method for maximizing information from radar returns from threat objects that may later be used in a detection algorithm.
- Improve on the state-of-the-art method of detecting weapons using radar, which uses the cross-polar reflection amplitude as the main detection feature.
- Verify the validity of the approach by undertaking systematic tests and producing Receiver Operating Characteristic (ROC) curves.

1.3 Contributions to Knowledge

The work presented in this thesis has provided a feasibility study on the application of polarimetric decompositions to standoff Concealed Weapons Detection (CWD) using fully polarimetric radar. The major outcome of this work is that polarimetric decompositions including the Pauli, Krogager SDH and H- α decompositions have been demonstrated as a viable means of interpreting data for the detection of concealed weapons. This will allow the next generation of radar based weapon detectors to reduce some of the orientation dependency on detection rates as observed in the current state-of-the-art systems. This work has resulted in a clear understanding of what is required to implement a fully polarimetric radar based weapon detector. The novel contributions from this work are listed as follows:

- It has been demonstrated that polarimetric decompositions provide information that is useful in the detection of concealed weapons.
- An investigation into the exploitation of polarization in radar based standoff weapon detection has been presented. This investigation goes beyond the scope of current knowledge by exploiting polarimetric decomposition algorithms.
- A comprehensive study of the polarimetric scattering effects from the body and a set of weapons has been presented in Chapter 5.
- An experimental fully polarimetric radar has been developed for the detection of weapons.
- A calibration and signal-processing algorithm has been developed as a pre-cursor to automatic classification of radar signals based around the use of polarimetric decompositions.
- A number of Artificial Neural Networks have been developed and trained to detect weapons using data from polarimetric decompositions.

1.4 List of publications

A list of the author's publications is provided:

1. O'Reilly, D., Bowring, N., Rezgui, N. and Andrews, D., "Target decomposition and polarimetric radar applied to concealed threat detection", Proc. of SPIE Millimetre Wave and Terahertz Sensors and Technology XVII, pp1-9, 18th Oct. 2013
2. O'Reilly, D., Bowring, N. and Harmer, S., "Signal processing techniques for concealed weapon detection by use of neural networks," IEEE 27th Convention of Electrical & Electronic Engineers in Israel (IEEEI), pp.1-4, 14-17 Nov. 2012.
3. O'Reilly, D., Bowring, N., Rezgui, N. D., Andrews, D. and Harmer, S., "Remote concealed threat detection by novel classification algorithms applied to multi-polarimetric UWB radar," Proc. of SPIE Radar Sensor Technology XVII, pp.1-8, 29th Apr. 2013.
4. Anani, N., O'Reilly, D., Ponnappalli, P. and Williamson, J., "Minimization of line current harmonics in single-phase AC-DC converter using a microcontroller," Universities Power Engineering Conference 2010 (UPEC), pp.1-5, 31st Aug. 2010.
5. Bowring, N., Southgate, M. J., Andrews, D., Rezgui, N. D., Harmer, S. and O'Reilly, D., "Development of a longer range standoff millimetre wave radar concealed threat detector," Proc. of SPIE Radar Sensor Technology XVII, pp.1-8, 29th Apr. 2013.
6. Rezgui, N., Bowring, N., Andrews, D., Harmer, S., Southgate, M. and O'Reilly, D., "Development of an ultra-wide band microwave radar based footwear scanning system," Proc. of SPIE Millimetre Wave and Terahertz Sensors and Technology XVII, pp1-9, 18th Oct. 2013.
7. Bowring, N., O'Reilly, D., Salmon, N., Andrews, D., Rezgui, N. and Harmer, S., "A feasibility study into the screening and imaging of hand luggage for threat items at 35GHz using an active large aperture (1.6m) security screening imager" Proc. of SPIE Millimetre Wave and Terahertz Sensors and Technology XVII, pp1-10, 18th Oct. 2013.
8. Salmon, N., Bowring, N., Hutchinson, S., Southgate, M., O'Reilly, D., "An aviation security (AVSEC) screening demonstrator for the detection of non-metallic threats at 28-35GHz," Proc. of SPIE Millimetre Wave and Terahertz Sensors and Technology XVII, pp1-10, 18th Oct. 2013.

1.5 Thesis Scope

The research presented within this thesis can be considered in three distinct phases. The first phase covers the development of an experimental radar with full polarimetric measurement capabilities. The second phase focuses on the measurement of the polarimetric scattering properties of various weapons when concealed on a person under clothing. The third and final phase covers the application of polarimetric decompositions to the measurement data and the results of an experiment designed to verify that the application of these decompositions results in a successful weapon detection system.

Chapter 2 presents a thorough and critical literature review of the most relevant techniques used for the detection of concealed weapons.

Chapter 3 discusses the development of an experimental system used to measure polarimetric scattering of weapons. Verification measurements are presented to assess the level of systematic errors in the measurement system.

Chapter 4 introduces the experimental procedures and methodology used in obtaining fully polarimetric measurements of weapons concealed on a person. This chapter also contains the resulting measurements with discussions.

Chapter 5 presents results from polarimetric decompositions applied to measurements from the previous chapter. In this chapter, an experiment is designed to test the suitability of a number of polarimetric decomposition techniques to CWD.

Chapter 6 draws conclusions from the work presented in this thesis; it also provides a discussion of areas for future research.

Chapter 2

Literature Survey

This chapter presents an in depth and critical literature review of the most relevant techniques used for the detection of concealed threats. Although the review is primarily focused on electromagnetic-based schemes, other methods such as acoustics techniques have also been addressed.

2.1 Introduction

Increased criminal and terrorists threats have placed onerous demands on improved technologies for the detection of dangerous items whether on body or in close proximity such as in passenger luggage.

There have been a number of high profile terrorist attacks in the UK over the last decade such as the London bombings of 2005 and the attack on Glasgow International Airport in 2007. These attacks resulted in loss of life and serious damage to infrastructure. Attacks like these have resulted in heightened security in high-risk areas like airports and government buildings. This drive to improve security has led to an increased demand for improvements in the capabilities and reliability of the technologies developed to detect concealed weapons and explosives. This increased demand has been the driving force behind much research in recent years. Consequently, many avenues have been explored in pursuit of a robust method of detecting concealed threats on the human body. The methods and technologies that have been developed have their own advantages and disadvantages when compared to one another. The following sections shall review

the benefits and limitations of each of the state of the art techniques. This review highlights any gaps in the research and shows that a solution has not yet been developed that tackles all of the aspects and issues involved in this area of research.

The scope of this review will be limited to state-of-the-art technological solutions including acoustic, electromagnetic radiation and inductive magnetic based methods of detecting concealed threats on the human body at standoff ranges.

2.2 Acoustic Detection

Methods based on the use of acoustic waves to detect the presence of objects concealed on the human body have been reported by a number of researchers, e.g. [7], [8], and [9]. There are two main acoustic-based methods of detection as explained below.

The first method was explored by Achanta [7]. This method involved the use of ultrasonic sources to generate acoustic waves capable of penetrating the clothing of an individual under investigation. Two ultrasonic sources of slightly different frequencies (140 kHz and 147 kHz) were used to form acoustic waves through non-linear interactions between the two sources, essentially the sources were mixed and the resultant signal was in the acoustic range [7]. Conventional ultrasonic beams have trouble penetrating clothing, hence the need to generate the lower frequency acoustic beam [7]. The acoustic waves interact with the target and the reflected waves are then measured using a microphone. This method relies on the reflection of the acoustic waves to detect the presence of a concealed object. The reflection of acoustic waves off an object is dependent upon the acoustic impedance of the material from which the object is constructed [8]. This impedance is related to the material's density [8]. Materials of a higher density have higher acoustic impedance and when an acoustic wave encounters a boundary with a large difference in acoustic impedance, for example between air and metal, there will be a large reflection of the wave. When a weapon

such as a gun or knife is concealed on the human body, there will be a larger acoustic reflection than when no weapon is present; this is because the human body has low acoustic impedance, relative to those of metals and hard plastics [8]. In Achanta's research, the detection method presented involves matching the acoustic signature from a scan to a database of known signatures from weapons. This presents problems due to the variable nature of an objects acoustic signature, which is aspect dependent [8]. Alongside the difficulties introduced by the aspect dependent signatures, it should also be highlighted that the size of the database that would be required would introduce serious problems in implementing this detection method. To summarize Achanta's research, it offers a promising method of acquiring acoustic signatures of objects concealed on the human body but the detection of concealed weapons from these signatures is not without its challenges.

Another method of using acoustics in concealed weapon detection was developed by Vadakkal [9]. This method uses a directional acoustic beam generated directly in the audio range to illuminate a subject under investigation [9]. The spectral characteristics of the reflected acoustic waves are analysed to classify the results from a scan. The acoustic wave is modulated in the presence of an object that is harder than the body and it is this modulation that is used to extract the natural resonant frequencies of the concealed object [9]. Vadakkal suggests that these natural frequencies could be used to detect the presence of a weapon concealed on the body by comparing the acquired frequencies to a database of known frequencies from weapons. This approach is similar to that of Achanta's and faces similar challenges. The issue with comparing signals to those of known weapons is that there exists many weapons with differing acoustic signatures and such a database would be difficult to manage effectively. Vadakkal's approach however does offer an appealing benefit compared to Achanta's in that the natural resonant frequencies could hold information regarding the shape of a concealed object, as outlined by Vadakkal [9].

The use of acoustic waves in the detection of concealed weapons has been attempted but as explained, there are challenges in implementation of a practical system. As such, there is not a great deal of open research on this method from recent years.

2.3 Magnetic Field Detection

The detection of concealed metallic/electrically conductive objects using electromagnetic field disturbance and pulse induction is a relatively mature technique. Metal detection systems are common in airports and other public areas with heightened security. There have been a number of research projects in recent years that have led to improvements and variations of the mature technologies that are widely used [10], [11], [12], [13] and [14].

Conventional metal detection systems used in high security areas such as airports require that each person be screened individually using either a portal or portable system [12]; this creates choke points when large volumes of people are to be screened [13] and [14]. To address this issue, a number of open/wide area detection schemes have been proposed including those by Nelson [13] and later Pati [14]. Nelson's proposed scheme, named Wide Area Metal Detection (WAMD), was a conceptual description in which a modification of Electromagnetic Induction (EMI) technology was suggested. EMI technology for concealed weapon detection involves exciting eddy currents in conductive objects using a transmitter coil and detecting secondary magnetic fields caused by the eddy currents when the transmitted field is switched off, as governed by Faraday's law [10] and [13].

Nelson proposed that an array of receiver coils and a wide area transmitter coil could be used to detect concealed weapons and identify the individual concealing the weapon. It was also suggested that the weapon could be classified using advanced signal processing techniques. It was claimed by Nelson that this solution would be a valuable tool in redirecting security resources and

reducing the inconvenience caused to the public, but was by no means a standalone solution. The reason as to why this method cannot be considered a standalone solution is relatively simple; it only detects electrically conductive objects. Weapons such as plastic guns or explosives would not be detected by this system and this is a serious limitation of Nelson's proposed scheme. Despite this Pati [14] later published simulation data validating a design based around the WAMD, this system was named Open Area Concealed Weapon Detection (OACWD). The OACWD system included more detailed designs such as transmitter and receiver coil designs alongside a new fast data acquisition system. The work by Pati [14] also included solutions to more practical issues, such as the inclusion of a Buck coil to the transmitter coil that ensured the transmitted field was switched off fast enough to prevent an overlap with the secondary field generated by eddy currents induced in electrically conductive objects. The research conducted by Pati [14] does not alter the system's inability to detect non-conducting objects and as a result, it cannot be considered a standalone solution to the weapons detection problem.

Most recently, research has been conducted to assess the possibility of resolving multiple threat objects in an EMI based detection system [11]. The motivation for this particular piece of research comes from the desire to solve a problem with conventional EMI based systems. The problem with these conventional systems is that a single parameter is used to trigger a detection of a concealed object. This single parameter, which is the fundamental time constant of the secondary field, limits the system capabilities. That is in terms of the separation and discrimination of objects with similar characteristic time constants. This work suggests that the resolution of multiple threat i.e. multiple similar time constants, and non-threat concealed objects is possible with improved Signal-to-Noise Ratio (SNR) that allows for the identification of these objects, providing a more robust solution than existing conventional systems.

To summarize, electromagnetic-based weapons detection technology is mature and is already used extensively in high security areas. However, the technology is only good for detecting

electrically conductive objects and as such cannot be considered a standalone threat detection solution. Consequently, the development of alternative technologies capable of detecting a wider variety of concealed objects is required.

2.4 Infrared Detection Methods

The utilization of infrared sensors for concealed weapon detection has been attempted [15], [16] and [17]. At first glance, infrared is an appealing choice due to the passive nature of the required sensors. However, there are fundamental limitations associated with using infrared systems in concealed weapon detection. The application of an infrared system relies on the measurement of thermal radiation that is naturally emitted by objects, which is related to an object's temperature [16]. Infrared systems, developed for weapons detection, generate an image in the infrared spectrum and the idea is that any concealed weapons show up as a temperature anomaly on the image [16] and [17]. This is because the body can be at a different temperature than the concealed weapon and emits more energy in the infrared spectrum. The main drawback with this method is that the wavelength in the infrared spectrum is too short to easily penetrate most clothing [16]. Therefore, what these systems are measuring is the radiation that has been absorbed and then re-emitted by clothing. This introduces a number of scenarios in which this method is unusable; the first scenario would be if a subject under investigation were wearing loosely fitted clothes the radiation would not go through the clothing. Another scenario would be if the subject was wearing thick or thermally insulating clothing, in this instance the radiation from the body would not be visible to the sensor. A third scenario would be if the weapon had been concealed against the body long enough for its temperature to rise to approximately that of the body there may not be enough contrast in the image to detect the weapon. It appears that infrared imaging only works if the subject

is wearing thin clothing that is tightly fitted and the concealed weapon is at a different temperature than that of the body.

As discussed, infrared imaging for concealed weapon detection is at an initial glance appealing but ultimately impractical as a stand-alone solution. The majority of the research suggests this method as a compliment to millimetre wave imaging. The research that is currently being undertaken on infrared-based systems is focused around sensor/image fusion and image processing techniques [15], [16] and [17].

2.5 Terahertz Detection Methods

The Terahertz region of the electromagnetic spectrum (300 GHz to 3 THz) is an appealing option to the developers of systems used to screen personnel for concealed contraband, explosives and weapons. The reasons behind this appeal shall be discussed in context of the technologies that have been developed in recent years. There are two main methods of applying Terahertz radiation to concealed explosives and weapons detection systems, which are imaging and spectroscopy.

2.5.1 Terahertz Spectroscopy

The method of remote detection of concealed explosives by Terahertz Spectroscopy, in theory, offers much promise to researchers due to the unique spectral characteristics of explosives above 500 GHz [18], [19] and [20]. The unique spectral characteristics can be analysed in either reflection or transmission mode [18]. Since the technologies for remote weapons and explosives detection are being discussed, only the reflection mode, which is suited to a radar based system, is considered. Such systems have been reviewed by Appleby [18], Kemp [19] and Sheen [20]. In their reviews, the practicalities of implementing a radar based spectroscopic explosives detector were

brought into question. The problems highlighted in these reviews included atmospheric absorption, scattering from clothing and the spectral characteristics dependence on the condition and surface of an object [19] and [20]. Atmospheric absorption of the electromagnetic waves is a real problem in the Terahertz region of the EM spectrum, this absorption is caused by water vapour and can be considerably worse in humid climates. The lack of ability to generate the power that would have to be transmitted to get a usable return signal containing spectral characteristics means that it is unlikely that a standoff remote detector will be developed in the near future [19] and [20]. The wavelength at Terahertz frequencies is very short (less than 1mm) and becomes comparable in length to the weave of the fabric in some clothing, as such some of the radiation is scattered and/or absorbed by such clothing [18]. Data presented in [18] illustrates this point; in this paper, transmission of radiation through a denim sample and a T-shirt are shown to reduce as the wavelength moves from sub-millimetre to terahertz (0.96 at 100 GHz down to 0.65 at 1 THz for the T-shirt and 0.9 at 100 GHz down to 0.1 at 1THz for denim). Additionally the reflectivity is observed to increase with a decreasing wavelength (0 at 100 GHz up to 0.05 at 1 THz for the T-shirt and from 0.01 at 100 GHz up to 0.05 at 1 THz for denim), data presented in [18], thus supporting the idea of the radiation being scattered by clothing. This is a considerable disadvantage of using Terahertz frequencies for concealed weapons detection. At lower frequencies, the clothing is far more transparent to EM radiation and this gives a better capability to detect weapons concealed under clothing, as seen with millimetre-wave systems. The shorter wavelengths in the Terahertz spectrum also mean that surface conditions of the material being illuminated can alter the way in which the radiation is scattered [20]. Rough surfaces can cause localized constructive and deconstructive interference of the scattered wave resulting in alterations of the material's apparent spectral characteristics [20].

To summarize, Terahertz Spectroscopy methods for the remote detection of concealed contraband, explosives and weapons, offers the ability to classify materials yet there are a number

of serious issues in the practical implementation of this technique. In fact the reviews conducted in the research by Appleby, Kemp and Sheen all reach the same conclusion; Terahertz Spectroscopy for the remote detection of concealed explosives is difficult, if not impossible with the current state of technology.

2.5.2 Terahertz Imaging

The other method of utilizing Terahertz radiation in concealed weapons detection is based around the formation images, much like millimetre wave imaging. Images can be formed from data acquired using both active and passive systems. An active system is essentially multi-pixel radar that measures the reflection of radiation that has been used to illuminate an object under investigation. Passive imaging systems work in a slightly different manner as nothing is transmitted towards the person, these systems measure radiation that is naturally emitted from the body. A number of Terahertz imaging systems, both active and passive, have been developed in recent years [21], [22] and [23].

The main properties of imaging systems in the Terahertz spectrum are spatial resolution, which is physically limited by diffraction [20], depth resolution and contrast. Spatial resolution is related to wavelength and aperture size and as mentioned is diffraction limited (in both active and passive systems), depth resolution is improved by increasing bandwidth (active systems) [20] and contrast is predominantly determined by the properties of the materials in the scene (mainly emissivity in a passive system and dielectric constant in an active system). The diffraction limited angular resolution is determined using the following equation (2.1).

$$\Delta\theta = 1.22 \frac{\lambda}{D} (rad) \quad (2.1)$$

Where D is the diameter of the antenna aperture and λ is the wavelength.

The Terahertz region of the EM spectrum offers short wavelengths capable of penetrating clothing, albeit with more attenuation than at lower frequencies. The short wavelengths are appealing as they offer very good spatial resolution in an imaging system. Such a system would produce the high-resolution images that are required for better detection capabilities [18]. The main drawback of using an active imaging system is specular reflection of the illuminating wave, meaning that it is scattered away from the receiver resulting in bright spots in image [18], [19], [20] and [22]. Specular reflection results in poor quality images, in which it is very difficult to find any concealed object with a reasonable degree of certainty. Yet it is active systems that are preferred at these frequencies in the research because of atmospheric absorption [18]. The contrast of an image formed by a passive imager operating in the millimetre wave or Terahertz region of the EM spectrum is related to background temperature [18]. There must be an observed radiometric temperature differential between the body and the background and also the body and any concealed threat item for any concealed weapon to appear visible enough to be detected in an image formed using a passive system [18].

As discussed, the short wavelengths of Terahertz radiation have been used to produce high-resolution images. Although these images show objects concealed under clothing there are issues affecting the quality of these images. Firstly, the specular reflections hamper an active system, whilst contrast can be an issue with passive imagers. There is also the issue regarding attenuation from both the atmosphere and clothing, which is less of an issue in the millimetre wave region of the spectrum, where clothing is more transparent. In [18] the transmission of a tee shirt is recorded as 0.65 at 1 THz and 0.96 at 100 GHz, this shows a difference of 0.31 in transmission. Finally, there are privacy concerns when imaging under a person's clothing that makes this method undesirable to the public.

2.6 Microwave and Millimetre Wave Detection

Much research on concealed weapons and threat detection at standoff distances makes use of the microwave and millimetre wave region of the EM spectrum. The reasons for which shall be discussed in this section. The research reviewed in this section is composed of the most recent significant papers relating to the main techniques of applying microwave and millimetre wave radiation to the CWD problem. These main techniques include imaging, non-imaging and the excitation of Complex Natural Resonances (CNR). All have their own advantages that shall be discussed alongside the drawbacks and limitations of each technique.

2.6.1 Complex Natural Resonances

One method of utilizing microwave radiation in the detection and identification of concealed threat items is to attempt to excite resonant frequencies in the concealed item using ultra wide band radar. This technique has been used extensively in the detection and identification of aircraft and missiles [24]. In recent years, researchers have attempted to apply this technique to CWD, however many difficulties have been encountered when a threat object is concealed on a human body [25]. These difficulties are due to the body obscuring both the resonant frequencies and the associated damping coefficients of the concealed object by altering the dielectric surroundings of the object [25]. The damping coefficient is a measure of the lifetime of the excited resonance(s). As such, it is a non-trivial process to apply this technique to CWD and consequently much research has been conducted [26], [27], [28], [29], [30] and [31].

The identification of concealed objects by exciting resonant frequencies offers an aspect independent option to CWD researchers. Aspect independence is important as it means that the features used to detect weapons would not be dependent upon the orientation of the weapon. Aspect

dependency is common with radar based weapon detectors because the radar cross section of a weapon is chaotic in nature and a small change in weapon orientation can lead to a large variation in the power reflected by the weapon. This aspect independence manifests in the form of the Late Time Response (LTR) where a concealed object re-irradiates an illuminating wave at resonant frequencies [27]. The LTR presents itself as exponentially decaying sinusoidal waves that are observed after the direct reflection from an object, after the object's resonant frequencies have been excited using Ultra Wide Band (UWB) radar (simulating a pulse). The LTR of an object is dependent upon the object's shape, size and local dielectric surroundings [25]. As this information is aspect independent the method is less prone to signal changes owing to the orientation of the concealed object and as such, it has benefits over other systems described in this review.

The LTR does have drawbacks when used for CWD as many of the threat objects that a system is required to detect have resonant frequencies in the low GHz (0.2 to 3 GHz) region of the EM spectrum [28]. This means that large antennae are required to excite these natural resonances making a portable system unfeasible and consequently the application of CWD using LTR is limited to portal style systems installed at fixed locations. The use of similar portal systems, such as current walk through metal detectors, in busy public environments leads to choke points. These choke points create delays in the security screening process, which are inconvenient and undesirable to both the public and security personnel [29]. As a result, the application of a LTR based detection portal relies on the ability to screen people quickly, in order for such a system to be commercially successful [29]. To address this issue Vasalos [29] conducted research into the relationship between detection accuracy and scan time. Vasalos obtained the LTRs of various target scenarios including body with and without a concealed object and it was observed in the experiment that reducing the scan time from 120 s to 15 s (multiple measurements made and averaged) had little effect on the LTR and it was deduced that fast scanning was achievable without degrading the detection accuracy. This suggests that scan times could be reduced to the point where the severity

of these choke points could be at a tolerable level. As mentioned previously many of the objects that need to be detected by security screening (knives, handguns, Improvised Explosive Devices etc.) have resonant frequencies in the low GHz region of the EM spectrum that require large antennae to excite them. This limited the LTR based systems portability; however, research conducted by Zhang [30] suggests that these objects have higher order resonant frequencies in the millimetre region of the EM spectrum. Exciting these higher order resonances could result in a practically portable system as the size of the required antennae would be reduced. It was found, through numerical simulation, that a kitchen knife has higher order resonant frequencies that extends into the millimetre wave region [30]. Although, these resonances have been shown to exist at these higher frequencies, the amplitudes are too small to detect reliably, also these higher frequency resonances would decay much faster than the fundamental resonances making them again very difficult to reliably measure [30]. Considering this difficulty, a portal based system that excites and detects the resonant frequencies in the low GHz region of the EM spectrum is more realistic for CWD using LTR.

As a result of the large antenna in such a system another problem occurs, which is related to the directivity of the illuminating beam. It has been realized that the illuminating beam needs to be commensurate in size with the concealed object (~10 cm) for the object to be reliably detected [28]. An optical system designed to focus the beam to such a size would be impractically large, meaning another solution was required. The solution presented by Harmer [28] was to use a phased antenna array where the beam could be focused and steered electronically. Additionally, an image can be formed using a phased antenna array allowing for the locality of the concealed object to be presented to security personnel [28]. In reducing the beam size using a phased array, the footprint of the antennae increases considerably making the system even larger and less portable, which may render such a system undesirable where space constraints are critical.

To summarize on the detection of concealed threat objects using the CNR, the aspect independence of this method is not matched by any of the other EM methods making this option appealing. However, there are many practicalities that hinder the progression of this technique into a deployable system and much research is still needed to address the issues highlighted in this section of the review.

2.6.2 Imaging Techniques

Millimetre wave imaging has been a popular technique employed in concealed weapon/threat detection over the last few years [20], [32], [33] and [34]. Many imaging systems have been developed and the technique used to form the image varies from one system to another. The imagers can be classified into two main groups; Active and Passive Imagers. Active imaging involves the use of an illuminating signal, which is then measured after being reflected from the scene in the image. Passive imaging works in a different manner, as it is the naturally emitted radiation that is measured from objects in the scene being imaged [33]. There are millimetre wave imagers being used at airports around the world, although the use of these systems is not without controversy. The controversy is in relation to privacy concerns as an image is formed in which the person being screened appears nude [35], this controversy may be unfounded as privacy filters are applied to the images and the images are analysed automatically using computer algorithms.

In this section a selection of recent papers are reviewed and the issues regarding the development of millimetre wave imagers are discussed. These issues include the detection of weapons that are constructed of dielectric materials (plastic based explosives and 3D printed guns) and improvements in image quality that are required for weapons detection to become more reliable. Also mentioned in this section is imaging using polarimetric, i.e. waves with dual polarization, information.

The detection of explosives and other dielectric based weapons is a challenge for researchers. A number of papers applying Terahertz spectroscopy to explosives detection have been published these can be found in the review by Kemp [19]. As outlined earlier in this review they all conclude that a deployable system is a long way off realization. Consequently a lot of emphasis has been placed on the ability of imaging systems to detect dielectric materials and hence explosives.

The detection of dielectric materials in millimetre wave images has proven to be a complex task as the dielectrics are fairly transparent at these frequencies (and frequency dependant) and are somewhat obscured by specular reflection when imaged on a body [34]. The reason for this is that the intensity of the reflection is dependent upon the material properties of the objects being imaged. For example, metallic objects have a higher reflection coefficient than dielectric objects and as a result have a higher intensity in the image, making them easier to detect, in an active imaging system. The detection of a dielectric object in an image from an active imager is strongly dependent on its reflectivity [34]. The detection of a dielectric object in an image from a passive imager is dependent upon the emissivity of the material(s) from which the object is constructed and the object's temperature. In an active imaging system, reflectivity of the material is the dominating parameter. The difference in reflectivity of skin with and without explosives is small. At 100 GHz there is a difference in reflectivity of 0.11 between skin with explosives and skin without explosives, at 500 GHz the difference is reduced to 0.04 and at 1 THz the difference is down to 0.01 [18]. This is noticeable when compared to the difference in reflectivity of skin and metal, which is 0.65 at 100 GHz, 0.91 at 500 GHz and 0.93 at 1THz [18]. In passive imaging, the difference in emissivity between skin and skin with explosives is 0.11 at 100 GHz, 0.04 at 500 GHz and 0.01 at 1 THz [18]. Again, this is noticeable when compared to the difference in emissivity of skin and metal, which is 0.65 at 100 GHz, 0.91 at 500 GHz and 0.93 at 1 THz [18].

To assess the detectability of dielectrics using an active millimetre wave imager Schiessl [34] performed a number of experiments. In these experiments, a multi-static planar array imager operating in the W-band was used to form images of various explosives placed on a reflective background (representative of the body). The conclusion drawn by Schiessl [34] from these experiments was that explosives detection using an imaging system is difficult. Schiessl also concluded that it is possible to estimate the relative permittivity of the explosive material through analysis of the temporal data. The conclusion drawn was that the best discrimination is provided in the presence of edge scattering (diffraction at the edges of the sample) from the explosive material [34]. The edge scattering from an object placed in front of a highly reflective background, such as the human body, has been found to be a good characteristic to use in the detection of explosives and weapons by other authors [36] and [32]. One method that has a lot of potential is to utilize polarization information in the formation of millimetre-wave image from both passive and active systems. Work conducted by Bernacki et al [33] showed that images formed using the Stoke's parameters, which describe polarization states, contain details not present in other imaging systems [33], such as the ability to see footsteps from a person walking on grass. In this work, the detection of buried targets using images formed from Stokes parameters was investigated, but no benefits for this application could be found. Further research on the use of polarimetric information in both imaging and radar must be conducted such that the potential benefits can be realized.

The use of millimetre-wave imaging in concealed weapons detection has been demonstrated by many and systems such as the L3 Provision millimetre wave imager are currently in use in airports around the world [37]. There are privacy issues concerning the formation of an image in which the subject appears to be nude, this makes this method undesirable to the public. There are issues surrounding the quality of images that are plagued by the same problems as described in the section on terahertz imaging, which are speckle and contrast. The detection of dielectric explosives and plastic weapons is difficult with millimetre wave imaging as the low

reflection coefficients of these types of material result in low contrast reflections from the weapons. Polarimetric imaging in the field of concealed weapon detection is relatively new and initial research shows new levels of information appearing in the images.

2.6.3 Non-Imaging Radar Techniques

One method of using millimetre-wave and microwave radiation to detect objects concealed on a human body under clothing is to scan the person with a radar system. This method offers the ability to scan a person without forming an image and thus avoiding the privacy issues that make millimetre-wave imaging undesirable. Much research has been presented to validate this approach [38], [39], [40], [41], [5] and [42]. In the research a number of experimental systems are described, such as Millimetre-wave Remote Threat Level Evaluation (MiRTLE) [5] and CounterBomber® [43]. The methods of implementing the radar vary, though they all use some form of swept frequency radar. The systems reported in the literature tend to use polarization changes in the reflected waves as an indication as to the presence of a weapon [6], [27] and [40]. This is because the weapons that these systems are screening for (knives, guns and explosives) tend to be complex in the way they scatter EM waves which results in these polarization changes [40]. The use of a cross polarized receiver tends to be favoured as the body gives little cross polarization and presence of a weapon on the body results in a significant cross polar component in the reflected wave. Some systems such as MiRTLE work based on a cross polar threshold triggering the alarm. Others use the time resolved radar signal and train a Neural Network (NN) to detect the weapon. One area that has set these systems apart from others mentioned in this literature survey is their ability to detect thin layers of dielectric material [38] and [39]. This ability is a result of the range resolution of these systems, which is governed by the system bandwidth. All of these systems tend to have Ultra Wide Band (UWB) capability and have bandwidths in the order of tens of GHz (35 GHz in the case

of MiRTLE). As the use of UWB components increases the cost of radar considerably, a system that uses cheaper amplitude only receivers (Direct Detection) was compared to conventional radars that have receivers that measure amplitude and phase [39]. In the research conducted by Bowring et al. [4] it was shown that the information related to the thickness of a dielectric material is conserved in a direct detection system. This showed that the detection of dielectric explosives using lower cost direct detection radar is a feasible option. It must be noted that the use of a direct detection system removes the ability to filter the returns based on range, a capability that is very powerful in conventional heterodyne-based radars.

One area in which these systems suffer is the detection of knives [40]. The reason for this is that the cross polar component that arises when a weapon is present is related to the orientation of the weapon. In the systems in the literature, a single illuminating polarization is used and the reflected wave is measured in the co-polar and cross polarizations. This results in targets such as knives avoiding detection when placed on the body in particular orientations [40] and [6]. Another issue with these systems is the classification of the time resolved radar signals. This tends to be difficult based on the variance in the data caused by the orientation of the weapon.

Very recently, a radar based weapon detector developed by the Centre of Sensing and Imaging at MMU was trailed by the National Ballistics and Intelligence Service (NABIS) and was independently verified as the first screening system capable of remotely detecting a plastic 3D printed gun concealed on a person under clothing [3]. This has since led to the technology receiving attention from the national press [44]. It should be noted that in this trial no other systems were tested.

In summary the use of radar in the field of standoff weapons detection is one the most promising options. The reasons are that there are no privacy concerns regarding images, weapons can be detected at standoff ranges using radar, the detection of both dielectric and metallic weapons is feasible and the systems can be given real time capability. This being said there are issues that

need to be addressed, mainly concerning the detection of targets such as knives. Polarization has been used as an indicator, yet a comprehensive survey of the way in which weapons change the polarization of an electromagnetic wave has not been conducted.

2.7 Dielectric Materials in CWD

In this thesis, polarimetric decomposition algorithms are tested in a concealed weapon detection scenario. The urban soft targets that were defined in the problem statement are typical of the scenario in which a proposed system would be deployed. These targets are vulnerable to attack from terrorists that may approach the target with a concealed weapon. The weapons that are considered in this thesis are guns, knives and Person Bourne Improvised Explosive Devices (PBIEDs). As discussed previously, a relatively new threat facing these targets is the printed gun. Printed guns are manufactured using 3D printers and are generally made of ABS plastic [2]; this type of weapon is worth noting but has not been included in the experiments within this thesis.

It is important to consider the effect of material properties on the ability of a proposed system to detect weapons concealed under clothing. In [18] it is reported that detection of weapons is dependent upon the optical properties of the clothing, metal and skin. The optical properties of these materials are frequency dependent and can be described by (2.2), taken from [18].

$$\varepsilon + r + t = 1 \quad (2.2)$$

The equation above contains three terms relating to emissivity (ε), reflectivity (r) and transmission (t). Emissivity is a measure of radiation that is naturally emitted by a material; this parameter is important when considering passive systems. Reflectivity is a measure of how much radiation will be reflected by a material, as a ratio of the radiation incident upon the material. Transmission is measure of the quantity of radiation that will pass through a material, as a ratio of

the radiation incident upon the material. Reflectivity and transmission are the most important properties to consider when investigating radar.

The detection of weapons concealed under clothing relies on the transmission of radio frequency waves through clothing and the reflection of the waves by a weapon and the body. Therefore, it is desirable for clothing to have a high transmission value. Equally important is that weapons and skin have a reflectivity that will enable the radar to see both. Typical values of the properties of metal, clothing, skin and explosives were reported in [18]. A table (Table 2-1) containing values of the optical properties of materials of interested has been extracted from [18].

<i>Material</i>	<i>Emissivity (ϵ)</i>			<i>Reflectivity (r)</i>			<i>Transmission (t)</i>		
	100 GHz	500 GHz	1 THz	100 GHz	500 GHz	1 THz	100 GHz	500 GHz	1 THz
<i>Explosives (on skin)</i>	0.76	0.95	0.94	0.24	0.05	0.06	0	0	0
<i>Metal</i>	0	0	0	1	1	1	0	0	0
<i>Skin</i>	0.65	0.91	0.93	0.35	0.09	0.07	0	0	0
<i>Denim</i>	0.09	0.49	0.85	0.01	0.01	0.05	0.9	0.5	0.1
<i>Tee-shirt</i>	0.04	0.2	0.3	0	0	0.05	0.96	0.8	0.65

Table 2-1 Optical properties of materials encountered in concealed weapon detection [18].

The table above shows measurements taken at 100 GHz, 500 GHz and 1 THz. The frequency of the radar used in the experiments within this thesis is 18 to 26 GHz. The measurements in the table are higher than the frequency used in this thesis, however the trends in the measurements are relevant. Data relating to measurements of these materials at frequencies between 18 and 26 GHz could not be found in the literature.

In Table 2-1 denim and a tee shirt are shown to have similar transmission values at 100 GHz. However, the materials behave differently at higher frequencies. Tee shirt remains more transparent (relative to denim) as the frequency rises to 1 THz. The reduction in transmission is

0.31 as the frequency increases from 100 GHz to 1 THz, for the tee shirt. The denim sample displays a larger reduction in transmission with a difference of 0.8 as the frequency increases over the same range. Both items of clothing display a trend of decreasing transmission with increasing frequency. If this data was to be extrapolated to lower frequencies (18 to 26 GHz) it would be anticipated the transmission would remain at the higher values in given in Table 2-1, or exhibit slight increases (based upon observed trend in data).

Table 2-1 shows that there is no transmission through metal or skin and that metal is purely reflective across all the measured frequencies. This shows that metallic weapons reflect incident waves making it feasible to detect them using radar. The skin is reflective but has a much lower reflectivity than metal, as the frequency increases the reflectivity decreases. At frequencies lower than those measured in Table 2-1, it is anticipated that the reflectivity of skin will be higher. As frequency increases, the emissivity of skin is also shown to increase. All of the weapons investigated in this thesis contained a significant amount of metal.

2.8 Literature Survey Summary

In this chapter, a critical literature survey has been presented. The survey detailed the work of others in the research field of concealed weapons detection. The work included in this survey has been constrained to state of the art technological solutions including acoustics, electromagnetic and inductive magnetic methods of detecting concealed weapons. The survey has shown that of these methods the use of electromagnetic radiation, especially millimetre-wave and microwave radiation, offers the most promising results. This is partly owing to the transparent nature of clothing at these frequencies, but also to the ability to detect both dielectric and metallic targets. The methods of utilizing millimetre-wave and microwave radiation vary in the literature, yet one method that has shown particular promise is the method of using UWB radar. This method offers standoff detection of a diverse range of targets. It is not without issues as shown in the survey. A gap in the research has been highlighted that requires an understanding of the role of polarization in concealed weapon detection using radar. Another gap that has been highlighted is in the classification of time resolved radar signals where variance in the data owing to aspect dependency causes difficulties in the robust classification of the radar data. This thesis will present an investigation into the use of polarization for weapons detection using Ultra Wide Band (UWB) millimetre/microwave radar. It will be shown, experimentally, that polarimetric measurements provide information for the robust detection of concealed weapons.

2.9 Methodology

This section provides an explicit description of the methodology used in terms of specifying the problem, assumptions made, scope and stages of development together with validation tests chosen. The hardware and software used for data collection and analysis are outlined, with some details on construction of the experimental radar. Further and more detailed discussions of experimental procedures specific to each experiment are provided in Chapters 3, 4 and 5.

2.9.1 The problem

The problem addressed in this work was the protection of urban soft targets using radar to detect weapons concealed under clothing. The author has suggested the use of polarimetric decomposition algorithms for extracting information from radar data that can then be used to detect weapons, with the aid of artificial intelligence (neural networks). A set of experiments have been designed that test the suitability of three polarimetric decomposition algorithms.

2.9.2 Assumptions and experimental boundaries

The scenario assumed in the experiments, was that a person would be scanned using radar in a clutter free environment and that the person would be cooperative. In a real world scenario, the person would likely be scanned in a cluttered environment and would either be unaware that they were being scanned or could potentially be non-cooperative. Justification for these assumptions was that the measurement system was experimental and had limitations that are discussed in this section.

The risk associated with the clutter free environment assumption, is that the presence of clutter could reduce the detection performance or increase the false alarm rate of a developed system in a real world deployment. This risk can be mitigated through appropriate design strategies. For example, the beam of the radar can be constrained to a spot on the body (using a lens). This means that if the person is in the line of sight, the beam will only be on that person and thus there would be no reflection from clutter around that person. If the person is not in the line of sight of the radar, i.e. they are obscured by another person/ people then it is not possible to scan that person. The human body is not transparent to the radio frequency waves used by the radar.

The person is assumed stationary at a given range whilst scans are being taken (cooperative target assumption). The reason the person is measured at a fixed range in the experiments is that the experimental radar uses multiple antennas whose beams are aligned at the fixed range. In a real world system, a confocal arrangement would be required where the beams of the antennae are aligned over the full working range of the radar. This is discussed at the end of the thesis and a diagram is provided of a proposed confocal arrangement in Figure 6-1.

Although the person was stationary in range, slow rocking movements (of a few cm) were made over the course of gathering multiple scans of the person. The inclusion of the rocking motion was to provide the radar with multiple looks at the target from various aspects. This practice allows for variance in data that was used to train, validate and test a supervised classifier (neural network) in an experiment. The scan speed was assumed faster than any movements of the person being scanned and no Doppler effects have been considered. This was a reasonable assumption as each scan takes less than a fraction of a second (~250 ms per scan).

2.9.3 Scope

The scope of the study was restricted to experiments that allowed the aim of the thesis to be satisfied. These experiments are discussed in the next section (2.9.4) along with stages of development required to conduct them.

A limited, but representative set of weapons have been investigated. This set included handguns and an Improvised Explosive Device containing fragmentation. No pure dielectric targets (i.e. sheet explosives containing no fragmentation) were included in the set and no benign items were included. The experiments in this thesis were used to make an initial assessment of the feasibility of using polarimetric decomposition algorithms in a radar based weapon detector. The experimental radar is limited in capability and the measurements were challenging to make with this system. The development of a portable radar with a confocal antenna arrangement capable of making real time measurements would allow for an increase in the variety and number of items included in the test set. These developments require significant further work.

Two weapon orientations have been used in the experiments. Ideally, the orientation of the weapon would incrementally adjusted. This would allow for further analysis of effects of weapon orientation on the polarimetric signatures that are used for detection. Given that the weapon is placed on a person and the person is making small semi-controlled movements, it is impossible to precisely align the weapon on the body. Assessment of the weapon in isolation would make it possible to incrementally adjust the weapon orientation. However, consideration of the weapon in isolation is not representative of the problem, as weapons concealed upon a body are of interest.

2.9.4 Stages of development

The stages of development of the work presented in this thesis are summarized using the following bullet points and discussions:

- Design of an experimental radar;

A radar was built around a Vector Network Analyzer (VNA). An antenna mount was designed and constructed that had two antennas arranged such that one was sensitive to vertical linear polarisation and the other was sensitive to horizontal linear polarisation. The antennas were angled such that their beams were co-aligned at a range of 2m. A laptop was used to interface to the VNA and a MATLAB script was created collected that data and subsequently processed it. This is discussed in Chapter 3.

- Perform verification measurements;

An experiment was conducted to verify the quality of measurements obtained using the developed radar. The technique used was to perform a quantitative measurement of a target radar cross section that could be solved analytically. To remove the effects of free space loss a relative measurement was selected. The chosen targets were two conducting spheres of different sizes. The radar cross section of the smaller sphere was measured relative to the larger one and the result was compared to the analytical solution. The measurement was made at 401 discrete frequencies across the frequency band used by the radar (18 to 26 GHz). The error between the measurement and analytical solution was presented as a function of frequency. This experiment is discussed in section 3.3.

- Gather data using radar under the defined detection scenario;

A data gathering experiment was conducted in which scans were taken of person with and without concealed weapons. The full details of the procedures used in this experiment are

discussed in Chapter 4. The results obtained from this experiment are presented and discussed. In this experiment, 1000 scans were taken for analysis.

- Perform polarimetric decomposition;

The data gathered in the previous experiment was processed using the polarimetric decomposition as described in Chapter 5. From the processed data three data sets were formed, one for each polarimetric decomposition that was investigated. The formation of these data sets is discussed in Chapter 5 and the results are presented alongside detailed analysis and discussion.

- Design an experiment to assess the proposed use of polarimetric decompositions algorithms to detect concealed weapons;

The last experiment in the thesis takes the three decomposition algorithms and tests their suitability in a weapon detection scenario. To each algorithm, a hypothesis test is applied. The hypothesis in each case was ‘This algorithm will provide data that can be used to detect concealed weapons’. The data sets from each algorithm (described in Chapter 5) were split in half. In each case half of the data was used to train and validate a neural network that was subsequently used to detect weapons. The other half of each data set was used in a test of the neural networks to detect weapons. The output from this experiment was three ROC curves, one from each algorithm. These ROC curves captured the detection rate and false alarm rate from the tests. To reach a decision on the validity of the hypothesis tests the area under the ROC curve was measured. The area under curve was compared to a value that represents a classifier with no useful purpose ($AUC = 0.5$). If the area under the curve was larger than the value quoted then the hypothesis was accepted. The confidence level in this experiment was calculated to be 95%, using the sample sizes. Chapter 5 section 5 documents this experiment and the results are analysed and discussed.

Chapter 3

Development of a Fully Polarimetric Radar

This chapter discusses the development of an experimental system used to measure polarimetric scattering of weapons. This experimental system is essentially a Frequency Modulated Continuous Wave (FMCW) radar constructed using a Vector Network Analyzer (VNA). This radar operates in the K-band (18-26GHz) and is fully polarimetric and has the potential to make a full measurement of a target's Sinclair scattering matrix. This scattering matrix can then be used to synthesize the polarimetric response of a target to an incident wave having any polarization. Verification measurements are presented to assess the level of systematic errors in the measurement system.

3.1 Introduction

Radio detection and ranging (Radar) is a tool used to detect remote objects using the reflection of radio frequency waves. A radar transmits an electromagnetic wave towards a target; this wave is often referred to as the incident wave. The incident wave then interacts with the target and a proportion of the wave is reflected back towards the radar, this wave is often referred to as the scattered wave. Only a proportion of the incident wave is reflected back towards the radar and the rest is either scattered away from the radar, absorbed by the target or transmitted through the target. On reception of the scattered wave, information about the target, including its range, can be

determined. Figure 3-1 below shows the interaction of an incident wave with an arbitrary target resulting in a scattered wave.

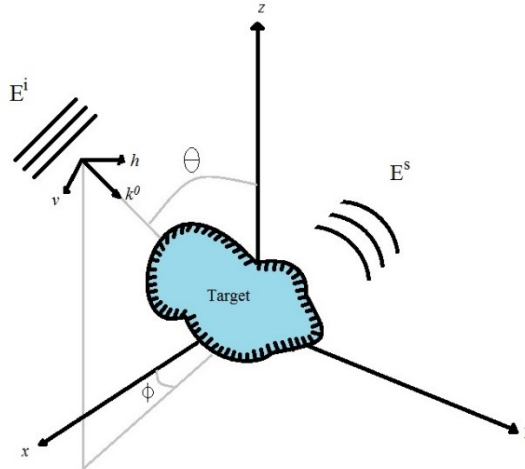


Figure 3-1 Interaction of an incident wave with an arbitrary target, resulting in a scattered wave.

One of the key characteristics of the scattered wave is its polarization and most importantly changes in polarization with respect to the incident wave. In the field of concealed weapons/threat detection, polarization changes have been used as a useful indicator of the presence of a weapon [25], [31], [38] and [41]. Radars can be designed with multiple polarizations to exploit any polarization changes that may occur because of the interaction of the incident waves with particular targets of interest. For example the use of multiple transmit polarizations ensures that cross-polarized reflections from knives are detected independent of rotation of the weapon in the target plane [45].

There are many types of radar available, each derived for specific applications. Some common types of radar include Pulsed radar, Doppler radar, Synthetic Aperture Radar and Frequency Modulated radar, to mention a few [46]. One of the more advanced forms of radar is Frequency Modulated Continuous Wave (FMCW) radar, which has good phase sensitivity making it ideal for polarimetric measurements. Additionally FMCW radar offers excellent range resolution,

this allows for range gating of clutter that is in close proximity to a target of interest. FMCW radar has been utilized in this research project and shall be described in detail.

3.2 The Radar

A block diagram showing the layout of the VNA measurement system used to form a FMCW radar is presented in Figure 3-2 below. In this measurement system, there are two sources, which are a Radio Frequency (RF) source and a Local Oscillator (LO) source. Both of these sources are voltage-controlled oscillators operating at different frequencies. The RF source will oscillate at the same frequency as the wave transmitted toward the target by the antenna and the LO source will oscillate at a much lower frequency. The purpose of the LO is to down convert the frequency of the transmitted and received signals such that they can be adequately sampled by the Analogue to Digital Converter (ADC) built into the VNA. Also in Figure 3-2 are four mixers that perform the down conversions of the signals. The mixers are fed by directional couplers that divert a proportion of the transmitted and reflected signals. In this measurement system, there are two antennas and only one RF source. The path of the RF source is switched to each of the antennas sequentially and the reflected signal is measured on both paths. The signals are sampled using receivers a1, a2, b1 and b2; these are then converted into complex s-parameters.

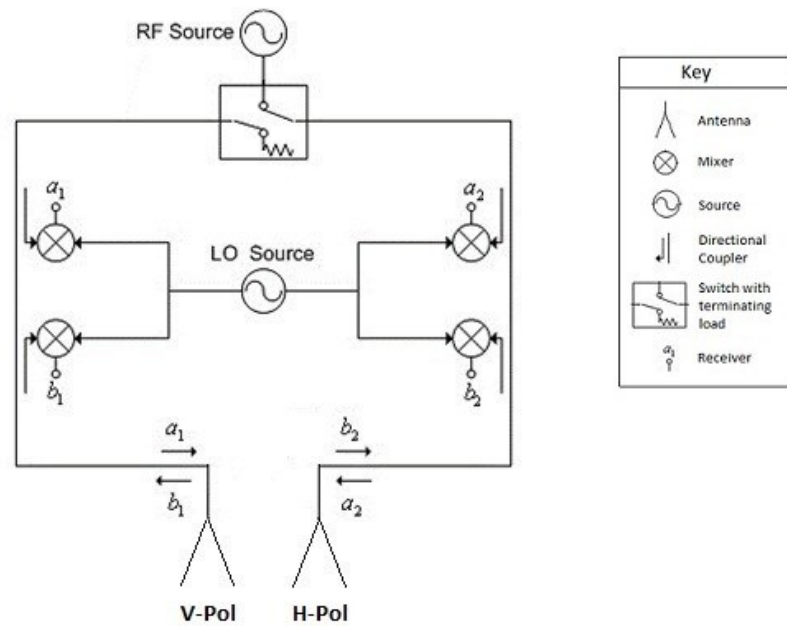


Figure 3-2 Simplified overview of measurement system using a VNA and two antennas, one with vertical linear polarization and the other with horizontal linear polarization, figure reproduced based on [47].

Complex S-parameters are used, as they are ideal for extracting amplitude and phase measurements from networks, which is a requirement for the intended polarimetric measurements. The radar described above can be treated as a 2 port network and the phase and amplitude of a signal reflected onto both ports can be measured relative to the signal transmitted on 1 of the ports, the transmit port is then switched to measure the response to the second transmitted signal which produces a wave of a different polarization. The receivers represented by a1, b1, a2 and b2 in Figure 3-2 are pairs of diode receivers that are fed via Q and I demodulators. The reflected signals are demodulated into Q and I in order to obtain both the amplitude and phase of the reflected signal with respect to the transmitted signal. The sampled signals are then converted into S-parameters using the following equation.

$$S_{mn} = \frac{b_m}{a_n} \quad (3.1)$$

All four s-parameters possible with a two-port network are measured and used to form the Sinclair scattering matrix as shown below.

$$S = \begin{bmatrix} S_{11} & S_{12} \\ S_{21} & S_{22} \end{bmatrix} = \begin{bmatrix} S_{VV} & S_{VH} \\ S_{HV} & S_{HH} \end{bmatrix} \quad (3.2)$$

The second form in equation (3.2) shows the s-parameters with subscripts representative of the antenna polarization connected to each port with V indicating vertical linear polarization and H indicating horizontal linear polarization.

Frequency Modulated Continuous Wave (FMCW) radar is a radar in which the frequency of the transmitted wave is modulated by a periodic reference signal. If a linear frequency sweep is generated using a triangular modulating signal then the resulting waveform is a chirp, as illustrated in Figure 3-3.

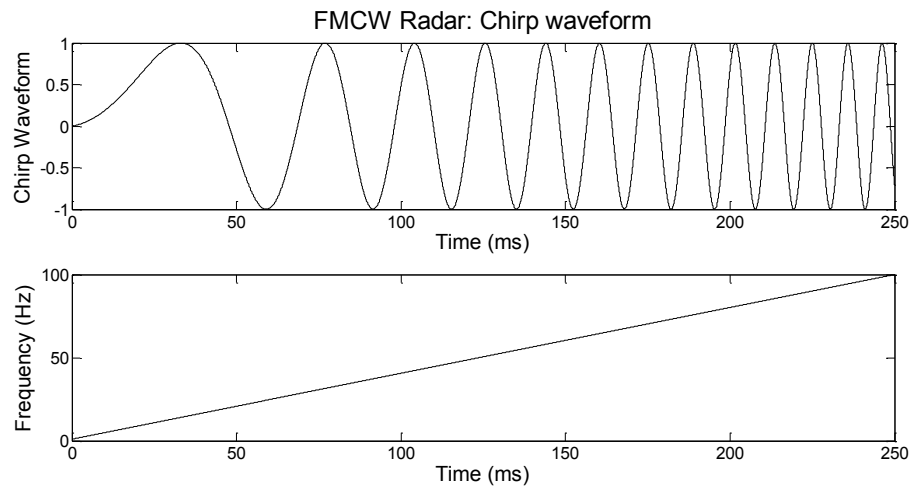


Figure 3-3 FMCW radar chirp (Top) and modulating (Bottom) waveforms.

The proportion of the wave that is reflected by a target is then mixed with the transmitted signal to generate a beat frequency; this beat frequency is directly related to the range of the target.

The beat frequency is the difference between the transmitted and reflected signal frequencies; this is shown in Figure 3-4. T_d is the time delay related to the time of flight of the signal and t_m is the period of the modulated signal.

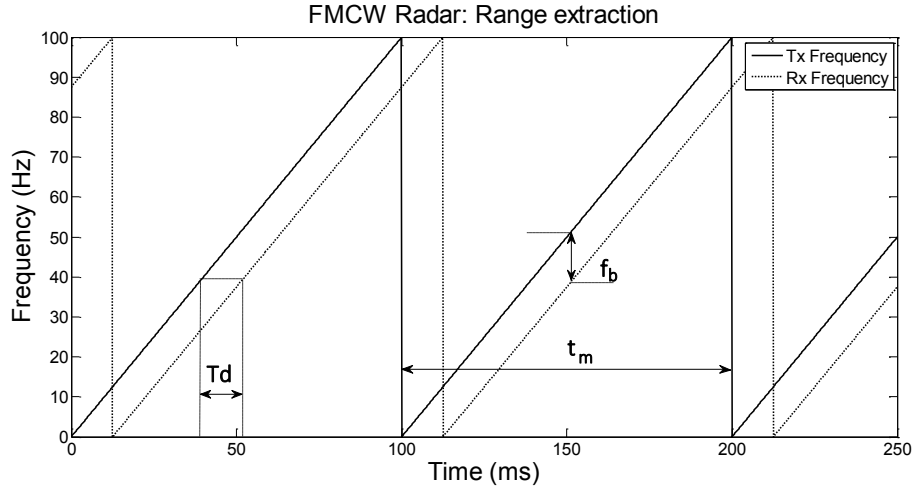


Figure 3-4 Range extraction from a FMCW radar.

The following equation governs the relationship between the beat frequency and the range of the target [46], this equation will later be used to determine the sampling criteria of the VNA.

$$f_b = \frac{2R\Delta f}{t_m c} \text{ (Hz)} \quad (3.3)$$

In equation (3.3) R symbolizes the range of the target, Δf the radar bandwidth, c the speed of light and t_m the period of the modulating waveform.

The radar equation is fundamental in understanding how much power is reflected back to the radar in a given scenario. The radar equation is given by (3.4) below [46].

$$P_R = \frac{P_T G^2 \lambda^2 \sigma}{(4\pi)^3 R^4} \text{ (W)} \quad (3.4)$$

Where P_R is the reflected power, P_T is the transmitted power, G is the antenna gain, λ is the wavelength of the transmit frequency and σ is the target's radar cross section.

To understand this equation, an isotropic antenna can be considered. An isotropic antenna is one that radiates energy equally in all directions. This gives a spherical radiation pattern. It is relatively simple to derive the power density for an isotropic antenna, since its radiating pattern is spherical, the power density, P_D , is just the transmitted power divided by the surface area of a sphere, as given in equation (3.5).

$$P_D = \frac{P_T}{4\pi R^2} \text{ (Wm}^{-2}\text{)} \quad (3.5)$$

In practice, a directional antenna is often used in radar. A directional antenna radiates more power in a particular direction. To account for this directionality a parameter, G , is defined which is antenna gain as given by (3.6) [46].

$$G = \frac{4\pi A_e}{\lambda^2} \quad (3.6)$$

Where A_e is the effective aperture of the antenna and λ is the wavelength of the electromagnetic wave that is radiated from the antenna. Considering the directional antenna the power density now becomes:

$$P_D = \frac{P_T G}{4\pi R^2} \text{ (Wm}^{-2}\text{)} \quad (3.7)$$

Now a parameter must be defined that takes into account the power reflected from a target in relation to the power density upon the target. The parameter σ used is the radar cross section (RCS); this parameter is defined as a ratio of the reflected power to the power density, as described in equation (3.8).

$$\sigma = \frac{P_R}{P_D} \text{ (m}^2\text{)} \quad (3.8)$$

Using the RCS and the power density for a directive antenna the power reflected back to the antenna from the target can be derived.

$$P_R = \frac{P_T G \sigma A_e}{(4\pi R^2)^2} \text{ (W)} \quad (3.9)$$

By transposing equation (3.6) for the effective antenna aperture and substituting this into equation (3.9) we arrive at the radar equation given by equation(3.4).

In reality, there is also noise in the system and this must be taken into consideration. The Signal to Noise Ratio (SNR) is a key parameter in any radar system and describes the severity of noise corruption in the received radar signal. The SNR is given by equation (3.10) [46].

$$SNR = \frac{P_R}{N} = \frac{P_T G^2 \lambda^2 \sigma}{(4\pi)^3 R^4 k T_e \Delta f L} \quad (3.10)$$

$$N = k T_e \Delta f \quad (3.11)$$

Where N is the noise power, k is Boltzman's constant, T_e is the effective noise temperature, Δf is bandwidth and L accounts for signal losses.

One of the key features of a radar is that it can provide a range to the detected target. The maximum range at which radar can operate can be derived from the radar equation. The equation is transposed for R and the reflected power is substituted with the minimum detectable power S_{\min} , which is derived from the levels of noise in the system. The maximum working range of a given radar system is calculated using equation (3.12).

$$R_{\max} = \sqrt[4]{\frac{P_T G^2 \lambda^2 \sigma}{(4\pi)^3 S_{\min}}} \text{ (m)} \quad (3.12)$$

As can be seen from the previous equation the maximum working range of a radar system can be extended by increasing the either the transmitted power, gain of the antenna or the wavelength. The RCS is governed by the targets the radar must be capable of detecting and hence little can be done about extending the working range as a function of the RCS. Finally, the range of a radar system can be improved by lowering the minimum detectable signal. This can be done by removing noise from the system where possible. Another crucial parameter in a radar system is

range resolution. Range resolution is a measure of the ability of a radar system to detect multiple targets in close proximity. If two targets are separated by a distance less than the range resolution of the radar then the radar will detect the two targets as a single target. In FMCW radar, the range resolution ΔR is determined from the bandwidth and is given by equation (3.13).

$$\Delta R = \frac{c}{2\Delta f} (m) \quad (3.13)$$

As can be seen from this equation the range resolution can be improved by increasing the system bandwidth. This however can result in increased cost of components.

3.2.1 Sampling

FMCW radar derives the range to a target using the beat frequency, which increases as the target moves away from the radar. Therefore, the beat frequency at the maximum working range of the radar is used to set the sampling criteria on the VNA as it results in the highest frequency signal that must be sampled. Nyquist's theorem states that for a signal to be reconstructed after sampling, the sampling frequency must be at least twice the bandwidth of the original signal. The sampling on the VNA is set using the Intermediate Frequency Band-Width (IFBW) and to satisfy Nyquist's theorem the IFBW must be twice the maximum beat frequency.

The VNA used in this radar has a set number of predefined IFBW settings, therefore an acceptable beat frequency must be chosen for the predefined IFBW setting that is to be used in the radar measurements. In this work, an IFBW of 10 kHz was chosen and therefore the beat frequency at the maximum working range of the radar must be at most 5 kHz. The beat frequency can be set using the sweep time following the equation below (3.14). Setting the beat frequency to 5 kHz at the maximum working range of the radar, the sweep time is found to be 53 ms. The maximum working range of the radar was chosen to be 5 m, this value was selected based on the area available

to conduct experiments and is used in the calculation below. In practice, targets were measured at a range of 2 m and a wall of radar absorbing material (RAM) was placed 5m from the radar, this helped to reduce background clutter.

$$t_m = \frac{2R_{\max}\Delta f}{f_b c} = \frac{2(5)(8 \times 10^9)}{(5 \times 10^3)(3 \times 10^8)} = 53(ms) \quad (3.14)$$

The unambiguous range of the radar is given by the number of points taken across the frequency sweep multiplied by the range resolution of the radar. The number of points in the frequency sweep has been selected as 401 (a pre-defined VNA setting) this will give the radar an unambiguous range of 7.5 m as shown in the following calculation (3.16), although the maximum working range will be shorter than this and will be set at 5 m by the sweep time and IFBW selections.

$$\text{points} = \frac{R_{\max}}{\Delta R} = \frac{2R_{\max}\Delta f}{c} \quad (3.15)$$

$$R_{\text{unambiguous}} = \frac{c \times (\text{points})}{2\Delta f} = \frac{(3 \times 10^8) \times 401}{2(8 \times 10^9)} = 7.52(m) \quad (3.16)$$

3.2.2 Calibration

Polarimetric analysis techniques that have been applied to data measured using the experimental radar require that systematic errors be kept to an absolute minimum. Typical acceptable errors are 0.4 dB in amplitude and 5° in phase for each element of the measured scattering matrices [48].

The main source of systematic error in this radar is the measurement errors on the VNA. These errors are primarily caused by poor impedance matching and directivity of components inside the VNA that lead to reflections and leakage respectively. Errors occur when reflections inside the measurement system generate beat frequencies that are observable in the measured data and these errors can be detrimental to the integrity of the signals related to the target being measured. Other sources of systematic errors come from the frequency response of the external cables, waveguide adaptors and the horn antennas. The effects of these systematic errors on measurements can be reduced or potentially removed altogether providing that time is taken to measure calibration standards [47]. A calibration standard is a piece of hardware or a definition of a connection that has a known response. These are placed in a system and the measured response is compared to the known response of the standard. This gives an indication of any system characteristics that lead to error in the measured data. The ability to measure system induced errors leads to the opportunity to correct the errors present in data measured through the process of calibration.

Literature reports that use of a two-port calibration (as was used in this work) can reduce measurement uncertainty from 10.4 dB to 0.44 dB in amplitude when a reflection measurement is made [49]. This would indicate that uncertainty in the two elements of the leading diagonal of the scattering matrix could be reduced to levels similar to the typical acceptable errors reported previously, if calibration is performed. Similarly, the same paper reports that transmission

measurement uncertainties can be reduced from 0.8 dB to 0.05 dB using a two-port calibration. The two elements on the trailing diagonal of the scattering matrix are essentially transmission measurements. This section later discusses the type of two-port calibration that has been applied to measured data in this study.

Typically, the impedance matching of components inside a VNA is good at certain frequencies; however, the broadband nature of these instruments means that the matching will be poor over many other frequencies. Impedance mismatches result in signal reflections at the points at which they occur. The greater the number of internal reflections and the greater the severity of the reflection the more difficult it becomes to analyse measurements made on the instrument. Ideally, the instrument would be factory calibrated to remove most of the effects of these mismatches; however, many of the negative effects can be corrected post-measurement by measuring calibration standards and using these measurements as references. These reference measurements are only valid whilst the VNA remains in the environment in which they were taken, for example if there is a variation in temperature the impedance of internal components will change resulting in a different mismatch to the one which would have been recorded through measurement of the calibration standards [47].

The directivity of the directional couplers inside a VNA can have an impact on the quality of measurements with low reflection coefficients. Although these components are typically of very high quality, there will still be leakage of signals and unintentional coupling between the transmitted and reflected signals. This is of particular concern in this work as some of the measurements that were made with this system have very small reflection coefficients. Again, the errors owing to the directional couplers can be removed providing that reference measurements of calibration standards are taken.

The frequency response of the external cables and waveguide adaptors results in large measurement errors, these errors can be removed by using the same cables and adaptors in the

measurement of the calibration standards. This error correction is only valid for measurements taken at and around the time of the calibration measurements, as the errors will change if the cables are unconnected or moved significantly from their original position.

There are many types of calibration that can be performed on a VNA such as Line-Reflect-Match, Short-Open-Load-Thru, Thru-Reflect-Match, Line-Reflect-Line & Thru-Reflect-Line (TRL) [47]. Each one of these calibration techniques requires different calibration standards. The calibration performed in this work was the TRL, the reason being that the standards are easy to build and this technique is highly accurate. To perform a TRL calibration the VNA parameters that will be used in the target measurements must be entered before starting the process and the cables and waveguide adaptors that are to be used for the target measurements should be connected to the VNA. Once this is done, measurements of the calibration standards must be taken.

The TRL calibration involves measurement of two transmission standards and one reflection standard. From measurements of these standards, eight error terms are calculated based on a two-port system error model. A diagram of a two-port system error model showing the sources of the eight error terms is provided in Figure 3-5.

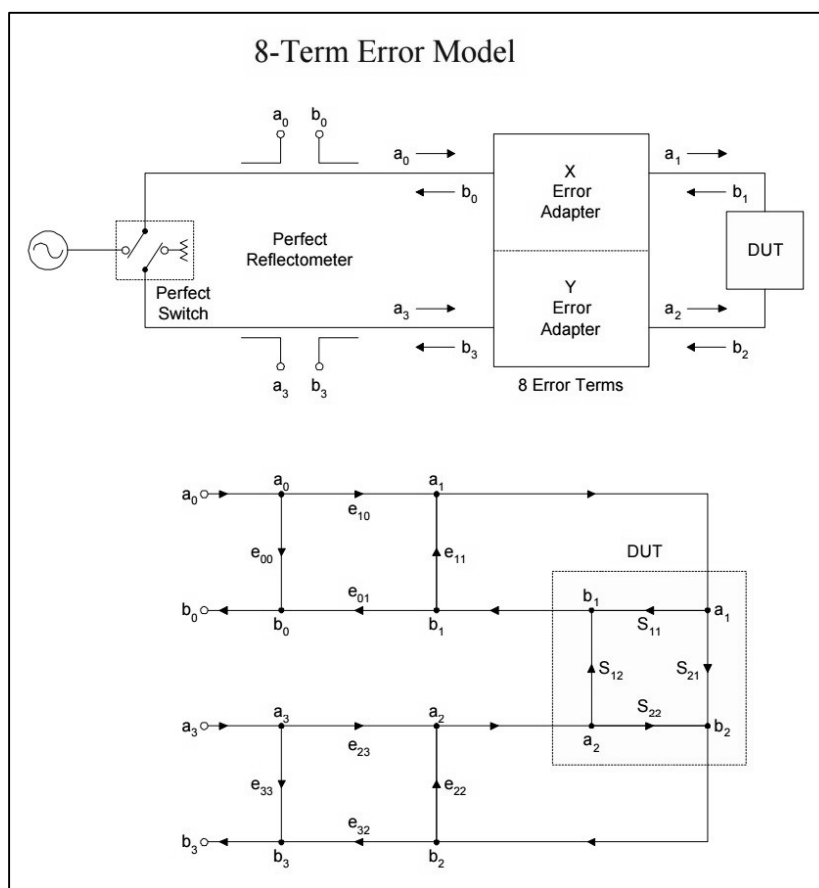


Figure 3-5 Diagram showing sources of measurement errors in a two-port VNA, produced using diagrams in [47].

Once the error terms are determined using information from the measurements and the known characteristics of the standards, the complex S-parameters of the system under test can be computed, as prescribed in [47]. In this work, the system under test is a target (person) within the working range of the radar. The error terms and corrected S-parameters were obtained using software provided on the VNA. A Short is used as a reflect standard, the short has a known S-parameter for S_{11} and S_{22} , with a magnitude of 0 dB expected at all frequencies. A line is the first transmission standard that is used as an impedance reference. The characteristic impedance of the line standard must be known and can be calculated from the length of the waveguide that was used as a line. The thru is the second of the two transmission standards and provides a third and final

impedance reference. The known S_{21} and S_{12} response of this standard is 0 dB magnitude and 0° phase, at all frequencies.

The Thru standard is not actually an additional piece of hardware; it simply involves connecting the waveguide adaptor that is connected to port 1 of the VNA to the waveguide adaptor on port 2 and measuring the scattering matrix. This is illustrated in the Figure 3-6.



Figure 3-6 Image showing connection of waveguide adaptors for measurement of a ‘thru’ calibration standard.

The short standard must then be connected to port 1 and port 2 and measurements taken on both. Figure 3-7 below shows a short connected to a waveguide adaptor.



Figure 3-7 Image showing short calibration standards connected to each port on VNA, close up view (Right).

The final standard to be measured is a line; this is simply a section of waveguide of known length. This is illustrated in Figure 3-8.

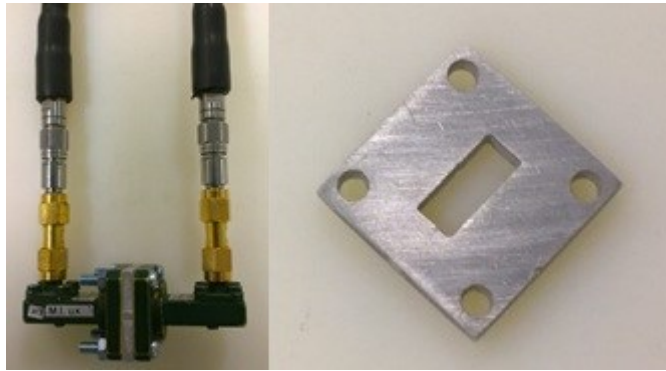


Figure 3-8 Image showing a line calibration standard connecting the two ports of the VNA, close up view on right.

There are a number of plots in Figure 3-9 below which show the raw data and calibrated data taken from measurements of the three calibration standards. The ideal characteristics of a thru are that the return loss in both directions is as low as or lower than the noise floor of the VNA ($S_{11} = S_{22} \leq -110$ dB) and that the thru path is un-attenuated and reciprocal ($S_{12} = S_{21} = 0$ dB).

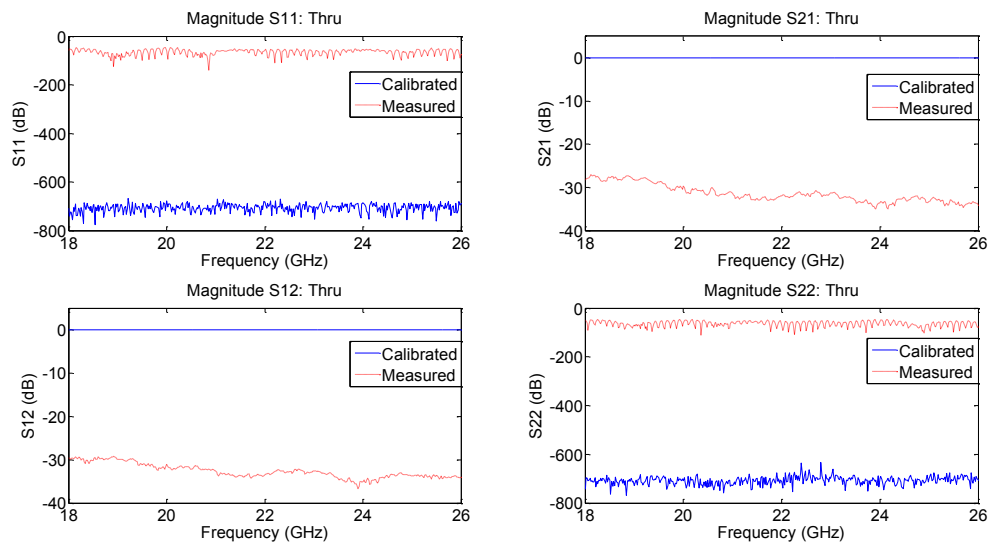


Figure 3-9 Plots showing measurements of a ‘thru’ calibration standard, each plot represents the log magnitude of the signal associated with each element of the complex S-matrix.

As can be seen in Figure 3-9 the measured data before calibration does not match the ideal characteristics of a thru. There is a significant return loss on both port 1 and port 2 of -70 dB, which is above the -110 dB noise floor of the VNA. The return loss on both ports shows strong frequency dependency that is untypical of an ideal thru. The thru characteristics before calibration are seen to be very poor, the thru is not seen to be reciprocal and is around -30 dB which is way below the ideal of 0 dB. After the calibration is applied to the measured data, the thru characteristics are much more like the ideal case, where the S12 and S21 parameters are reciprocal and at a flat 0 dB across the frequency range. The return loss on both ports is way below the -110 dB noise floor after calibration.

The ideal characteristics of the next standard, the short, are that a reflection of 0 dB is observed on both port 1 and 2 and that the leakage on both ports is way below the noise floor ($S_{12} = S_{21} \leq -100$ dB). Figure 3-10 shows that prior to the calibration process being applied, the reflection on each port is below the expected value of 0 dB and has a strong frequency dependency, and it is observed that each port has a distinctly different reflection characteristic. Post calibration the observed reflection and leakage characteristics are more like the ideal with a 0 dB flat reflection on both ports and leakage across both ports in each direction way below the noise floor of the VNA.

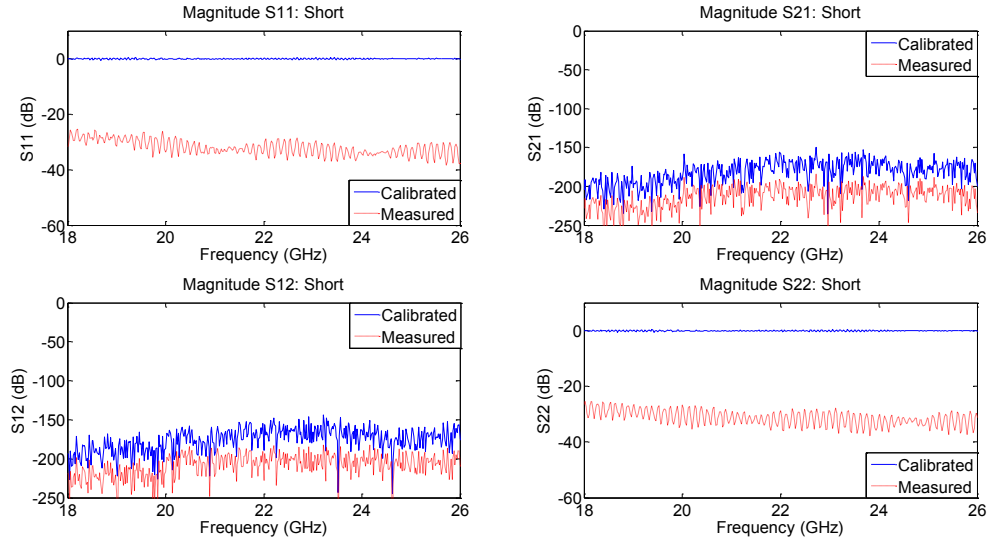


Figure 3-10 Plots showing measurements of a Short calibration standard, each plot represents the log magnitude of the signal associated with each element of the complex S-matrix

The final standard in the calibration process is the line; a short piece of waveguide is used as the line standard. The length of the line has been selected at approximately a quarter of the wavelength at the centre frequency of the system (~ 3 mm). The anticipated characteristics of this standard are a flat and reciprocal thru with very little attenuation ($S_{12} = S_{21} = \sim 0.3$ dB) and that both port reflections are below the noise floor ($S_{11} = S_{22} \leq -110$ dB).

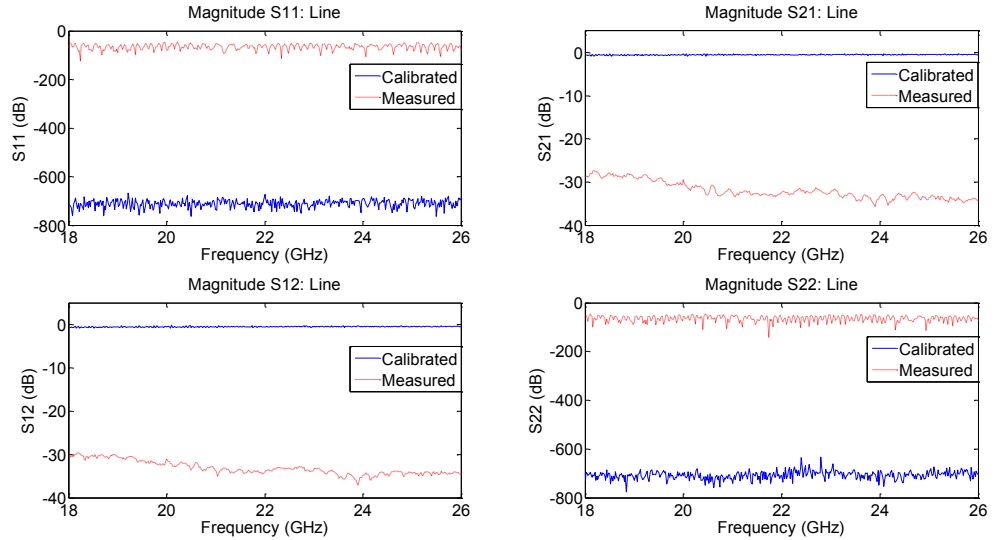


Figure 3-11 Plots showing measurements of a Line calibration standard, each plot represents the log magnitude of the signal associated with each element of the complex S-matrix

Figure 3-11 shows that again the un-calibrated response of the system yields measurements that are unlike the anticipated characteristics of the standard. The observed behaviour of the thru standard that can be seen in the figure shows a large attenuation of $\sim 30 \text{ dB} \pm 5 \text{ dB}$ which is not reciprocal; this is untypical of a waveguide section of only a quarter wavelength long. After calibration is applied the thru is observed in Figure 3-11 to be at $\sim 0.7 \text{ dB}$ flat across frequency and reciprocal across ports, the port reflections are seen to be below the system noise floor.

The frequency response and mismatch of the horn antennas will result in large reflections that are much higher in amplitude than the target reflections. These reflections can easily be removed with a measurement of an open (background) with the horns connected. This measurement is then subtracted from any subsequent measurements effectively suppressing these large reflections from the horns. There is potential for the target signal to be altered or suppressed whilst using this type of error correction if the target is very close to the horn antennas. This is not a

problem here, as the polarimetric analysis techniques applied to the measured data require that the target be in the far-field (Fraunhofer Region) of the antennas, which begins at 0.5 m from the antenna as calculated by equation (3.17).

$$R_{Fraunhofer} = \frac{2D^2}{\lambda_{min}} \quad (3.17)$$

Where D is the maximum linear dimension of the antenna. The next section will discuss range gating, followed by a section that will characterize the antenna used in the radar and will discuss the configuration in which the antennae have been utilized in the radar.

3.2.3 Range Gating

After systematic errors have been removed using calibration, some features that are not related to the target of interest remain. These features are a reflection from the interface between the waveguide adaptor and horn antenna and a reflection from a wall of Radar Absorbent Material (RAM) at the end of the test range (see section 4.3). The calibration described in the previous section removes errors present in the system up to the point of the waveguide adaptor, where the calibration standards were fixed and measured. A mismatch between waveguide adaptor and the horn antenna is the cause of the reflection at this point (this will appear close to 0 m in range). The RAM at ~6.5m on the test range was put in place to reduce any stray reflections from the wall at the end of the lab. As the RAM is not perfect, a reflection from this can be seen in the data. Figure 3-12 shows a sample measurement taken from a person not carrying a weapon; clutter is visible in the signal and has been labelled for illustration. These reflections are considered clutter and can be removed from the signal leaving only the response of the target of interest using range gating.

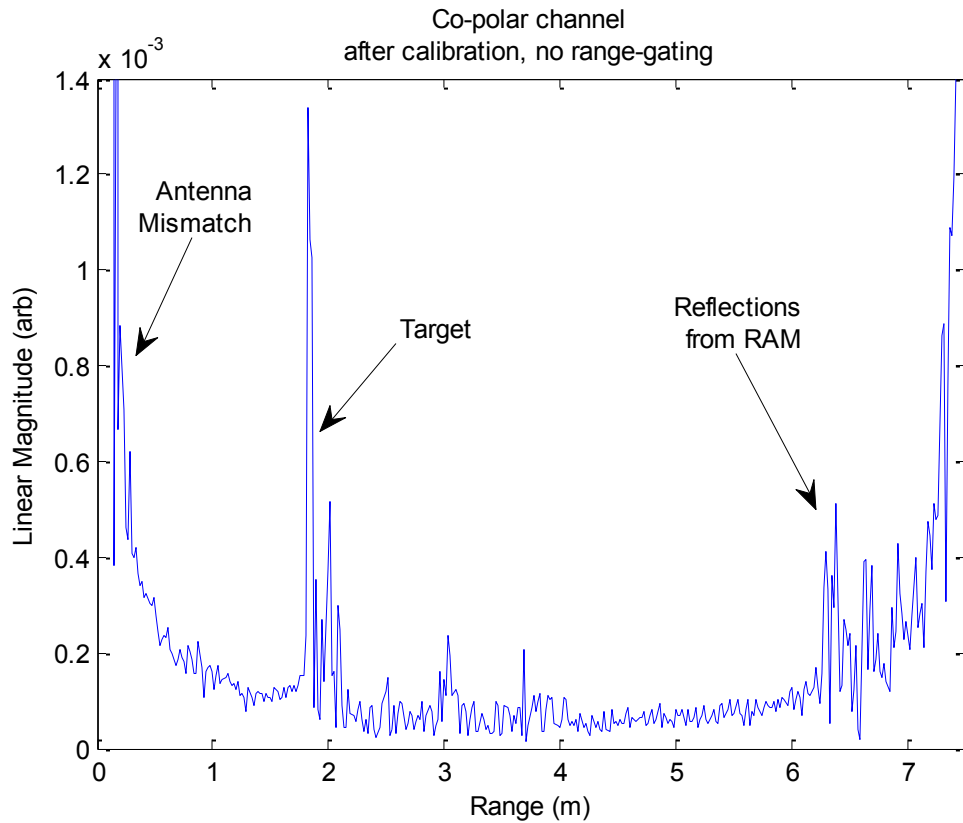


Figure 3-12 Plot showing a co-polar signal relating to a body that was scanned using the radar. A calibration has been applied, but no range gate has been used.

Applying a window at the range that the target was measured removes unwanted signals (clutter), such as the ones described. In all of the experiments the target has been measured at a range of 2m, this is due to a limitation of the measurement system caused by beam alignment of the two antennas; this is discussed in the next section. As the target is always located at 2 m, a rectangular window centred at 2 m is applied to the range resolved data. The window is given an arbitrary width equivalent to 1m in range (no clutter visible in data over this range). This ensures that the target is captured in isolation from the clutter described previously. The gating is applied by taking a signal like the one shown in Figure 3-12 and multiplying it by the window described. For illustration, a sample measurement that has been range-gated is shown in Figure 3-13.

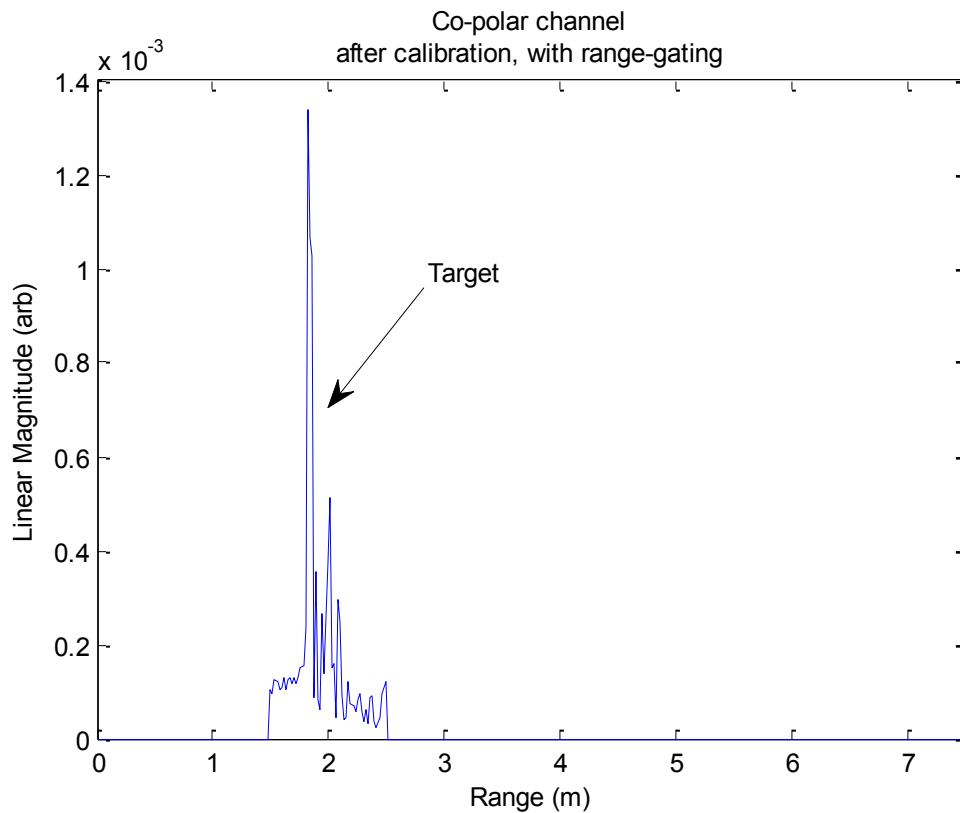


Figure 3-13 Plot showing a co-polar signal relating to a body that was scanned using the radar. A calibration and range gating have been applied.

As Figure 3-13 shows, the reflections from the antenna mismatch and RAM have been removed. This process of range gating has been applied to all the measurements presented in the thesis. The use of range gating has provided a method of isolating the target in the measurements. This ensures that any data extracted from the polarimetric decompositions will be corresponding solely to the target and will not contain features from the clutter that has been observed here.

3.2.4 Antenna

The antennae used in this radar are pyramid horn antennas and there are two of them mounted in a quasi mono-static arrangement with one antenna having vertical polarization and the other cross polarized with a horizontal linear polarization. The forward facing antennae have been angled slightly towards one another to bring the beams into alignment at a range of 2 m. To assess the beam pattern of the antenna and calculate the mounting angles a simulation was run on a 3D electromagnetic solver (COMSOL), the simulation was required as manufacturer test data was unavailable for these antennae. From the simulation, the far-field radiation pattern was obtained which allows for the measurement of beam width and directivity. Once the beam width is known, the spot-size at any given range can be estimated. The extracted far-field pattern at 18 GHz is presented in Figure 3-14.

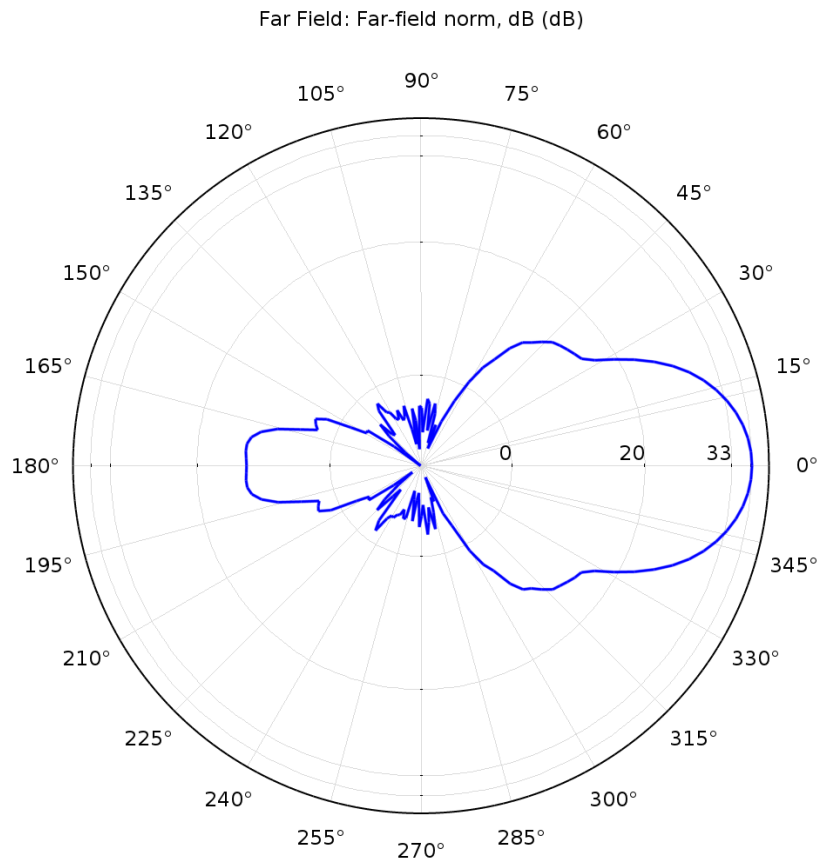


Figure 3-14 Far-field radiation pattern of a horn antenna used in the radar, pattern taken at a frequency of 18 GHz.

The figure shows the far-field radiation pattern of one of the horn antennas at a frequency of 18 GHz, from this plot the Half Power Beam-Width (HPBW) was measured to be 25.5°. The HPBW at the upper frequency in the sweep (26 GHz) was measured at 17°, showing that the antenna becomes increasingly directional at higher frequencies. Figure 3-15 illustrates the far-field pattern at a range of frequencies between 18 GHz and 26 GHz, which shows there is not a great deal of change in the main lobe of the far-field pattern as the frequency changes across the range used for this radar.

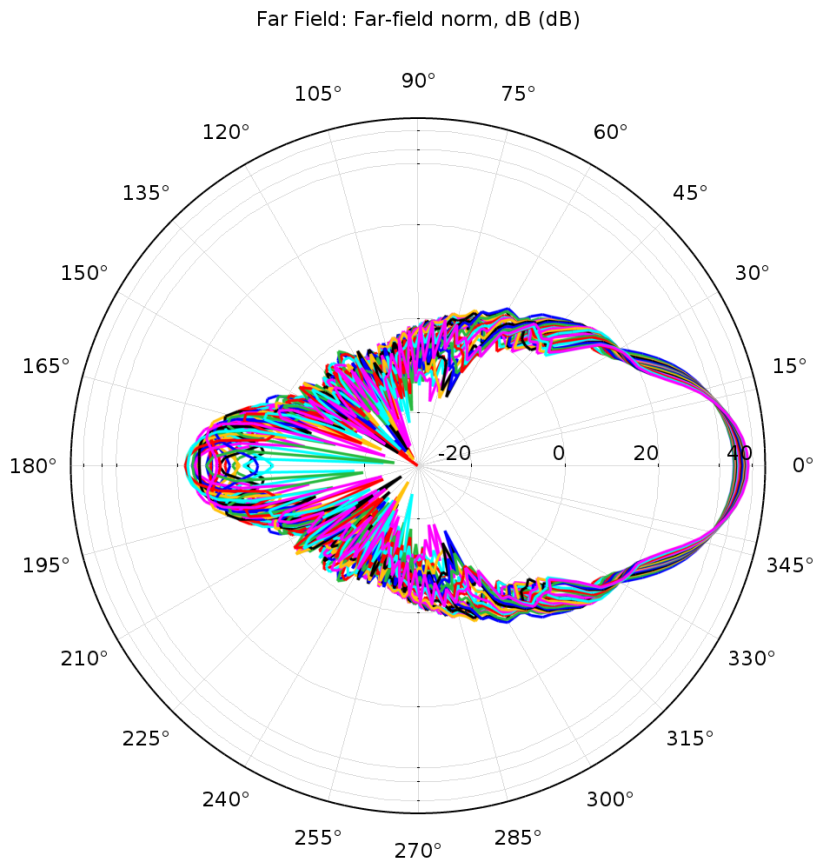


Figure 3-15 Far-field radiation pattern of horn antenna at multiple frequencies across the bandwidth of the radar (18 to 26 GHz).

The measured beam-widths of the antenna were used to calculate the angle at which the antennas should be orientated in order to align the beams at a given range. The reason for doing this is to ensure that the target is illuminated equally from each antenna, if it was not there would be a difference in RCS of the target as measured on each antenna. This difference is not tolerable in the post processing that will be applied in order to extract the polarimetric properties of the target. This is the main reason for taking the time to design an experimental radar system that has low systematic errors.

The geometry of the antenna beams are shown in Figure 3-16. The figure shows that the receivers have been angled such that the two beams come into alignment at a range of 2 m, this

diagram has assumed that the beams diverge linearly with an angle equal to the simulated HPBW angle.

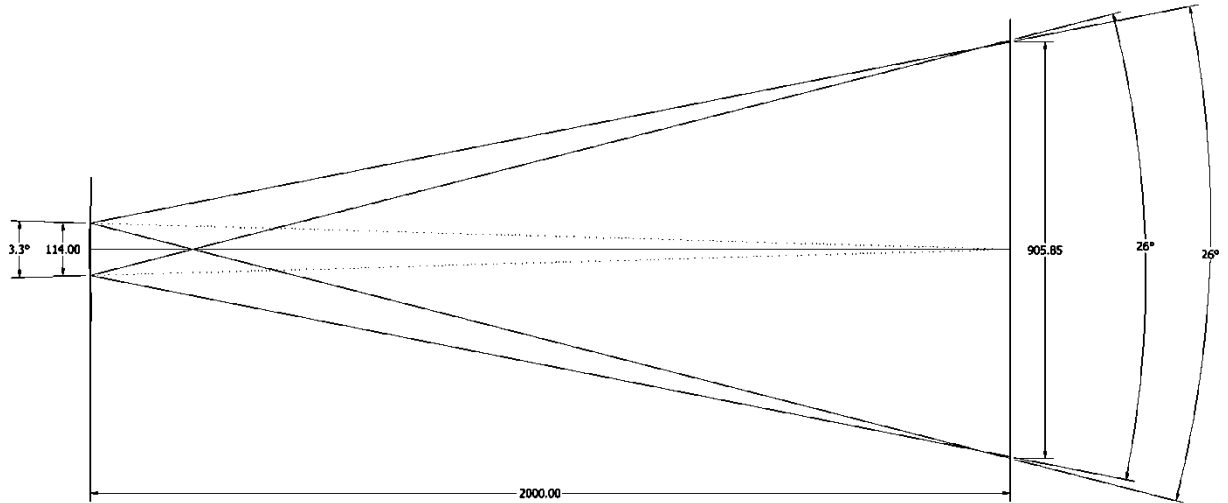


Figure 3-16 Image showing geometry of the beams from each of the horn antennas, angled such that the beams from both antennas are aligned at 2m range (linear dimensions in mm).

The simulations also proved useful in assessing the antenna return loss, which is a measure of how much of the excitation power is reflected by the antenna. For an antenna to effectively couple radiation from a circuit/waveguide to free space the return loss must be low. In fact, the antenna bandwidth is defined by the frequency range for which the antenna return loss is below -10 dB. The power transmitted by the antenna at -10 dB is 96% of the excitation power, with only 4% being reflected by the antenna. The return loss of the antenna used in this research is presented in Figure 3-17; both results from simulation and practical testing are presented in this figure.

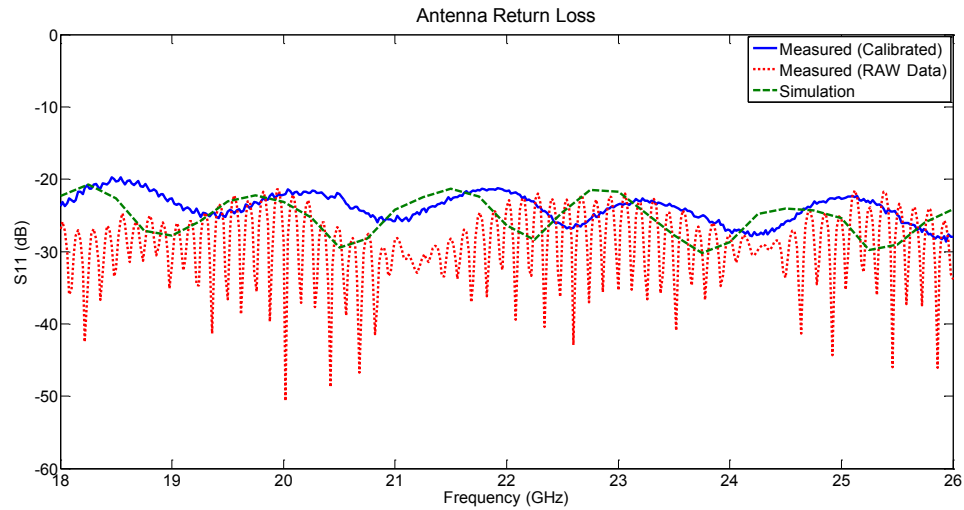


Figure 3-17 Plot showing the return loss of the antenna used in the radar.

As Figure 3-17 shows, the return loss is below -20 dB across the full range of frequencies tested and therefore the antenna is being used within its bandwidth and effective coupling of radiation into free space is achieved. Figure 3-17 shows that there is good agreement between the simulation data and the measured data (post calibration). The measurements were taken using the Agilent E8363 VNA and the calibration used was a TRL that has been explained previously.

Care has been taken to calibrate the VNA to avoid any systematic effects from being recorded and attributed to a measured target and for this reason, the effects of the antenna must also be considered. To do this a measurement of the transmission of the antenna was conducted. In the test the two matched antennas were placed facing each other and in the far field (0.5 m apart) and the transmission through free space and the antennas was recorded (S21). The results of this test are shown in Figure 3-18.

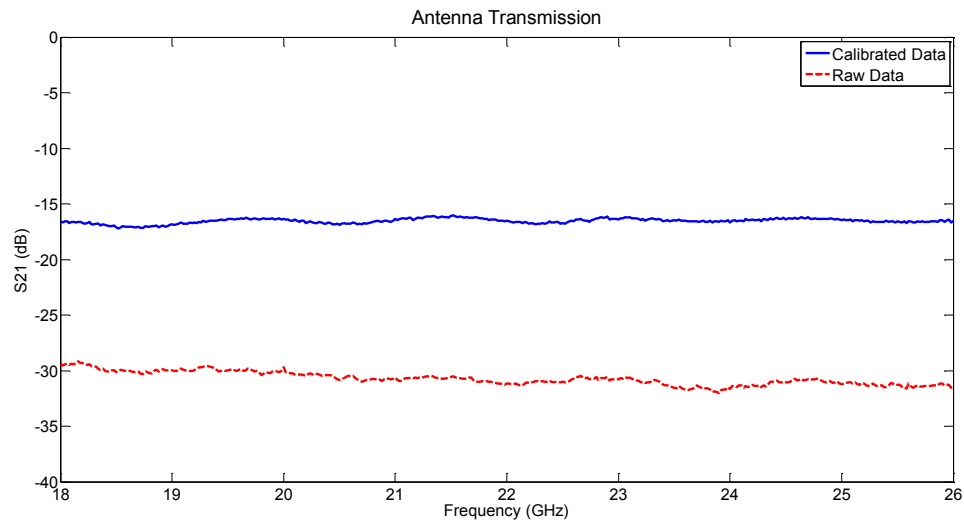


Figure 3-18 Plot showing the transmission characteristics of the horn antenna pair selected for use in the radar.

As the figure shows, the transmission is reasonably flat across the fully range of frequencies measured. This would indicate that there are no resonant effects from the horn in this frequency region and that the horns will have very low systematic effects on any subsequent measurements.

3.3 Verification Measurements

Now that all the major aspects of the measurement system have been discussed, some verification measurements will be presented. The purpose of these measurements is to obtain an indication of the quality of the radar system and quantify any remaining errors after calibration. To do this a large conducting sphere is considered, the radar cross section (RCS) of this target can be calculated and compared to a measured value. The radius, r of the sphere has been chosen such that the sphere scatters independent of frequency across the full frequency range of the radar and therefore the RCS of this target will be frequency independent. The RCS of the sphere is calculated using the following equation.

$$RCS_{Sphere} (m^2) = \pi r^2 \quad (3.18)$$

In the experiment to verify the radar's performance, two different sized spheres were measured. The purpose of measuring two spheres is that RCS measurements are always made with respect to a reference target. One sphere is used as a reference and the other to obtain a RCS measurement. In this experiment, the larger sphere has a radius of 32.5cm and the smaller sphere has a radius of 27.5cm, the larger sphere will be used as the reference target. The calculated values for each of the sphere's RCS is captured in Table 3-1.

<i>Sphere Radius</i>	<i>Calculated RCS</i>
27.5 (cm)	-4.79 dB
32.5 (cm)	-6.24 dB

Table 3-1 Calculated RCS values for two different sized conducting spheres.

The two spheres were then measured using the radar described previously and the TRL calibration was performed on these measurements. The measurements were then referenced to the larger sphere using the following equation.

$$\sigma_{target} = \frac{\sigma_{target}^{measured} - background}{\sigma_{reference}^{measured} - background} \times \sigma_{reference}^{calculated} \quad (3.19)$$

The background measurement was taken with the radar pointing towards a wall of radar absorbent material. The first case where the larger sphere is measured and then referenced to itself, the results yield the theoretical value for the RCS and no error is anticipated. The results from the measurement of the larger sphere are presented in Figure 3-19 against frequency.

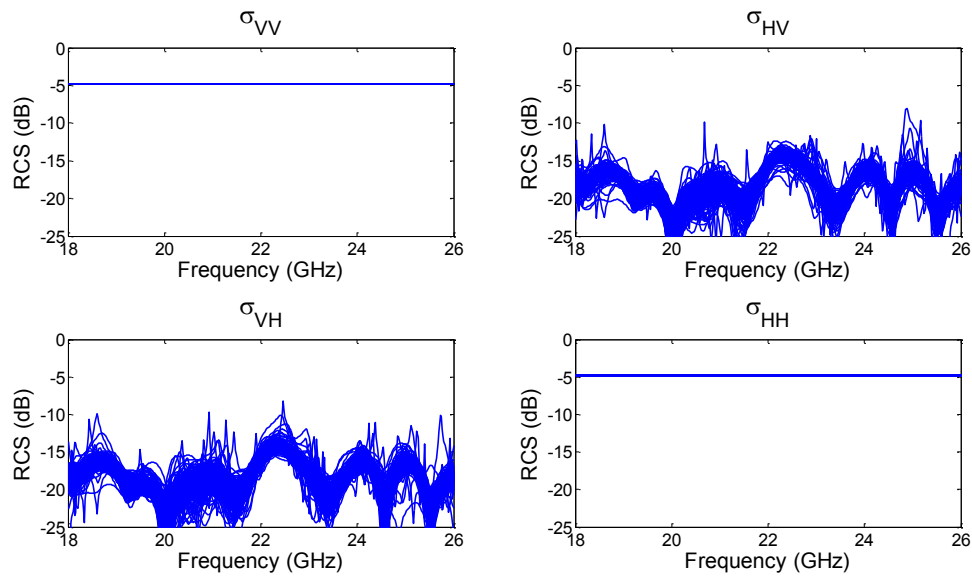


Figure 3-19 Plot showing the measured Radar Cross Section (RCS) of a 65 cm diameter conducting sphere against frequency for each polarization on the radar.

As the figure shows, the larger sphere has a RCS that is independent of frequency on the co-polarized channels, which are the VV and HH channels. The value of the RCS is exactly that which was calculated, this is because the measurement has been referenced to itself. The two cross-polar channels are observed to show a highly frequency dependent RCS which is much lower in value compared to the co-polarized RCS. A perfect conducting sphere would produce no reflection on the cross polarized channels (VH and HV). The observed reflections on the cross polar channels (VH and HV) are caused by imperfections in the targets construction. The target was constructed using a yoga ball covered in tin foil and the foil had crinkles resulting in small amounts of cross-polar reflections. The figure shows the results of 200 successive measurements and only the cross-polar channels are displaying signs of drift in the measurements, these are of low level. The temporally resolved S-parameters from these measurements of the larger sphere are presented in Figure 3-20.

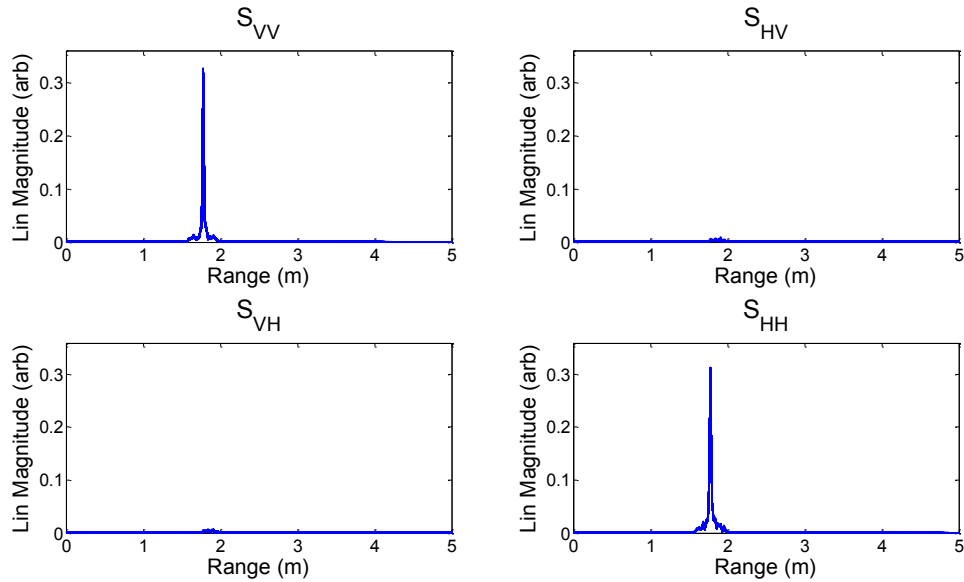


Figure 3-20 Plot showing the range resolved signals from a conducting sphere of 65cm diameter for each polarization on the radar.

Figure 3-20 shows that there are well-resolved single reflections on each of the two co-polarized channels and that there is very little cross-polarized reflection from the target. This result is a good sign that the target is isolated from the measurement system and background clutter as there are no observed reflections near the 0 m range, or anywhere other than the range that the target was placed at (2 m). The results do not show any sign of background clutter, which would appear as peaks at ranges before or after the target. As the plots clearly show, the target was placed at a range of approximately 2 m from the radar. The small amounts of cross-polarized signal that are reflected are seen to originate from the target at ~2 m. This would suggest the target is producing small amounts of cross-polarized reflections. These are most likely caused by imperfections in the construction of the target and undesirable reflections from the netting used to suspend the target in place during the measurements. At this point it should be noted that the spheres were constructed using yoga balls carefully wrapped in metal foil and despite the care taken to wrap the balls there were surface imperfections on the completed conducting spheres. To show that the measurements

of the large sphere, when referenced to themselves, yield the calculated RCS the mean errors on the two co-polarized channels were measured and are presented in Table 3-2.

<i>Channel polarization</i>	<i>Mean Error</i>
<i>Vertical</i>	Undetectable
<i>Horizontal</i>	Undetectable

Table 3-2 Mean errors on the co-polarized RCS measurements from a conducting sphere of 65cm diameter.

This shows that the process of measuring a target to a reference yields the theoretical value, when the measured target is also used as the reference, thus verifying (3.19).

The smaller sphere was then measured using the radar and the resulting RCS values, referenced to the larger sphere, are plotted against frequency for each of the radar polarizations in Figure 3-21.

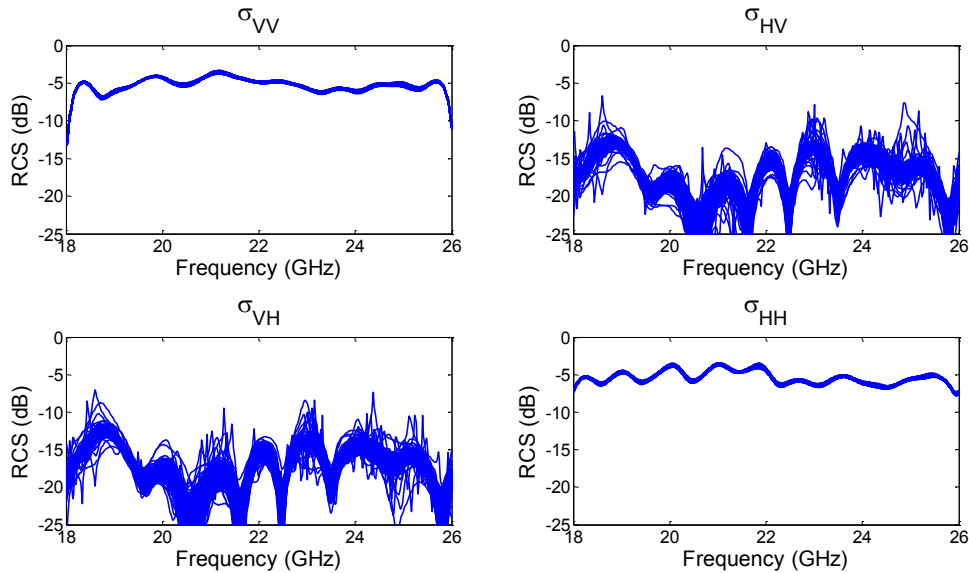


Figure 3-21 Plot showing the measured Radar Cross Section (RCS) of a 55cm diameter conducting sphere against frequency for each polarization on the radar.

As Figure 3-21 shows, the two co-polarized measurements show different characteristic ripples against frequency. This indicates that there are measurement errors present in the system. Again, the cross-polarized RCS is observed to be significantly lower than the co-polarized RCS values as would be expected. The temporally resolved S-parameters for each of the measured polarizations are plotted in Figure 3-22 and the target is seen at a range of approximately 2m.

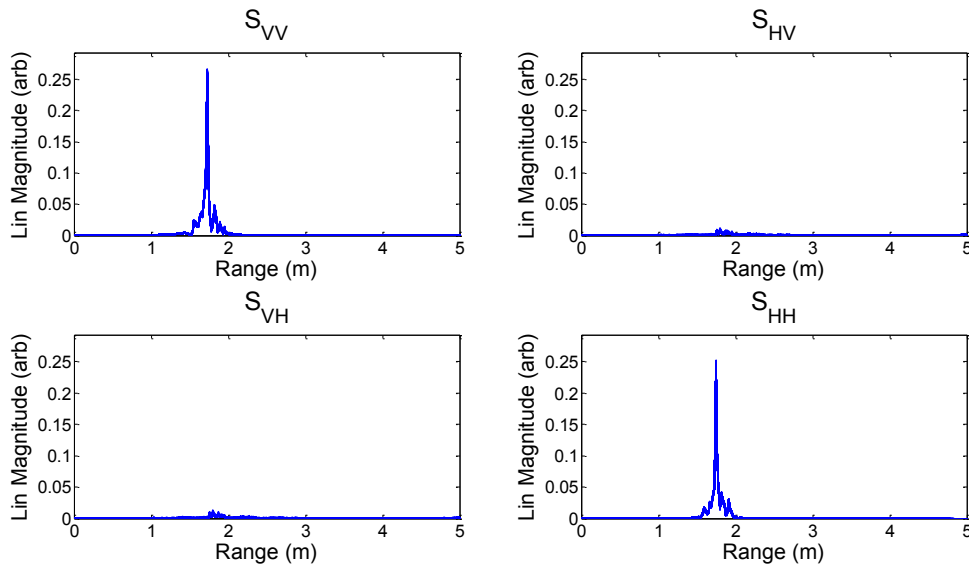


Figure 3-22 Plot showing the range resolved signals from a conducting sphere of 55cm diameter for each polarization on the radar.

The figure shows that again, the targets seem isolated in free space and no background clutter is observed. Yet there remains a small cross-polar reflection from the target. This was also observed with the larger sphere and is likely caused by surface imperfections on the sphere.

The co-polarized RCS of the smaller sphere was observed to vary with frequency, see Figure 3-21; therefore the error between the measurement and calculation was recorded and has been plotted for both co-polarized channels in Figure 3-23.

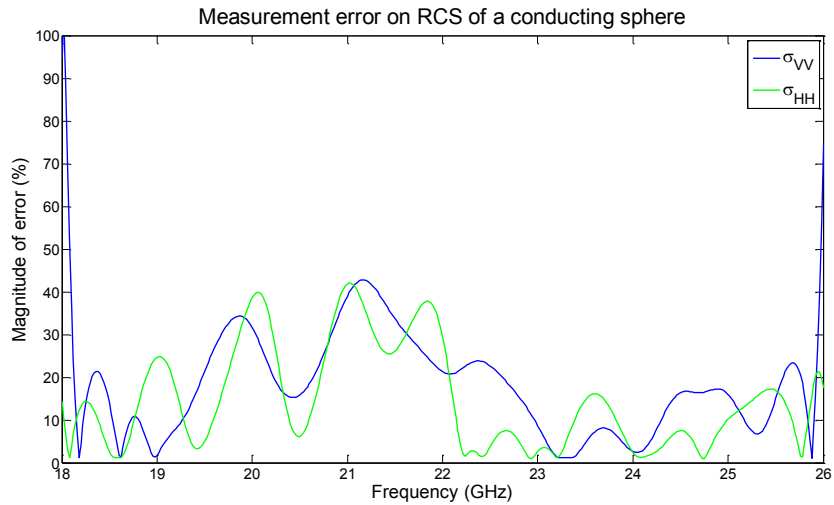


Figure 3-23 Plot showing the measurement error on the RCS of a conducting sphere of 55cm diameter, for each of the co-polarized RCS parameters.

The plot shows that the error varies significantly with frequency and that the error is different for each channel. The error is observed to reach 100% for the first and last frequency on the vertical co-polarized channel and this seems to be an anomaly as the error is much lower elsewhere. To attempt to quantify the error into a single number for each of the co-polarized channels the mean errors in Figure 3-23 were taken and are presented in Table 3-3.

<i>Channel polarization</i>	<i>Mean Error</i>
<i>Vertical</i>	18.6 %
<i>Horizontal</i>	14.7 %

Table 3-3 Mean errors on the co-polarized RCS measurements from a conducting sphere of 55cm diameter.

The mean errors on each channel initially seem high, but as the literature shows, these are respectable errors for RCS measurements made using a VNA based radar [50].

3.4 Summary

This chapter has introduced a radar system capable of making fully polarimetric measurements. All aspect of the radar have been discussed and careful consideration has been given to the selection of some key parameters. These key parameters have been captured and summarized in the table below.

<i>VNA Radar Parameters</i>	<i>Value</i>
<i>Start Frequency</i>	18 GHz
<i>Stop Frequency</i>	26 GHz
<i>Bandwidth</i>	8 GHz
<i>Number of points</i>	401
<i>IFBW</i>	10 kHz
<i>Max Range</i>	5 m
<i>Range Resolution</i>	18.75 mm
<i>Sweep time</i>	53 ms
<i>Power</i>	2 dBm
<i>Polarization</i>	HH, VH, VV & HV
<i>HPBW @ f_c</i>	25°
<i>Beam size @ 2m</i>	0.9 m

Table 3-4 Summary of key selected radar parameters.

Furthermore, a validation study has been conducted in which the radar cross sections of conducting spheres of varying size have been measured and compared to calculated values. The validation study has given an indication as to the measurement uncertainties of the system post calibration.

Chapter 4

Polarimetric Measurements of Weapons and the Body

This chapter introduces the experimental procedures and methodology used in obtaining fully polarimetric measurements that are used in subsequent chapters. A representative group of targets are introduced and their concealment on a person for screening is discussed. Furthermore, measurements are presented that show the signals prior to any polarimetric decompositions, this will assist the reader in appreciating the nature of such signals.

4.1 Introduction

The previous chapter introduced an experimental VNA based radar that was developed for this research. This radar was used to measure the polarimetric scattering of electromagnetic waves caused by the human body with and without various concealed weapons present. These measurements shall be the focus of this Chapter. The main reason for making the measurements presented in this Chapter was to explore the use of polarization in the detection of concealed weapons. The use of polarization has been investigated in the literature, for example [5], [6] and [42], however the extent to which polarization has been utilized in practical systems is limited. These papers describe the development of radar systems that measure the power (direct detection) in the co-polarization and cross-polarization. This information is then used to detect weapons via simple thresholding algorithm or pattern recognition [5]. The research presented in this thesis takes a step further and applies algorithms that translate the changes in polarization into physical descriptors of the target itself. For this to happen the developed radar collects all of the information

in a target's Scattering matrix or matrices for multi-frequency measurements, as is the case in this work. Each matrix contains four S-parameters, all with an amplitude and phase. An advantage resulting from recording the amplitude and phase is that the target can be isolated by the use of range gating; this provides another step to ensure that only the target of interest contributes to the recorded scattering properties.

The radar developed in this work was used to test the feasibility of applying the polarimetric decomposition algorithms to weapons detection, but this has been done with the intention of further developing this radar into a commercial product. The commercialization of this radar will depend upon the devices ability to detect weapons that are a current threat to the safety of the public or present a threat to the security of public infrastructure. These include handguns that can easily be concealed upon the body and Person Borne Improvised Explosive Devices (PBIED).

4.2 Weapons & Concealment

The set of weapons chosen for this research represents the type of weapons that must be detected by the proposed type of security screening radar. The chosen weapons are a handgun, a small revolver type handgun and a Person Borne Improvised Explosive Device (PBIED) containing metallic fragmentation. These weapons are pictured in Figure 4-1 for reference.



Figure 4-1 Image showing weapons used in measurements, starting from the left a handgun, a smaller revolver type handgun and a Person Borne Improvised Explosive Device (PBIED).

All of the measurements that were taken with a concealed weapon, used the same method of concealment. The weapon was in each case positioned on the torso of the individual being scanned and then concealed under the individual's clothing (a t-shirt and sweater). The larger handgun was measured in two different orientations whilst still concealed under the individual's clothing, these two positions were with the barrel vertically aligned with the body and with the barrel at an angle of 45° to the previous vertical alignment. The measurement at two different orientations provides a rotation of the weapon around the line of sight of the radar; this proves useful in analysing the results of the polarimetric decompositions in the next Chapter.

4.3 Experimental Procedures

To conduct the measurements presented in this thesis a radar range was set-up in the laboratory at the Centre for Sensing and Imaging. This range provided a clutter free environment in which to make the required measurements, the range provided a 5m long space and had a wall of radar absorbent material located at the end. The absorbent material helped prevent undesirable reflections from the wall at the back of the lab and any multipath reflections that may arise from subsequent reflections from walls and equipment around the lab. An image of the range is provided in Figure 4-2 for reference.



Figure 4-2 Image showing the measurement set-up, with a calibration target (conducting sphere) in place.

The image shows a large conducting sphere suspended in front of the radar on the range, this sphere was taken as a reference target and measurements of this target are used in the polarimetric decomposition results analysis in the next Chapter. The measurements of a person with and without a concealed weapon were performed using the same equipment and the same range, the person stood in place of the sphere. In each case the person stood facing the radar such that the concealed

weapon would be in the main beam of the radar, the beam occupied a 0.9 m diameter space of the range at 2 m. As the person stood in place for the measurements small movements (of a few cm) were made to present the body or weapon (when present) to the radar in a number of different aspects, this is representative of a realistic screening scenario. The presentation at multiple aspects allows an artificial intelligence based classifier to search for patterns in the measurement data and ensure robust detection of the weapon as the aspect changes slightly. This will be tested in the next Chapter where an Artificial Neural Network (ANN) is trained on data from each of the considered polarimetric decomposition techniques and then used to detect weapons.

Prior to the measurements for each target being taken a measurement of the background (range with no target) was recorded, measurements of the calibration standards that were introduced in the previous chapter were also recorded. The full procedure for measuring a target and the subsequent processing that was applied to the measurements is detailed in the block diagram in Figure 4-3.

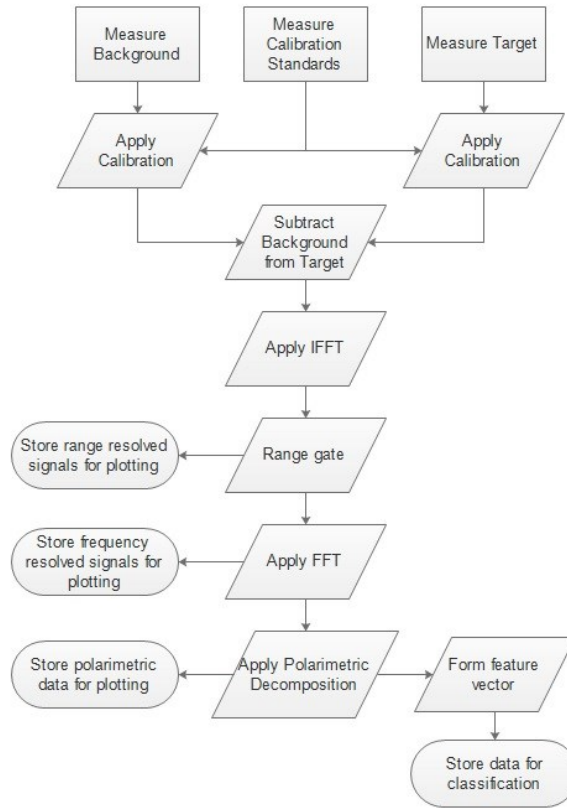


Figure 4-3 Flowchart showing process of taking measurements.

The data that was processed from the measurements was recorded at various stages as shown in Figure 4-3 for a number of purposes. The post-calibration data was transformed into the range domain via an Inverse Fast Fourier Transform (IFFT) and range gated. This ensures that the target was isolated on the range and no background clutter was recorded in the target's polarimetric scattering measurements. The gate that was applied was a simple rectangular window with a width corresponding to 1 m, which was centred at 2 m. The width of this window was determined empirically and the centre point was set by the range at which the target was placed. Range gating also had the effect of band-pass filtering the frequency domain data, which helped eliminate small levels of noise from the instrumentation. The data was recorded at this point whilst in the range domain for plotting and introducing the measurements in this chapter. The data was also stored after being transformed back into the frequency domain via a Fast Fourier Transform (FFT). The

reason for transforming back into the frequency domain is that the Polarimetric Decomposition algorithms, which are investigated in the next Chapter, are applied in the frequency domain and applied discretely at each frequency. The diagram in Figure 4-3 shows the application of the polarimetric decomposition techniques. This will be discussed further in the next Chapter.

4.4 Sample Sizes

The number of scans taken per target was chosen to ensure that the sample size for the classification experiment in the next chapter resulted in a statistically significant result. The method of assessing the classification of the measured data was chosen to be Receiver Operating Characteristic (ROC) curves. The test applied to each polarimetric decomposition was that it would provide data which could be used to classify data into two groups ‘threat’ and ‘non-threat’ with a ‘better than chance’ probability. This was deemed adequate for this research as these methods had never before been applied to weapons detection and their suitability was the primary concern of this research, not necessarily the absolute performance of the methods. To choose a sample set size the following criteria was imposed: Type I (probability of rejecting null hypothesis when in fact it is true) and Type II (probability of accepting the null hypothesis when in fact it is false) error less than 5%. This would result in a minimum statistical power of 95% and a confidence level of 95% or greater, meaning that the results of the experiment had sound statistical significance and that the results would be an accurate indication of reality. The benefit of using ROC curves is that the Area Under the Curve (AUC) can be used to choose sample set sizes for a chosen Type I and Type II error. Calculating the required sample size for a given experiment ensures that the results obtained are useful in making a convincing argument.

To calculate the minimum sample size required, the Colton sample size formula was used to calculate the number of samples in each normal and abnormal set (threat and non-threat). The formula is given by (4.1) and was taken from [51].

$$n = \left[\frac{z_{\alpha} \sqrt{2V_1} + z_{\beta} \sqrt{V_1 + V_2}}{\delta} \right]^2 \quad (4.1)$$

Where z_{α} is the z-score associated with a confidence interval of 95% (Type I error 5%, $z_{\alpha}=1.645$), z_{β} is the z-score associated with a statistical power of 95% (Type II error 5%, $z_{\beta}=1.645$), δ is the difference between the predicted AUC and the AUC corresponding to the random chance line, V_1 and V_2 are parameters calculated using (4.2) with AUC of the random chance line and the predicted AUC respectively.

$$V = \frac{AUC}{2 - AUC} + \frac{2AUC^2}{1 + AUC} - 2AUC^2 \quad (4.2)$$

These formulas were used with a predicted AUC of 0.7 and the result was a sample set size of 86 normal (non-threat) samples and 86 abnormal (threat) samples. As the sample size increases, the statistical significance increases for a given test. Therefore, the results of the sample size calculations should be treated as a minimum criterion and any additional samples will only increase the power of the test. Given the ease of which measurements can be taken with the designed experimental radar it was decided that 200 measurements per target set would be recorded. Of these measurements, half are to be used in the training of the ANN (100 of each target) and half used to test its ability to detect weapons (100 of each target). Since there are three weapons, one of which is measured at two different orientations, and the case of the body without a weapon a total of 1000 radar scans were taken. These measurements will now be presented and discussed.

4.5 Results & Discussion

The first measurements to be presented were taken without a weapon concealed on the body. The plots in Figure 4-4 show the frequency dependent S-parameters for each of the measured polarizations. All measurements presented herein have been calibrated as described previously.

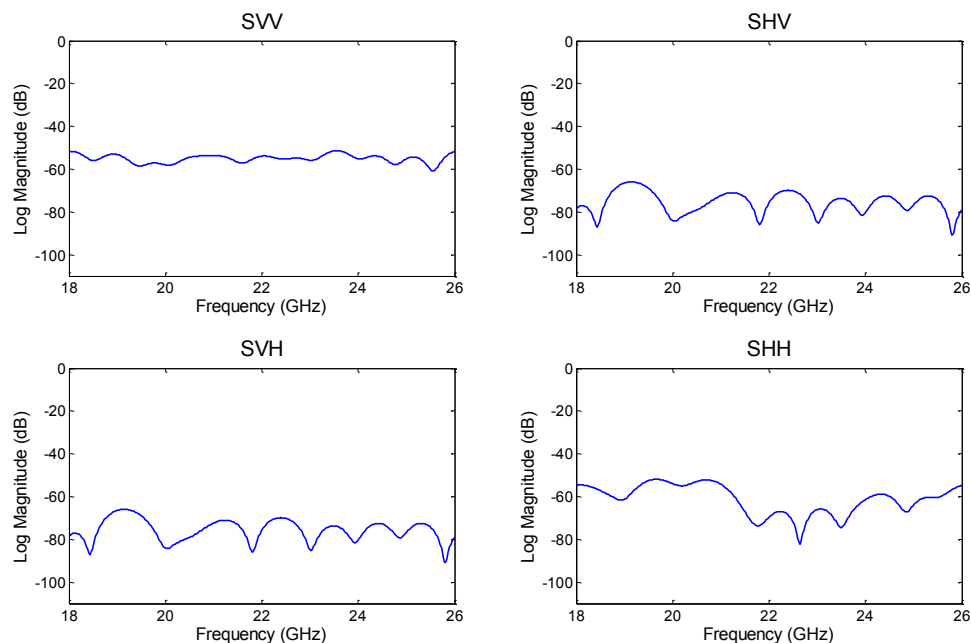


Figure 4-4 An example of a measurement made with no weapon concealed on the body against frequency.

The results presented in the figure are an example of one of the 200 measurements taken for this target. The frequency response of the target is shown in the first instance, as this is the format in which the measurements are subsequently processed using the polarimetric decomposition algorithms. The format that is often easier to relate to is the range resolved signals were the frequency data has been transformed using an Inverse Fast Fourier Transform (IFFT). In this format, the target reflection appears at the range corresponding to the actual range of the target

during the measurement. The plots in Figure 4-5 show the results of 200 measurements in this format.

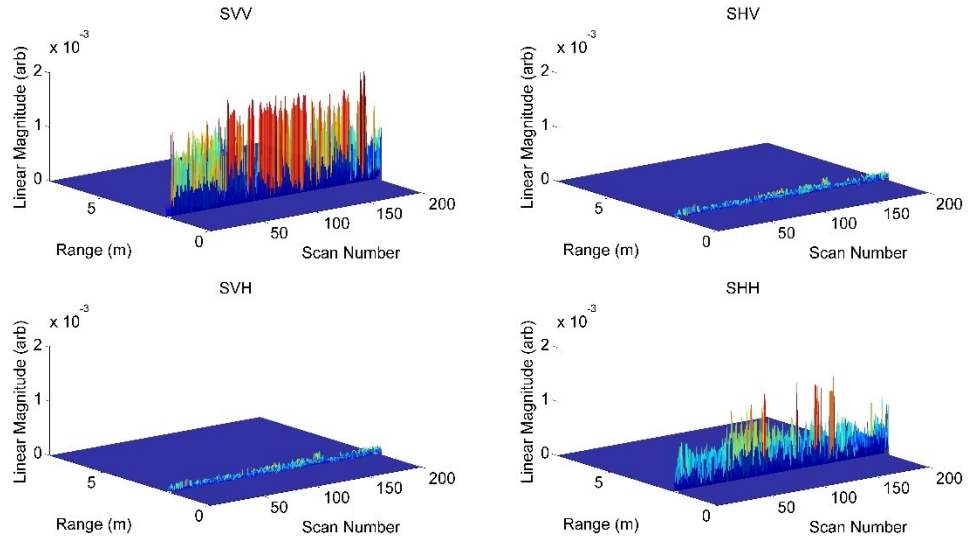


Figure 4-5 A plot showing 200 range resolved measurements of a person with no concealed weapon.

The plots clearly show a reflection from a target at approximately 2 m. The target was measured at a range of 2 m as stated previously so this is a positive indication that a good measurement of the target has been achieved. An observation to take from the plots is that the cross-polar reflection from the target (body no weapon) are extremely weak. This observation indicates that the body produces low amounts of cross-polarization and is in agreement with the literature [5]. Another observation to take from these plots is that there exists significant variance in the amplitude of the reflection in consecutive measurements; this is due to the movements made by the person being scanned. This is because the RCS of the target varies as the target is presented at varying aspects. The experimental procedure outlined previously stated that the person would make small movements as to present the weapon at multiple varying aspects. This is crucial as the radar cross

section of the targets measured varies significantly with aspect and a range of viewing aspect must be taken for an artificial intelligence based classifier to classify the measurements accurately.

The next set of plots presented in Figure 4-6 show an example of a measurement taken of a person carrying a concealed gun with the barrel vertically aligned to the torso.

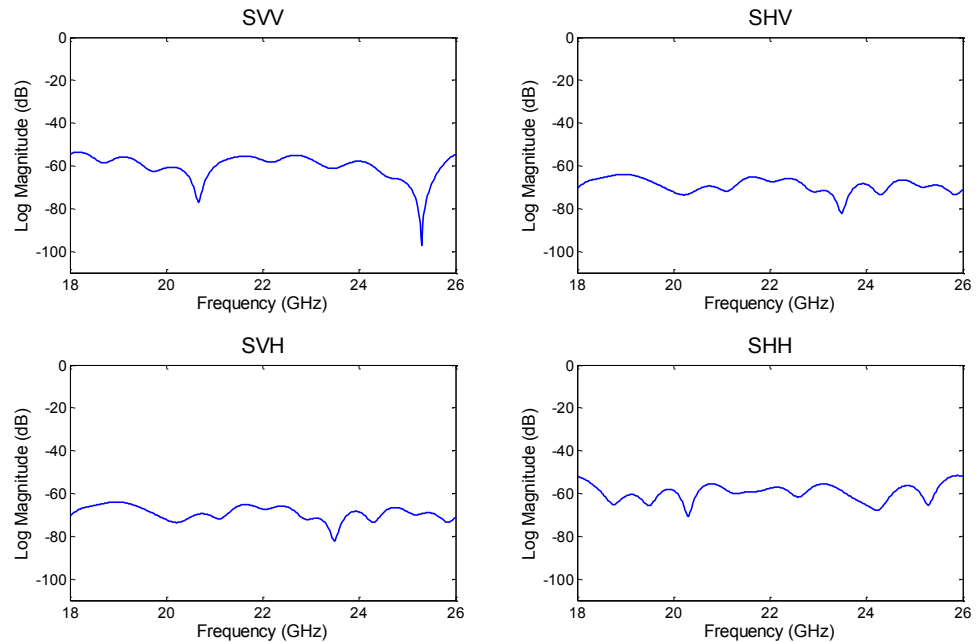


Figure 4-6 An example of a measurement of a person carrying a concealed gun with the barrel vertically aligned to the torso.

The results are presented in the frequency domain and each plot corresponds to a different polarization. In this set of plots, the magnitude of the cross-polar is subtly larger than was the case with the measurement of a person with no concealed weapon (~ 70 dB compared to ~ 80 dB without weapon), this was consistent with all weapons tested. This indicates that the weapon induces the cross-polar reflection and gives strength to the argument for using the level of cross-polar reflection as a primitive method of detecting weapons using radar as is the case with current state of the art weapon detection radars [52].

Presented in Figure 4-7 are plots showing 200 consecutive measurements of a person carrying a gun concealed on the torso and in a position with the barrel vertical. Each plot represents a different element of the target's Sinclair scattering matrix, which was introduced in the previous chapter.

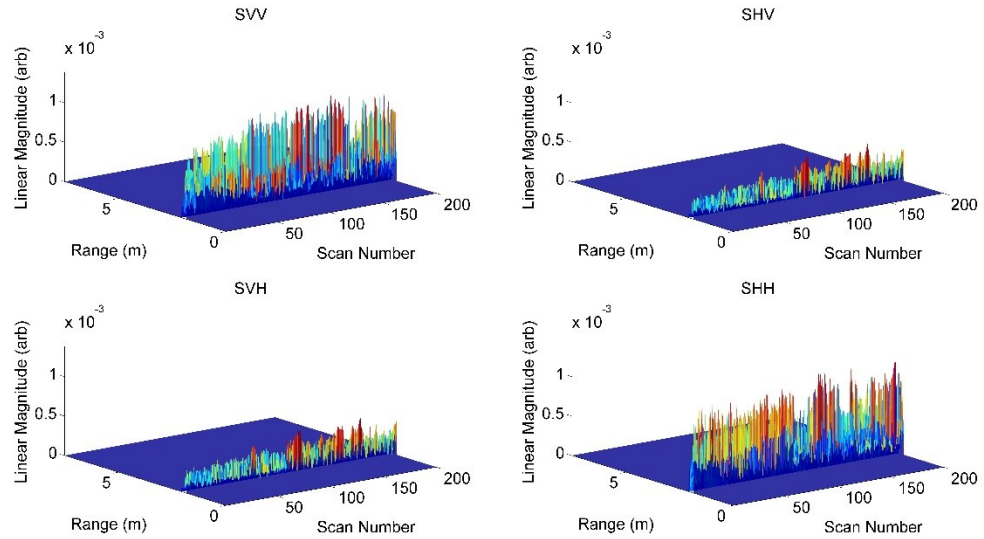


Figure 4-7 A plot showing 200 range resolved measurements of a person with a vertically aligned gun concealed on the torso.

As was the case with the previous target it is clear that a reflection from the target at a range of approximately 2 m after the frequency recorded data has been transformed using the IFFT. The cross-polar reflections are noticeably larger compared to the body alone when viewed along range (post IFFT). As the results show there are no reflections before the target or down range indicating that the target is isolated, this is desirable as only the desired target will be contributing to the scattering and therefore the polarimetric decomposition will give a true indication of the target's scattering properties without undesirable effects creeping in from background clutter.

The next set of plots corresponds to measurements of a person carrying a concealed handgun with a 45° orientation. An example of these results is presented in the frequency domain in Figure 4-8.

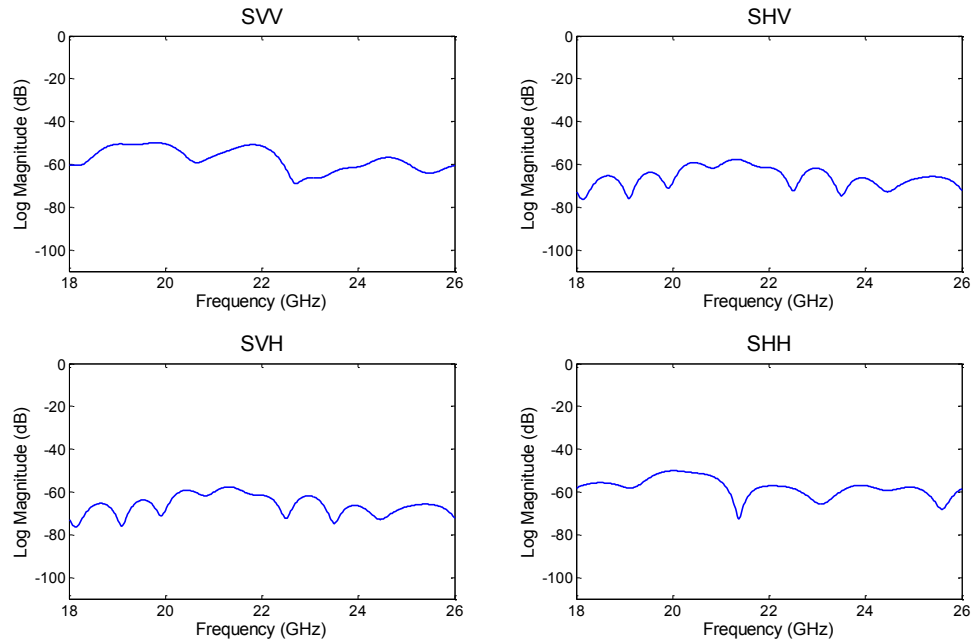


Figure 4-8 An example of a measurement of a person carrying a concealed gun with the barrel aligned at 45° to the torso.

Again, with these results there is an increase in the amount of cross-polarized reflection of ~10dB in the presence of the concealed handgun. The cross-polar reflections caused by the weapon are smaller than the main co-polarized reflection from the body, as was the case with the handgun in both orientations.

The full set of measurements from the 45° orientated handgun are now presented post IFFT in Figure 4-9. Again, the results are presented in the range domain as it is easier to assess the quality of the measurements and interpret any features that may be observed.

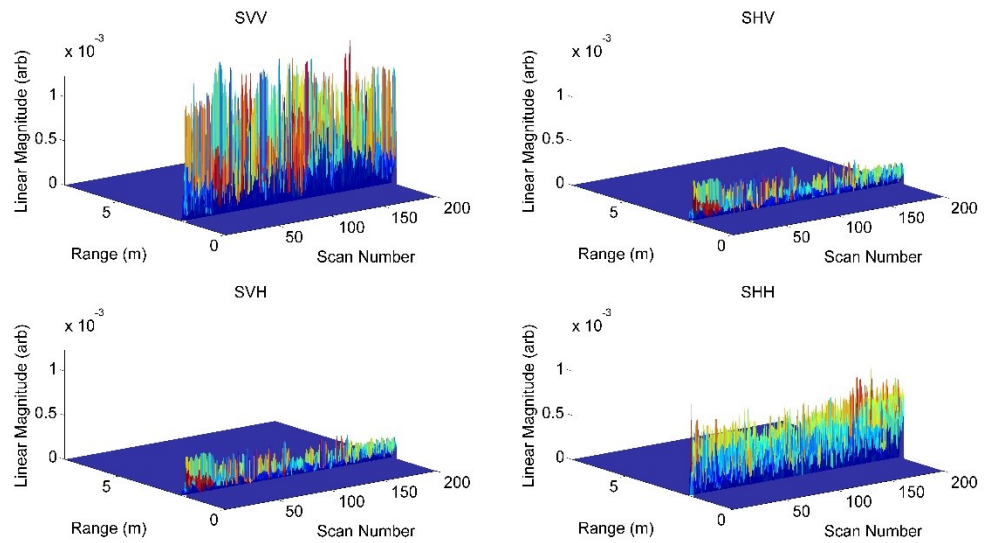


Figure 4-9 A plot showing 200 range resolved measurements of a person with a concealed gun with the barrel aligned at 45° to the torso.

The results in Figure 4-9 show that once again, the target reflection is observed in isolation and there are no undesirable reflections from background clutter. There remains a visible difference in the cross-polar reflection with the weapon present; this is more prominent in the results when presented in the range domain. The larger cross-polar reflection can be observed in the top right and bottom left plots in Figure 4-9.

An example of measurements of the PBIED concealed upon the body is presented in Figure 4-10, in this figure each plot represents an element of the target's scattering matrix. The results in this plot are presented in the frequency domain.

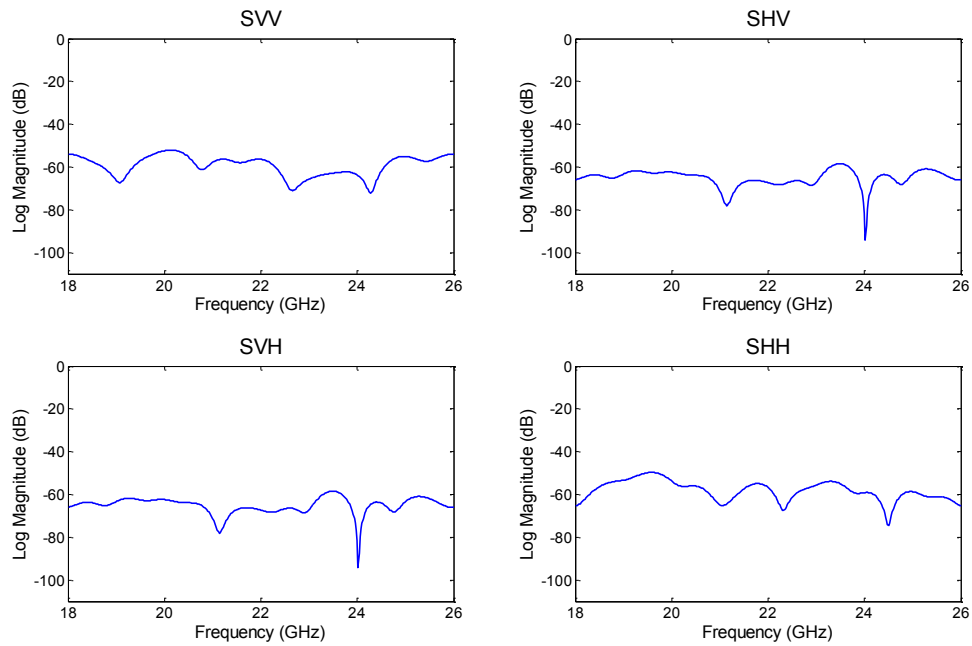


Figure 4-10 An example of a measurement of a person carrying a concealed Person Borne Improved Explosive Device (PBIED).

The results from the PBIED measurements show a large cross-polar reflection of ~ 65 dB, this is similar to that observed from the handgun measurements. The cross-polar reflections are again observed in the top right and bottom left plots of the figure. This is expected as the PBIED is filled with randomly orientated pieces of metal that alter the polarization of the incident waves.

The presentation of the PBIED measurements in the range domain is given in Figure 4-11.

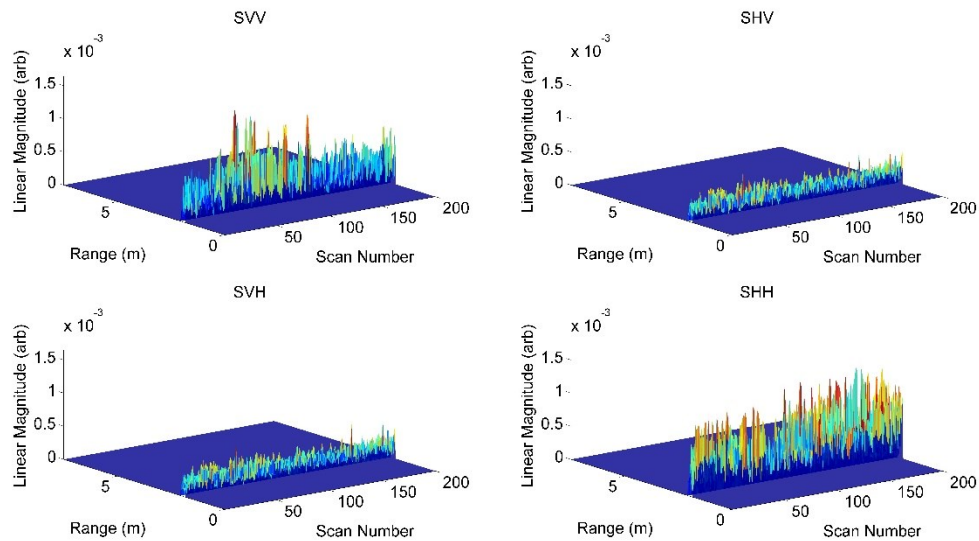


Figure 4-11 A plot showing 200 range resolved measurements of a person with a concealed Person Borne Improvised Explosive Device (PBIED).

All 200 scans of the PBIED show a strong cross-polarized reflection that is more substantial in terms of the ratio of amplitude of the co-polarized to cross-polarized signals when compared to the two data sets corresponding to the handgun. This is because the incident waves are interacting with a physically larger target that has polarization altering properties. The PBIED produces a cross polar reflection of ~ 60 dB as compared to ~ 70 dB produced by the gun.

The final set of measurements to be presented in this chapter were taken with a person concealing a small revolver type handgun. The first set of plots from the measurements of this target are in Figure 4-12.

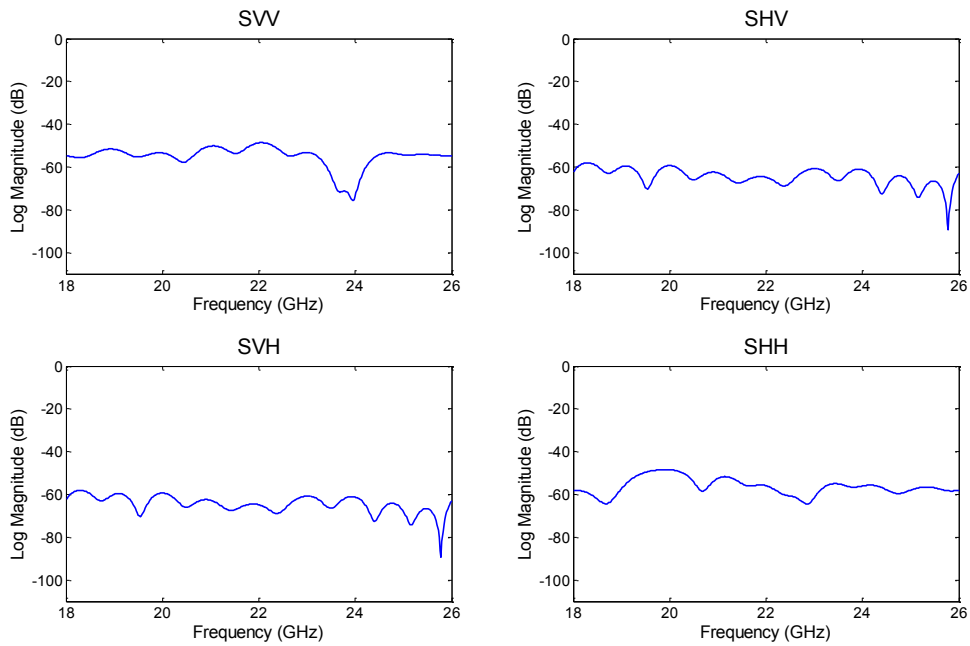


Figure 4-12 An example of a measurement of a person carrying a concealed small revolver type handgun.

The figure shows the frequency domain S-parameters that make up the scattering matrices. In these plots, the cross-polar reflection is observed to be significantly larger than the body alone with the difference as large as 20 dB at certain frequencies. The reason for the large cross-polar reflection is mostly owing to the complexity of the shape of the small revolver. The revolver has many facets with edges having many orientations, see Figure 4-1. These facets and almost random orientation of edges alters the incident wave's polarization through the process of diffraction.

All 200 scans of a person concealing a revolver are displayed in Figure 4-13 after being transformed into the range domain using the IFFT.

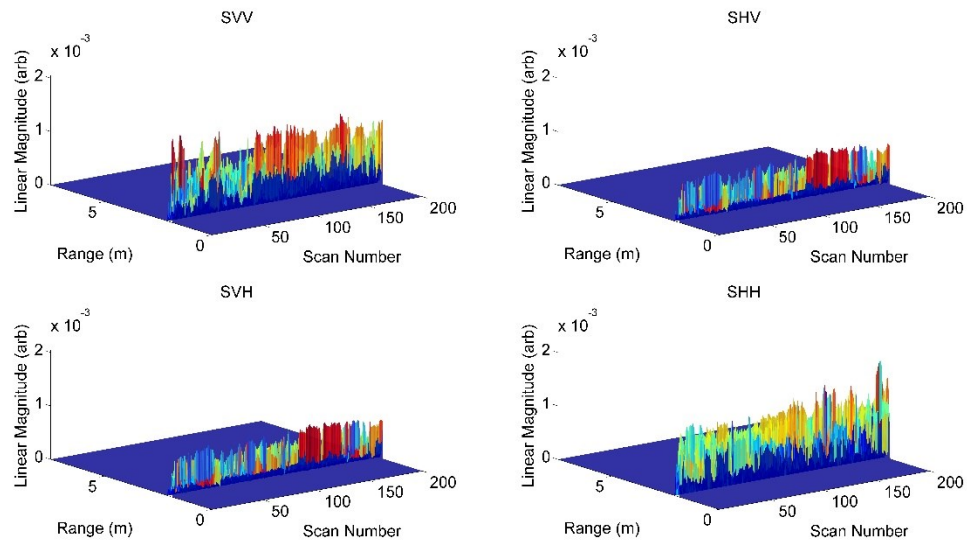


Figure 4-13 A plot showing 200 range resolved measurements of a person with a concealed small revolver type handgun.

The magnitude of the cross-polarized reflection from the revolver is clearly larger than any of the previous targets, see Table 4-1. This is consistent across all of the scans taken for this target, which due to the movements of the person being scanned have presented this weapon at a number of aspects. The measurements presented in Figure 4-13 have also displayed a clear reflection at the range of 2 m, where that target was stood, and lack any background clutter.

A table collating the magnitude of the average co and cross-polar reflections from each target is presented for reference in Table 4-1.

<i>Target</i>	<i>Co polar (dB)</i>	<i>Cross polar (dB)</i>
<i>Body no weapon</i>	-50	-80
<i>Body with gun (vertical)</i>	-55	-70
<i>Body with gun (45°)</i>	-55	-65
<i>Body with PBIED</i>	-60	-60
<i>Body with revolver</i>	-55	-60

Table 4-1: Table of average values of the co and cross-polar reflections from the targets that were measured in this thesis.

4.6 Summary

In this Chapter, the set of weapons used in this research have been presented and the procedures for concealing these weapons upon a person for measurement has been discussed. The experimental procedures used to take the measurements have also been introduced and discussed. The set-up of a dedicated measurement range in the Centre for Sensing and Imaging laboratory has been described. Furthermore, measurement taken using the developed radar and experimental procedures have been presented and discussed, with key observations taken from these results.

The next chapter introduces a number of polarimetric decomposition techniques taken from the field of Earth Observation. These techniques are then applied to the measurements presented in this chapter and finally the use of these techniques to detect weapons is assessed.

Chapter 5

Polarimetric Decomposition Techniques Applied to CWD

This chapter presents results from polarimetric decompositions applied to measurements from the previous chapter. The use of three polarimetric decompositions in automated classification algorithms are investigated. It is shown that each of the techniques explored provides good classification performance. The major contribution to knowledge from this thesis is presented in this chapter, as an experiment that shows that polarimetric decompositions are a useful tool in the detection of concealed weapons using fully polarimetric radar.

5.1 Introduction

The application of polarimetric decomposition techniques to concealed weapon detection using fully polarimetric radar, to the author's knowledge, has never before been attempted. This thesis provides the first survey of polarimetric scattering phenomenology resulting from the interaction of electromagnetic waves and weapons concealed on a person. This survey is a key contribution to knowledge and detailed discussions of the findings of the survey are provided throughout this Chapter. The findings will aid the design of the next generation of radars for the detection of concealed weapons, by providing key information about how weapons, when concealed on a body alter an electromagnetic wave's polarization. The work presented in this chapter then takes a further step and the detection of concealed weapons using polarimetric decomposition techniques, alongside signal processing and artificial intelligence in the form of neural networks is presented. This is the first ever demonstration of these algorithms being used to detect concealed weapons and is a major contribution to knowledge, that provides a new method

for detecting concealed weapons with a reduction in the aspect dependency that is currently experienced by state-of-the-art radar weapon detectors.

The Pauli, SDH and H- α polarimetric decompositions that have been investigated in this thesis have been around since the 1990s and have been used extensively by the Earth Observation community. These algorithms have been used to classify land use from radar images, they have also been used to monitor crop conditions, de-forestation and snow coverage, a recent review of uses for these algorithms is provided in [53].

As standoff weapon detection using radar is an emerging technology the uses of polarization has been limited, as discussed in the literature review, in Chapter 2. The application of radar to weapon detection and separately the development of the polarimetric decompositions are both relatively new and this is probably a contributing factor as to why this work has not previously been undertaken. The application of polarimetric decompositions can only be achieved when a target's scattering matrix is measured in its entirety including phase information. This leads to increased cost and complexity of the required measurement system and this has definitely contributed to the delay in this work being conducted. The increased cost and complexity is down to the requirement of a fully polarimetric heterodyne/ homodyne radar operating at bandwidths > 8 GHz (required for range resolution capable of resolving a weapon on the body), these are more expensive and more technically challenging than the direct detection systems reported in the literature. In fact, the development of the polarimetric decomposition techniques was only realized when complex and costly radar imaging instrumentation was designed for space and airborne missions, all of which required extensive funding and resources.

5.2 Polarimetric Decompositions

Polarimetric decomposition techniques are used to extract target information from radar data. The advantage of using polarimetric decompositions over analysing temporally resolved radar signals or ratios of co-polarized to cross-polarized returns, as is the case with current state of the art systems, is that polarimetric decompositions yield parameters which have physical interpretations. These physical interpretations present an opportunity to classify radar returns into groups of objects. The physical interpretations that can be taken from the polarimetric decompositions are essentially descriptions of the type of scattering that is caused by the target. These interpretations are often placed into three groups with the following terminology used to describe these groups: single/odd bounce, double/even bounce and diffuse/volume scattering. To put these interpretations into context of the research presented in this thesis the following diagrams are used, see Figure 5-1.

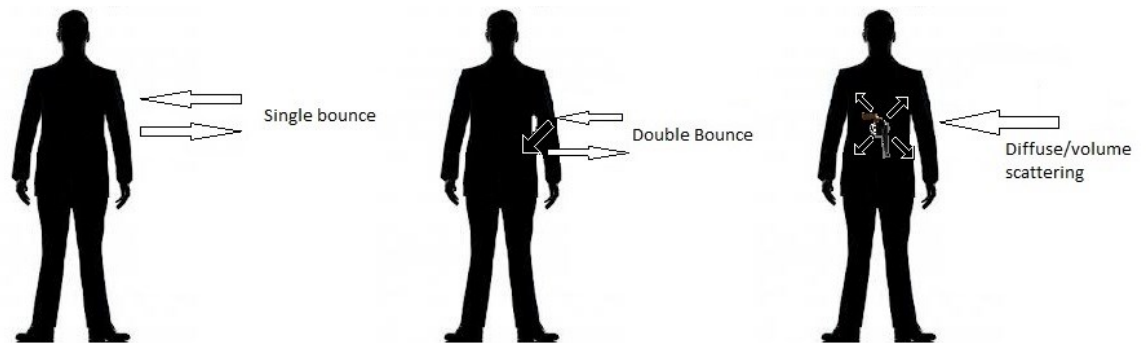


Figure 5-1 Diagram showing different scattering mechanisms that occur from a person with and without a concealed weapon.

Figure 5-1 shows the three types of scattering described by the polarimetric decomposition techniques and as can be seen the presence of the weapon is anticipated to cause diffuse/volume scattering.

Additionally some of the decomposition techniques offer roll-invariant parameters, in this thesis SDH and H- α decompositions are investigated, both of which offer roll-invariant parameters. The significance of roll-invariant parameters is that they offer the ability to reduce the aspect dependence of radar based weapon detectors. The orientation of a weapon can significantly alter the ability to detect the weapon when using radar that analyses temporally resolved signals or ratios of co-polar to cross-polar backscatter.

In the field of Earth Observation, a number of polarimetric decomposition techniques have been developed to aid in the interpretation of Polarimetric Synthetic Aperture Radar (PolSAR) images [53], [54], [55], [56] and [57]. These decompositions can be separated into two main groups, which are Coherent techniques and Incoherent techniques, both of these groups will be introduced in this Chapter.

5.3 Coherent Techniques

The techniques in this group of decompositions are used to express a measured scattering matrix as a weighted summation of scattering matrices which represent canonical radar targets, for example a sphere or a di-plane. Each of the coherent techniques has a different base set of canonical targets. In creating a weighted summation, comparison between the measured target and each of the canonical objects can be made. For this reason, it is important that the canonical targets express independent behaviour where possible. This will prevent a measured scattering matrix of a canonical target from having more than one non-zero weighted term in the decomposition. To ensure that this condition is satisfied each of the canonical targets defined in the base group is usually selected to be mutually orthogonal to each of the others.

$$\left[S^{measured} \right] = \sum_{n=1}^N a_n \left[S_n^{canonical} \right] \quad (5.1)$$

The above equation arbitrarily represents a coherent decomposition of a measured scattering matrix into an undefined group of scattering matrices each with an associated weight a_n .

5.3.1 Pauli Decomposition

The Pauli decomposition uses scattering matrices obtained in an orthogonal linear polarization basis that is the responses to illumination in vertical and horizontal linear polarizations sequentially are used to form the targets scattering matrix. The base group of canonical targets are defined as the set of scattering matrices presented below.

$$\begin{bmatrix} S^{measured} \end{bmatrix} = \begin{bmatrix} S_{VV} & S_{HV} \\ S_{HV} & S_{HH} \end{bmatrix} = \alpha[S_1] + \beta[S_2] + \gamma[S_3] \quad (5.2)$$

$$[S_1] = \frac{1}{\sqrt{2}} \begin{bmatrix} 1 & 0 \\ 0 & 1 \end{bmatrix}, [S_2] = \frac{1}{\sqrt{2}} \begin{bmatrix} 1 & 0 \\ 0 & -1 \end{bmatrix}, [S_3] = \frac{1}{\sqrt{2}} \begin{bmatrix} 0 & 1 \\ 1 & 0 \end{bmatrix} \quad (5.3)$$

The base group is shown in equation (5.3) to contain a single bounce target S1, a double bounce target S2 and a target which only reflects cross polarized waves S3. The weights α , β and γ associated with each of these targets are given by the three equations below.

$$\alpha = \frac{S_{VV} + S_{HH}}{\sqrt{2}} \quad (5.4)$$

$$\beta = \frac{S_{VV} - S_{HH}}{\sqrt{2}} \quad (5.5)$$

$$\gamma = \sqrt{2}S_{HV} \quad (5.6)$$

To investigate the application of the Pauli decomposition to CWD a number of targets were measured under semi anechoic conditions and their scattering matrices were recorded. The measured scattering matrices were then decomposed using the Pauli decomposition and the weight parameters were plotted.

The plot in Figure 5-2 shows the weights for a control target, which was a large conducting sphere. The weights have been normalized and the figure clearly shows that the control target yields a value of one for the alpha parameter across the measured frequency spectrum; the other weights are near zero.

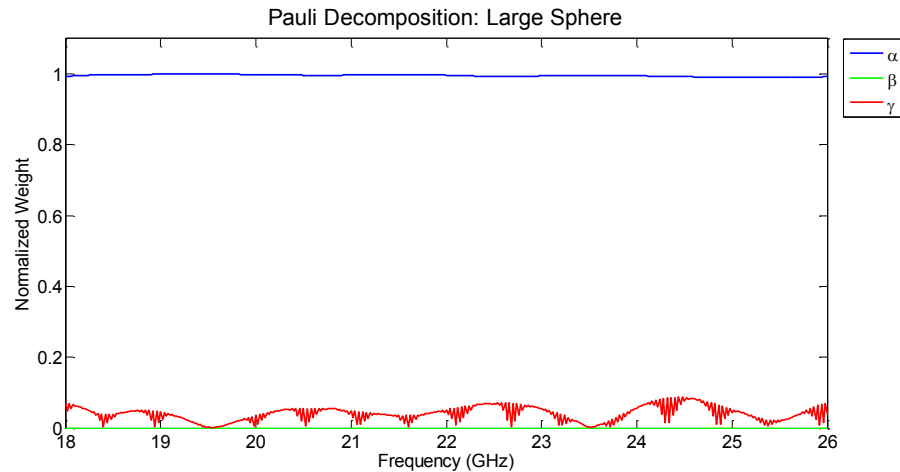


Figure 5-2 Plot showing weights associated with the Pauli decomposition of a large conducting sphere.

The results in Figure 5-2 are no surprise considering that the control target is a conducting sphere, whose radius ensures that the target scatters independently of frequency in the proportion of the spectrum measured in this work. The gamma component does display a non-zero value with frequency dependency; this must be owing to residual errors in the measurement of the target scattering matrix as no cross polar component is anticipated from a surface conducting sphere.

The other targets measured include a person without a concealed weapon, a person carrying a concealed gun in two different orientations (vertical and 45°), a person carrying an improvised explosive device and a person carrying a small revolver pistol. In all instances where the person has been carrying a weapon, the weapon has been concealed under clothing on the front of the torso.

The plot in Figure 5-3 shows the Pauli decomposition weights corresponding to a person not carrying a concealed weapon.

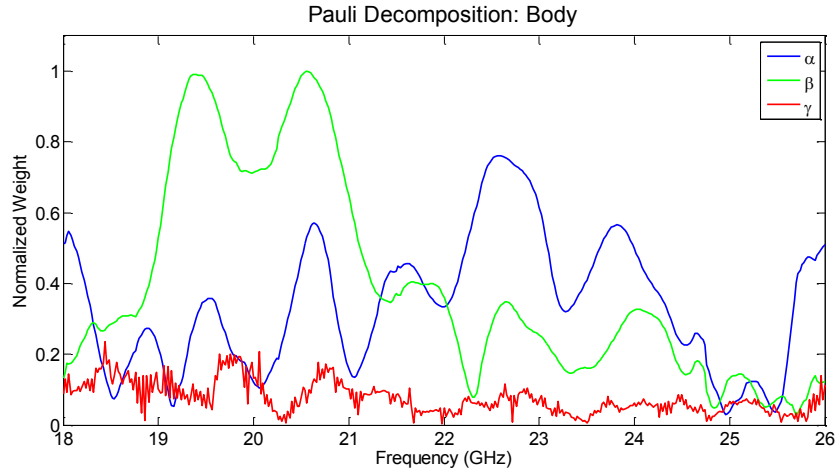


Figure 5-3 Plot showing weights associated with the Pauli decomposition of a person without a concealed weapon.

Again, the weights have been normalized; here it can be observed that two of the parameters have large values with strong frequency dependency. This suggests that the body has features or structures that have scattering mechanisms with strong wavelength dependency, as the body is causing frequency dependency in these parameters. This is not an unreasonable or suspicious observation, as the complex shape of the human body would be expected to have structures both large and small; these structures would give rise to multiple scattering phenomena, which would be wavelength dependent. For example, structures around the hand, like fingers, would be likely candidates to cause cross polarization through edge diffraction at most wavelengths in the spectrum considered. In addition, the torso would be expected to cause a large single bounce reflection at lower frequencies. This would become more complex as the wavelength decreases because the dimensions in the curvature of the body would become comparable to the wavelength itself, causing more complex scattering of the incident waves. Yet another scattering phenomenon can be expected as the arms and torso create cavities that cause double bounce scattering. Figure 5-3 does show the

cross-polar scattering, represented by the gamma parameter, to be contributing less to the scattering process than the single and double bounce mechanisms. An explanation to justify the last statement would be that the structures that cause single and double bounce scattering would occupy a larger area of the incident beam of radiation than the structures causing cross polarization, hence the contribution is partly determined by the proportion of the structure that is in the beam.

The next target that was measured was the gun concealed on the body with a 45° alignment; the weights from the Pauli decomposition are plotted in Figure 5-4.

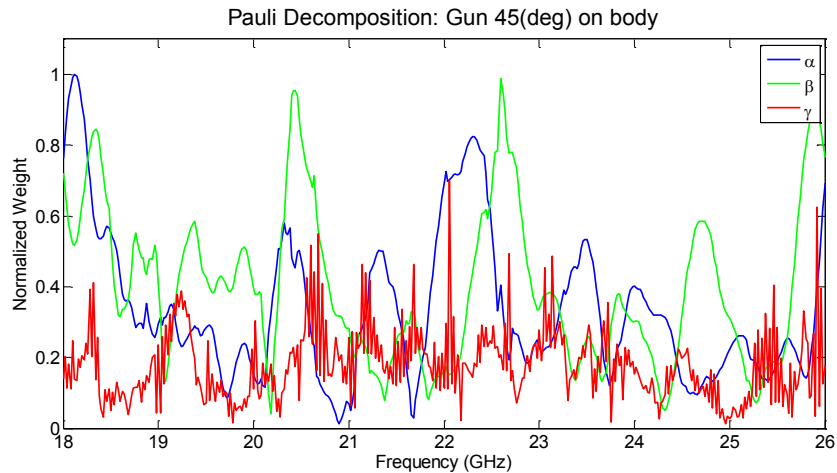


Figure 5-4 Plot showing weights associated with the Pauli decomposition of a person carrying a concealed gun on the torso at an alignment of 45°.

The plot in Figure 5-4 shows that the presence of the concealed weapon has caused a significant increase in the amplitude of the gamma parameter, representing larger cross polarization scattering contribution. This result is reassuring as it has previously been reported in the literature [52] that a cross-polar reflection can be used as an indicator to the presence of a weapon. Again, this plot shows that both single and double bounce scattering is produced by this target, and that both scattering types have strong frequency dependency. The presence of single and double bounce scattering can be accounted for because this behaviour was previously observed in Figure 5-3 from

the body, here both the body and the weapon are in the incident beam and will therefore both contribute to the scattering process.

A measurement of the gun concealed in a second orientation (vertically aligned) is decomposed and the values of the Pauli decomposition parameters are plotted in Figure 5-5.

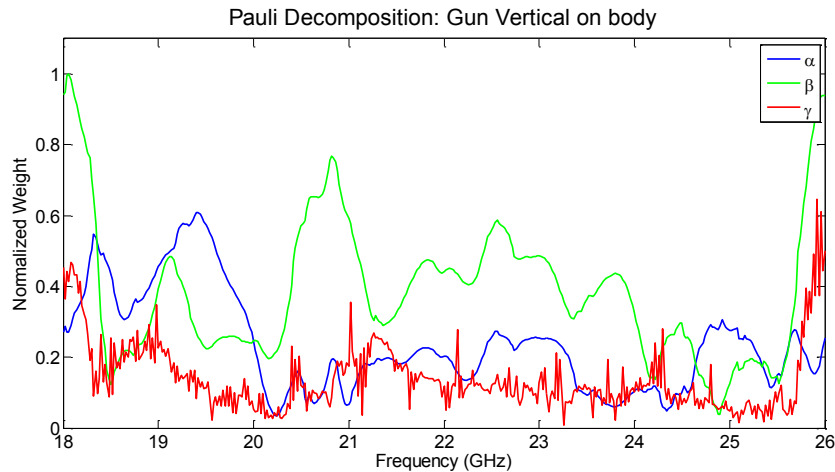


Figure 5-5 Plot showing weights associated with the Pauli decomposition of a person carrying a vertically aligned gun concealed on the torso.

The reorientation of the gun still gives a rise in amplitude for the gamma component compared to the body alone; however, there are differences in the amplitude of the parameter as the gun has changed orientation. The amplitude when vertically aligned is lower than when the gun is at a 45° alignment. At this point, it is worth noting that the Pauli decomposition does not provide any roll invariant parameters and with this in mind, the lower amplitude in the vertical alignment becomes explainable by considering the barrel of the gun. The barrel of the gun will give a maximum cross polarization when at an angle of 45° to the illuminating linearly polarized wave. Once again, large frequency dependent single and double bounce scattering is observed from the body structures.

A measurement of a person carrying a concealed improvised explosive device was decomposed and the resultant weights can be seen in the plot presented in Figure 5-6.

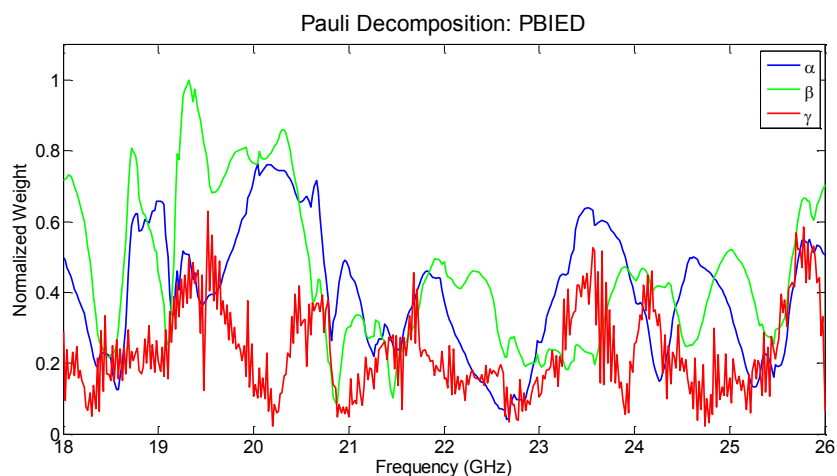


Figure 5-6 Plot showing weights associated with the Pauli decomposition of a person carrying a concealed Person Borne Improvised Explosive Device (PBIED).

This time the gamma component is observed to be much greater, with respect to the alpha and beta parameters, than the previous targets where a person was carrying no weapon and a gun in two different orientations. This significant increase is caused primarily by the structure of the IED, this target is constructed of a wax explosive simulant and a considerable amount of fragmentation, which is made of nuts, bolts and nails all randomly orientated in the wax matrix. The presence of the randomly orientated fragmentation greatly increases the cross polarized reflections through edge diffraction. Another reason for the increase in the amplitude of the gamma component compared to when the person has previously carried a weapon is the physical size of the IED, which is much larger than the gun that was used. This again shows that the weights are related to the proportion of the scattering structure that is presented in the illuminating beam. The single and double bounce scattering caused by the body is also observed in Figure 5-6.

The final target that was decomposed using the Pauli decomposition was the person carrying a small revolver pistol concealed under clothing and on the front of the torso. The results from this decomposition are presented in Figure 5-7.

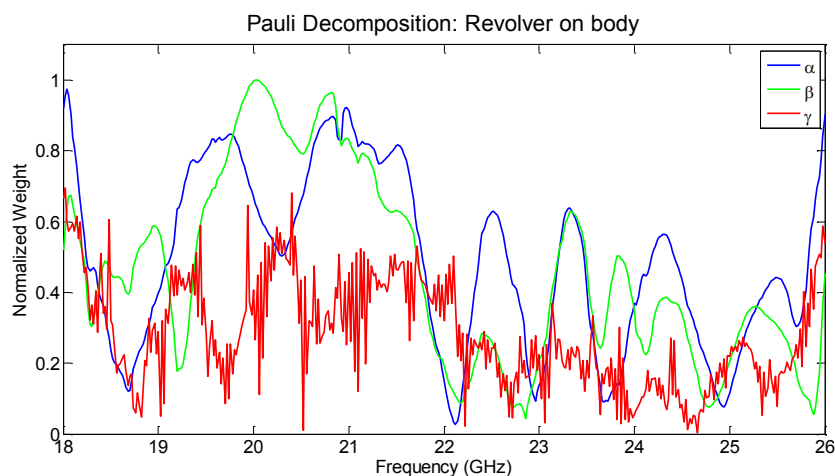


Figure 5-7 Plot showing weights associated with the Pauli decomposition of a person carrying a small revolver pistol concealed on the torso.

The results in Figure 5-7 are much alike the other results in that a single and double bounce scattering behaviour is observed and attributed to the larger structures on the body. The interesting observation from these results comes from the gamma parameter; this target is creating similar levels of cross polarization to the PBIED. The larger cross-polar signal from this gun is likely caused by the number of facets or sharp edges; this gun is smaller but more complex in shape than the larger gun seen previously.

The analysis of the results obtained via the Pauli decomposition has shown that the gamma parameter that represents a likeness to a target that reflects cross polarization is larger in amplitude when a weapon is concealed on the body. The gamma parameter has been shown to vary for the same target at two different orientations (gun at vertical and 45°) the vertical position has been observed to give a lower value of gamma. This is expected as the decomposition is performed on a scattering matrix in the linear polarization basis and therefore does not offer any roll-invariant parameters. The other two parameters, alpha and beta, are observed to have strong frequency dependency and are observed to be similar in nature for each of the targets measured where a person

is present. The Pauli decomposition presents three parameters which could be used to classify signals into groups of ‘threat’ and ‘non-threat’ and this hypothesis will be tested later in the thesis.

5.3.2 SDH Decomposition

The Krogager decomposition, also referred to as the Sphere Diplane Helix (SDH) decomposition, is another coherent decomposition technique with its own distinct base group of canonical targets. This decomposition along with the Pauli and H- α decompositions has been used extensively in the field of Earth Observation, although the coherent techniques are falling out of favour for the H- α decomposition, this technique remains a valid option. As the SDH name suggests the base group is composed of scattering matrices that describe the behaviour of a Sphere (single bounce), a Diplane (double bounce) and a Helix. This can be formulized as follows:

$$\begin{bmatrix} S^{measured} \end{bmatrix} = \begin{bmatrix} S_{VV} & S_{HV} \\ S_{HV} & S_{HH} \end{bmatrix} = e^{j\varphi} \left\{ e^{j\varphi_s} K_s [S_{Sphere}] + K_d [S_{Diplane}] + K_h [S_{Helix}] \right\} \quad (5.7)$$

$$\begin{bmatrix} S^{measured} \end{bmatrix} = e^{j\varphi} \left\{ e^{j\varphi_s} K_s \begin{bmatrix} 1 & 0 \\ 0 & 1 \end{bmatrix} + K_d \begin{bmatrix} \cos 2\theta & \sin 2\theta \\ \sin 2\theta & -\cos 2\theta \end{bmatrix} + e^{mj2\theta} K_h \begin{bmatrix} 1 & \pm j \\ \pm j & 1 \end{bmatrix} \right\} \quad (5.8)$$

To calculate the values φ_s , φ , θ , K_s , K_d and K_h a transformation of polarization basis on the measured scattering matrix is performed and the following relationships between the transformed matrix elements and the decomposition parameters exist [57].

$$K_s = |S_{rl}| \quad (5.9)$$

$$\begin{bmatrix} K_d \\ K_h \end{bmatrix} = \begin{bmatrix} |S_{ll}| \\ |S_{rr}| - |S_{ll}| \end{bmatrix} \left\{ \begin{array}{l} \\ |S_{rr}| > |S_{ll}| \end{array} \right. \quad (5.10)$$

$$\begin{bmatrix} K_d \\ K_h \end{bmatrix} = \begin{bmatrix} |S_{rr}| \\ |S_{ll}| - |S_{rr}| \end{bmatrix} \Bigg|_{|S_{ll}| > |S_{rr}|} \quad (5.11)$$

$$\varphi = \frac{1}{2}(\varphi_{rr} + \varphi_{ll} - \pi) \quad (5.12)$$

$$\theta = \frac{1}{4}(\varphi_{rr} - \varphi_{ll} + \pi) \quad (5.13)$$

$$\varphi_s = \varphi_{rl} - \frac{1}{2}(\varphi_{rr} + \varphi_{ll}) \quad (5.14)$$

The above equations were taken from [58]. One potential issue with this method is that not all the canonical targets are mutually orthogonal, the Dipole and the Helix are the two targets, which are not. This could lead to a canonical target giving non-zero values for both K_d and K_h , however the targets in this work are complex and will present non-zero values on all parameters, therefore this should not be a problem in the work presented here. One advantage of this decomposition is that the three parameters K_s , K_d and K_h are roll-invariant, however they remain aspect dependent. This does add a degree of robustness by reducing the aspect dependency through the roll-invariant nature of these parameters. The roll invariance of these parameters is a direct result of the transformation of polarization basis, i.e. the switch from linear to circular. A circular polarized wave will ensure a reflection from an elongated target, such as a dipole, irrespective of its orientation in the plane perpendicular to the direction of propagation of the wave; the same cannot be said of a linearly polarized wave where a strong orientation dependent reflection would be observed. A method of reducing the aspect dependency on parameters used to detect weapons is needed if radar based weapons detectors are to be successfully commercialized and this is the main justification for presenting this decomposition in this thesis.

The transformation of polarization basis from VH (linear) to rl (circular) can be performed using the following equations to compute the new matrix in rl .

$$S_{rr} = jS_{HV} + \frac{1}{2}(S_{VV} - S_{HH}) \quad (5.15)$$

$$S_{ll} = jS_{HV} - \frac{1}{2}(S_{VV} - S_{HH}) \quad (5.16)$$

$$S_{rl} = \frac{j}{2}(S_{VV} + S_{HH}) \quad (5.17)$$

Once the transformation of basis is complete, the elements of the new matrix are used to compute the SDH parameters using the above equations. In the study only the roll-invariant parameters have been computed and presented, the other parameters may be useful for extracting information about the targets orientation as they are not roll-invariant, but this is beyond the scope of the research in this thesis. To clarify the use of the phrase roll-invariant is a substitute for rotation invariant around the radar line of sight. The phrase comes from the Earth Observation community who mounted Polarimetric Synthetic Aperture Radar (PolSAR) systems on satellites and the satellites rotate on the axis representing the radar line of sight, thus making the radar roll invariant using polarimetric decompositions was deemed desirable.

The first target to be decomposed using the SDH technique was the control target. The control target was a conducting sphere with a radius that ensured that the sphere would reflect independent of frequency over the spectrum used in this work. The anticipated result would be that K_s would have a value of one over the full frequency sweep and that the other parameters would be zero. The results from this decomposition are plotted in Figure 5-8.

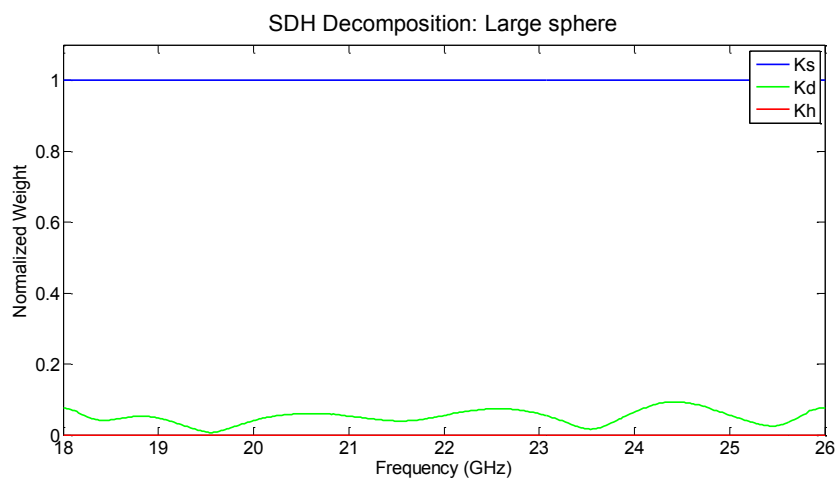


Figure 5-8 Plot showing weights associated with the SDH decomposition of a large conducting sphere.

The plot shows that the anticipated values of K_s and K_h were observed in practice; however, the value of K_d was not as anticipated. This value is non-zero and displayed a frequency dependency, which may be attributed to scatter caused by surface imperfections on the sphere, the same measurements were used in this decomposition as was used in the Pauli decomposition where scatter were also observed.

The plot in Figure 5-9 shows the results of the SDH decomposition of the measured scattering matrices corresponding to a person without a concealed weapon.

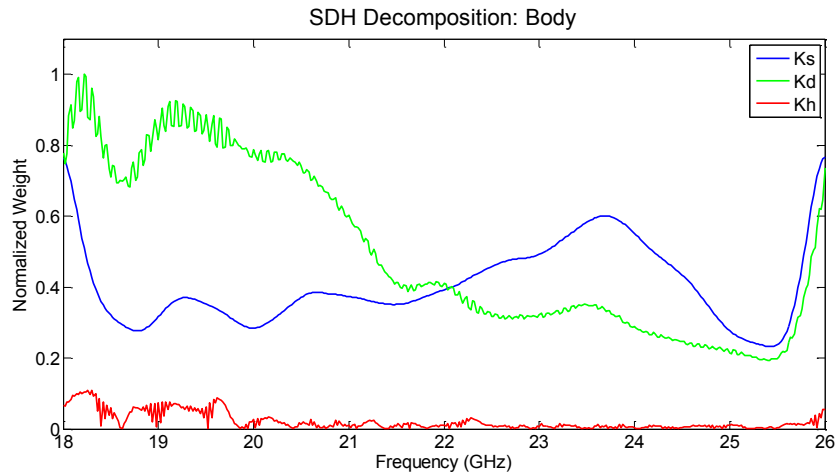


Figure 5-9 Plot showing weights associated with the SDH decomposition of a person without a concealed weapon.

In Figure 5-9 the K_s parameter associated with single bounce scattering is seen to contribute large proportion to the total scattering behaviour of the body, with a modest ripple across the frequency range. This is similar to the observations taken from the Pauli decomposition where single bounce scattering was shown to contribute a large proportion to the overall scattering behaviour of the body. One point worth noting is that the frequency ripple for the SDH decomposition is less chaotic than that of the Pauli decomposition. This could be due to the reduction in the aspect dependency when using a circular polarization basis to form the scattering matrix prior to decomposition, although this is theory unproven. The double bounce parameter in the plot also demonstrates a large contribution to the scattering process, again in agreement with the Pauli decomposition. The frequency dependent nature of the double bounce parameter is different for the SDH decomposition compared to the Pauli decomposition, as was the single bounce component. The difference this time being that the ripple appears smoother barring the high frequency features that are superimposed on this parameter. Finally, the helical scattering component represented by K_h is much smaller in amplitude than the other parameters. The helical scattering gives a measure of the twist in polarization of the reflected wave and can loosely be compared to the cross polar scattering

component in the Pauli decomposition. The helical contribution is anticipated to be the most useful of the SDH parameters, it will be demonstrated that the presence of a weapon causes a significant and detectable change in the value of the helical component. Given that this parameter is roll-invariant there exists an opportunity to use this parameter to detect weapons with a reduction in the detrimental effect that the orientation of a weapon has on detection rates.

The first case of the SDH decomposition being performed on data measured with a person carrying a concealed weapon is presented in Figure 5-10. In this plot the SDH parameters are presented that correspond to a person carrying a concealed gun at an alignment of 45°.

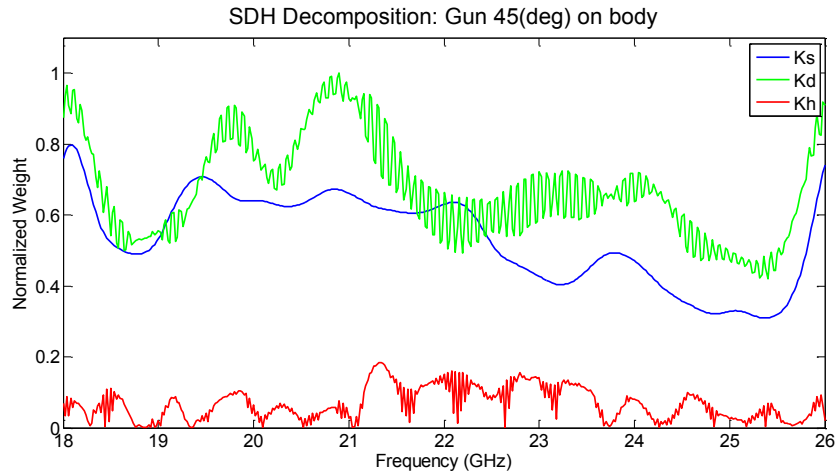


Figure 5-10 Plot showing weights associated with the SDH decomposition of a person carrying a concealed gun on the torso with an alignment of 45°.

The first and most critical observation to be taken from Figure 5-10 is the difference in the helical scattering component compared to that of the person without a concealed weapon. The helical component, although still being the smallest of the three scattering mechanism is noticeably larger than the body without a weapon, especially above 20 GHz. The second key change when compared to the body alone is the change in the high frequency features superimposed on the diplane/double bounce scattering component, these appear to be amplified by the gun. It was mentioned previously that the diplane and helix canonical targets scattering matrices, which are used in the base target

group, are not mutually orthogonal. This means that targets that cause a difference in one parameter may also cause a difference in the other and this seems to be the case with the gun. The third parameter K_s is different when the gun is present on the body but the general shape and amplitude of the parameter is still similar to the body alone. The differences will be down to the slight change in the aspect/position of the body during the measurements taken with a concealed gun.

The next target to be measured and investigated using the SDH decomposition is the person carrying the gun concealed in a vertical position. The results of which are plotted in Figure 5-11.

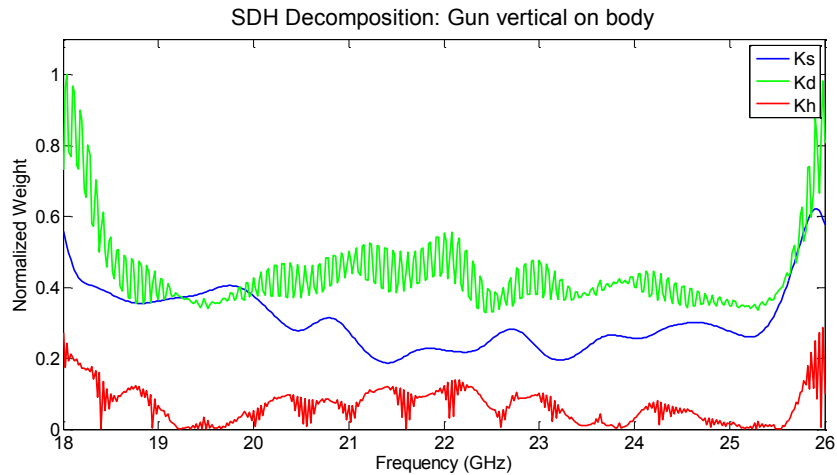


Figure 5-11 Plot showing weights associated with the SDH decomposition of a person carrying a vertically aligned gun concealed on the torso.

Recall that the difference in position of the gun resulted in a lower cross-polar component when looking at the vertical gun using the Pauli decomposition. This is not the case with the helical scattering component K_h of the SDH decomposition; this parameter has a similar amplitude for the gun in both positions. The slight difference can be put down to changes in aspect when taking measurements, it is important to clarify that the SDH parameters are only invariant in roll around the radar line of sight and that changes in aspect will still alter that values of these parameters. That being said, the results do indicate that this decomposition would reduce the effect of the orientation

of the weapon and this is the main motivation for using polarimetric decomposition techniques in weapon detection.

The SDH parameters corresponding to the next target, a person carrying a concealed PBIED, are plotted in Figure 5-12.

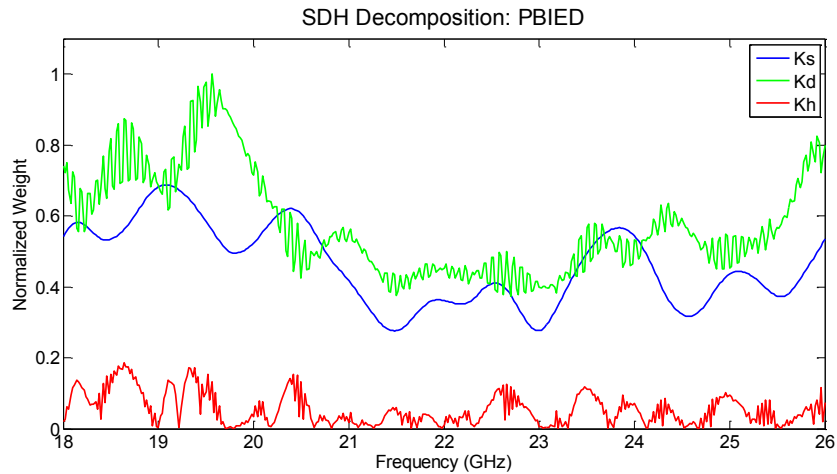


Figure 5-12 Plot showing weights associated with the SDH decomposition of a person carrying a concealed Person Borne Improvised Explosive Device (PBIED).

The helical scattering component shown in Figure 5-12 is weaker than that from the gun yet it is still noticeably larger in amplitude compared to the body alone. This suggests that both guns and PBIEDs could be detected using this parameter. The diplane or double bounce parameter still has high frequency features superimposed upon it, which also seem amplified by the PBIED as with the gun. The single bounce component still has a form that is alike that of the body alone which indicates that, as with the other measurements and decompositions the body remains a significant contributor to the scattering process even in the presence of a concealed weapon. This is expected but means that the single bounce component may not provide information that is as useful as the helical and diplane parameters when used in weapons detection.

The final target to be analysed using the SDH decomposition is the small revolver pistol concealed on the body. The results of this analysis are illustrated in Figure 5-13.

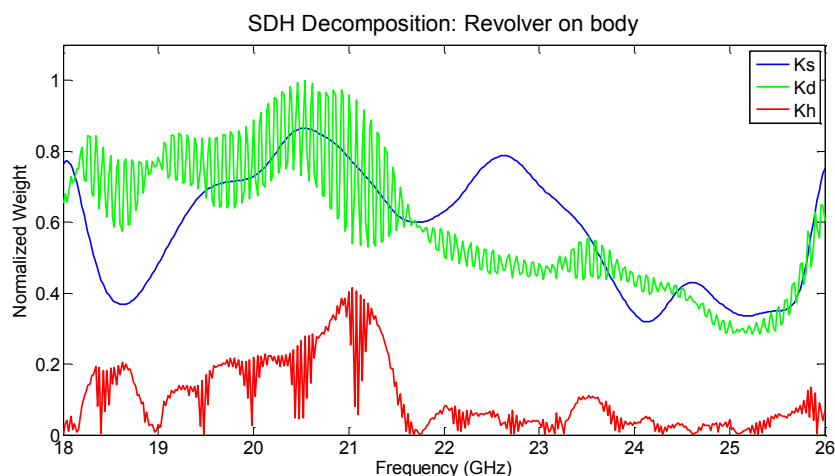


Figure 5-13 Plot showing weights associated with the SDH decomposition of a person carrying a small revolver pistol concealed on the torso.

Of all the weapons, the revolver seems to give the largest helical scattering response and this is clear to see in Figure 5-13. The helical scattering from the revolver is as much as twice the level of that observed from the gun or PBIED, this is interesting given that the physical size of the revolver is smaller than the gun and much smaller than the PBIED. This would indicate that the small features and complex structure of this target are more important than the size of the target in detecting it using the helical scattering parameter as a classification feature. Again, with this target, the high frequency features superimposed on the diplane parameter are amplified in the presence of the weapon, indicating that this parameter could be used in the classification of data into groups of ‘threat’ and ‘non threat’. The sphere or single bounce component is slightly larger in this instance but still displays a likeness to the case of body alone and the differences can be attributed to the change in aspect/position of the body between measurements.

The results presented for the SDH decomposition have shown that two of the roll-invariant parameters offer the potential to be used as distinct features in a classification scheme. The most promising of the parameters has to be the helical scattering parameter K_h , which has been shown to change significantly when a concealed weapon is introduced on the body, but even more appealing

is the lack of significant change of this parameter as the gun was presented at two different orientations. The other useful parameter is the diplane scattering parameter K_d which has been observed changing in the presence of a weapon, the changes being the amplification of superimposed oscillations on the parameters frequency response.

5.4 Incoherent Polarimetric Decomposition

This group of decomposition algorithms uses second order statistical methods to obtain parameters related to the measured scattering matrix that have direct physical interpretations. This is in contrast to coherent techniques that only provide a factorization of a scattering matrix with weights to each term providing a measure of likeness to each of the base group canonical targets. The use of incoherent techniques proves to be of most benefit when analysing distributed targets. Typically, these targets are complex in construction and shape. Incoherent techniques operate on a target's covariance or coherency matrix that can be derived directly from the measured scattering matrix. In this thesis, only one of the incoherent techniques has been analysed, this being the H- α algorithm based on an Eigenvalue decomposition of a target's coherency matrix. The reason for considering only one of the incoherent techniques is that the chosen method is widely regarded as the superior method in the literature, in fact Cloude and Pottier showed this to be the case [56].

5.4.1 H-alpha Decomposition

The H-alpha decomposition developed by Cloude and Pottier in 1990s has proven to be an extremely valuable tool in the field of Earth Observation [58]. This decomposition provides a roll invariant method of analysing radar returns, making this method an attractive option in the field of Concealed Weapon Detection. Successful application of H- α in CWD could remove an element of

the aspect dependency that is detrimental to most state of the art classification techniques employed within CWD.

The method as outlined in [56] and [58] is applied to a target's measured scattering matrix, this matrix must be measured in a linear polarization basis and can be arbitrarily represented by the matrix below.

$$S^{measured} = \begin{bmatrix} S_{VV} & S_{HV} \\ S_{HV} & S_{HH} \end{bmatrix} \quad (5.18)$$

Once the targets scattering matrix has been measured it is converted into a target vector using the Pauli spin elements. The vector and the measured scattering matrix are related by (5.19).

$$k = \frac{1}{\sqrt{2}} \begin{bmatrix} S_{VV} + S_{HH} \\ S_{VV} - S_{HH} \\ 2S_{HV} \end{bmatrix} \quad (5.19)$$

Taking the target vector and multiplying it by its own complex conjugate results in the target's Coherency matrix, as shown in equation (5.20). The Coherency matrix contains the second order statistical information about the scattering process.

$$T = k \cdot k^{*T} \quad (5.20)$$

The H- α decomposition is in essence an Eigenvalue decomposition of the coherency matrix and this is shown by equation (5.21), furthermore the resulting Eigenvectors have been parameterized as equation (5.22).

$$T = [U_3][\Sigma][U_3]^{-1} = \begin{bmatrix} \hat{u}_1 & \hat{u}_2 & \hat{u}_3 \end{bmatrix} \begin{bmatrix} \lambda_1 & 0 & 0 \\ 0 & \lambda_2 & 0 \\ 0 & 0 & \lambda_3 \end{bmatrix} \begin{bmatrix} \hat{u}_1 & \hat{u}_2 & \hat{u}_3 \end{bmatrix}^{-1} \quad (5.21)$$

$$[U_3] = \begin{bmatrix} \cos \alpha_1 & \cos \alpha_2 & \cos \alpha_3 \\ \sin \alpha_1 \cos \beta_1 e^{j\delta_1} & \sin \alpha_2 \cos \beta_2 e^{j\delta_2} & \sin \alpha_3 \cos \beta_3 e^{j\delta_3} \\ \sin \alpha_1 \cos \beta_1 e^{j\gamma_1} & \sin \alpha_2 \cos \beta_2 e^{j\gamma_2} & \sin \alpha_3 \cos \beta_3 e^{j\gamma_3} \end{bmatrix} \quad (5.22)$$

To extract the H and α values the probability of each of the Eigenvalues must first be computed using equation (5.23).

$$P_i = \frac{\lambda_i}{\sum_{n=1}^3 \lambda_n} \quad (5.23)$$

The two key parameters in this decomposition are now obtained using equations (5.24) and (5.25)

$$\underline{\alpha} = \sum_{n=1}^3 P_n \alpha_n \quad (5.24)$$

$$H = -\sum_{n=1}^3 P_n \log_3(P_n) \quad (5.25)$$

The parameter α describes the average scattering behaviour of the target, this value can range from 0° to 90°. The lower value representing a single bounce scattering and the upper value representing a double bounce scattering behaviour, the mid-range value of 45° represents volume scattering. The significance of the H parameter is described in [58] as a measure of polarimetric disorder, and the value of this parameter tends to one when all three scattering mechanisms are contributing equally to the overall scattering process. The value tends to zero in the presence of a single scattering type, i.e. a pure/canonical target.

The research presented here intends to investigate whether or not these parameters can be used to successfully classify radar scans of people with and without concealed weapons into two groups ‘threat’ and ‘non-threat’. Firstly, the decomposition is used to extract the parameters for a control target, which as with the other techniques a conducting sphere has been used. The sphere’s radius was such that the target would reflect independent of frequency. The H and α parameters were extracted for the target at each frequency point measured by the radar the values were then plotted onto a scatter plot as shown in Figure 5-14.

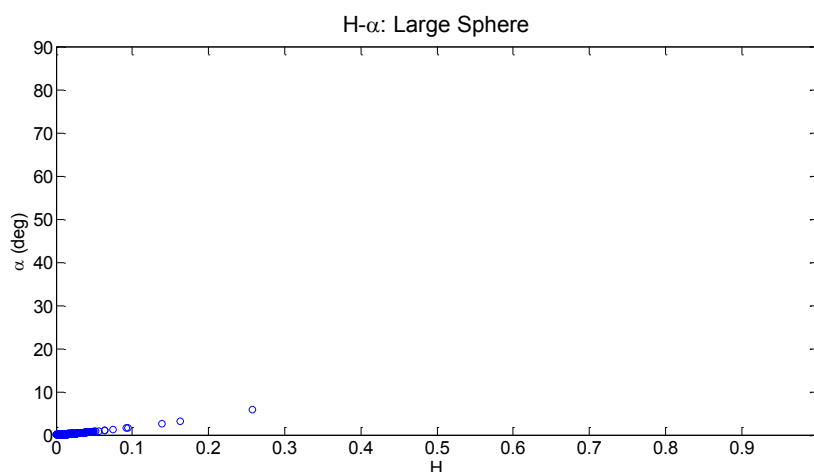


Figure 5-14 A scatter plot of the H- α parameters corresponding to a large conductive sphere, at various frequencies (18-26 GHz).

The scatter plot above shows a tight distribution of points around the lower left hand corner of the plot. The lower left hand corner is the region where the values of α are low meaning that single bounce is the main scattering mechanism and also the H value is low indicating low disorder and the presence of a pure/canonical target. This is a positive result as the control target is considered a canonical target and should look like a single bounce scattering target. There are a number of points on the scattering plot that are away from the bottom left corner and display H up to 0.25 and α values up to 5° , these points are most likely corresponding to frequencies at which the scattering from surface imperfections on the sphere are most prominent.

The plot in Figure 5-15 shows the results from the H- α decomposition of measured scattering matrices in which a person without a concealed weapon was recorded by the radar.

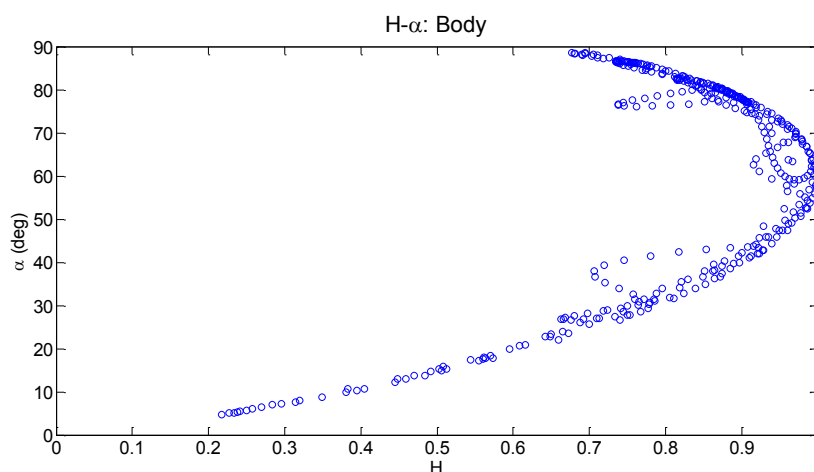


Figure 5-15 A scatter plot of the H- α parameters corresponding to a scan of a person without a concealed weapon, at various frequencies (18-26 GHz).

The scatter plot shows that the points are distributed along a curve. The curve represents the extent of the feasible region of the H- α plot space, see [58]. The plot shows that there is a strong frequency dependency on the H- α parameters and that the parameters display a high degree of disorder. This can be seen in Figure 5-15 where all of the points are spread across a large proportion of the plot space and each one of the points represents a single frequency. This high degree of disorder indicates that all three scattering mechanisms are contributing to the scattering process, with varying levels of contribution from each type dependent upon the frequency. The points are seen to span the range of possible α values again showing that all scattering mechanisms are present in the measurements. In Figure 5-15 a number of points are observed to deviate from the curve at the extent of the feasible region, the significance of this observation is not clear at this point.

The next measurements to be decomposed using the H- α decomposition are presented in Figure 5-16. These measurements were recorded when a person carrying a concealed gun on the torso at 45° was scanned using the experimental fully polarimetric radar.

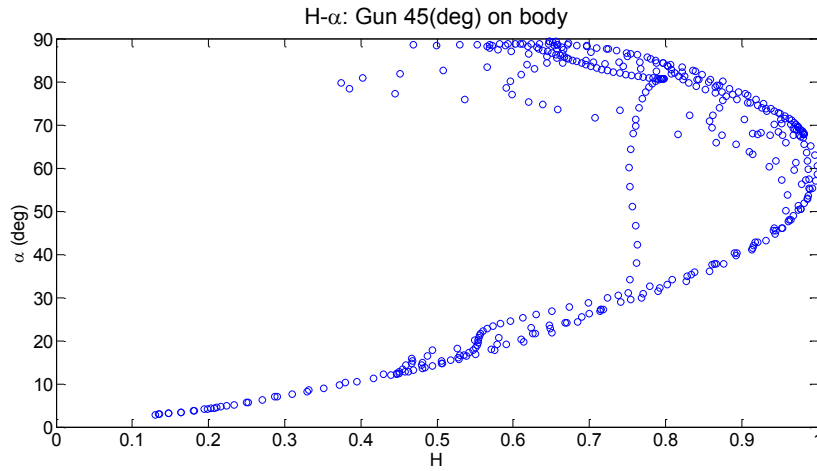


Figure 5-16 A scatter plot of the H- α parameters corresponding to a scan of a person carrying a concealed gun on the torso at a 45° alignment, at various frequencies (18-26 GHz).

The results here show that more of the frequency points result in H- α parameters that deviate from the curve at the extent of the feasible region of the plot space. This initial observation may indicate that the presence of a weapon concealed on the body causes this deviation. If this is the case the deviation from this curve may be used as an indicator or feature of the presence of a weapon and could result in successful classification of the radar scans into the ‘threat’ and ‘non threat’ groups as proposed earlier.

The next set of results in Figure 5-17 are again corresponding to a person carrying a concealed gun, this time the gun is orientated vertically with respect to the person.

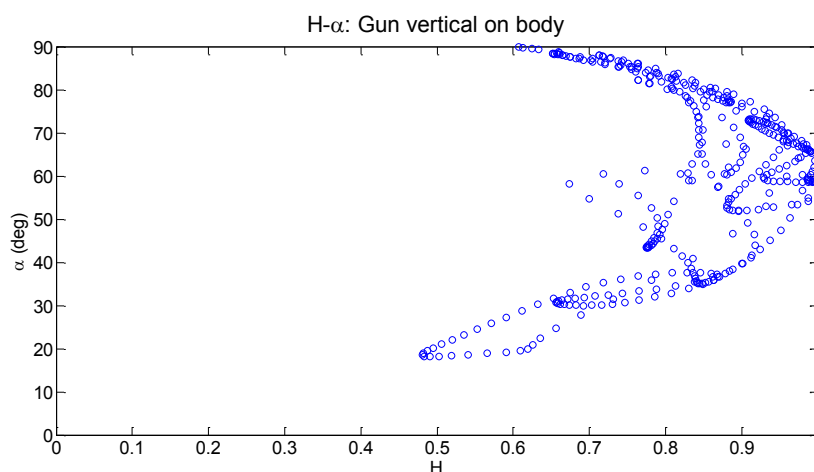


Figure 5-17 A scatter plot of the H- α parameters corresponding to a scan of a person carrying a vertically aligned gun concealed on the torso, at various frequencies (18-26 GHz).

In this plot, there is a significant proportion of the points deviating from the curve bounding the feasible region and the coverage of points along this curve is reduced when compared to Figure 5-16. The reduction in the coverage of points is clearer when looking to values of α below $\sim 25^\circ$. An interesting observation to take from Figure 5-16 and Figure 5-17 is that the plots look significantly different when the gun is re-orientated on the body. This was not anticipated as this method is supposed to provide the property of roll-invariance in all of its resulting parameters. An explanation to these differences could be that there is a sensitivity to orientation in planes other than that perpendicular to the radar line of sight. This is plausible as the chaotic nature of the targets RCS would mean that a small misalignment in the target would yield a significant change in RCS. It should be noted that the measurements were taken with the person making small movements and that there will be differences in aspect between measurements as well as the weapon being rotated 45° around the radar line of sight. The aspect dependency is still expected when using all of the polarimetric techniques considered in this thesis, however the property of roll-invariance in a single plane is expected to reduce the detrimental effect that the orientation of the weapon has on detection probabilities of existing radar systems.

The next plot in Figure 5-18 shows the H- α values at various frequencies for scattering matrices measured with a person carrying a concealed PBIED.

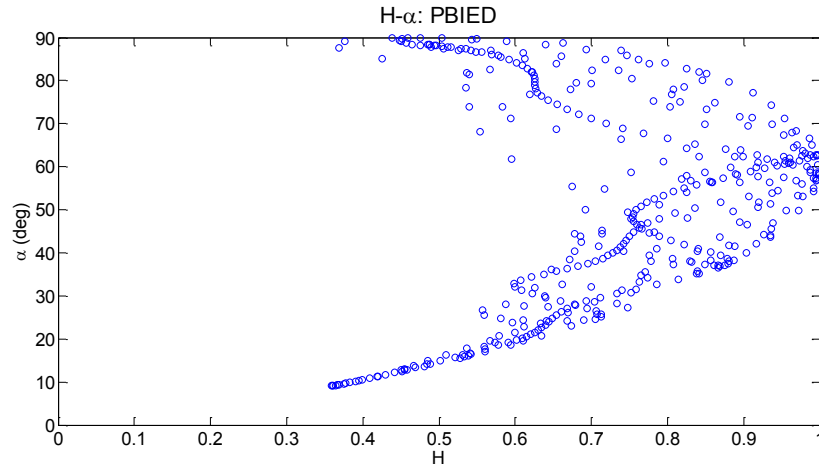


Figure 5-18 A scatter plot of the H- α parameters corresponding to a scan of a person carrying a concealed Person Borne Improvised Explosive Device (PBIED), at various frequencies (18-26 GHz).

In Figure 5-18 the largest deviation of points away from the limit of the feasible region of the plot is observed. Since this deviation has now been observed with both a gun, a PBIED and more critically has not been observed without a concealed weapon present, it seems likely that this technique gives potential information that could be used to classify the radar returns data. This theory will be tested later in Section 5.5 with an experiment.

The final measurements to be decomposed using the H- α technique were recorded by the radar when a person carrying a concealed revolver pistol was presented. The results from this final decomposition are presented in Figure 5-19.

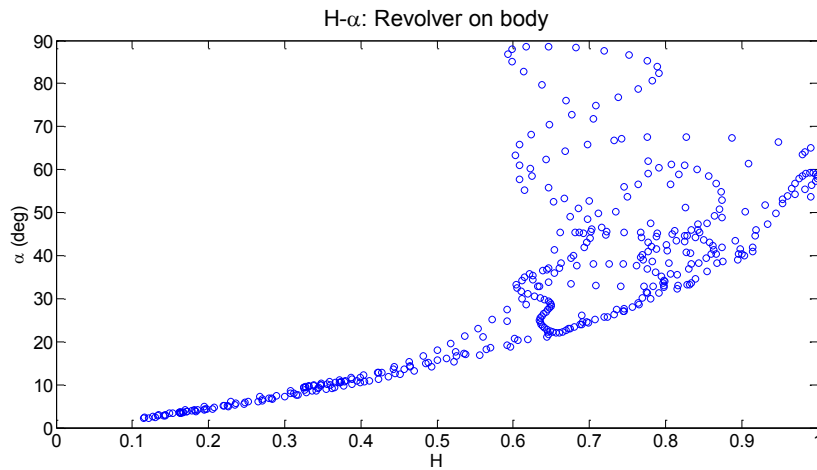


Figure 5-19 A scatter plot of the H- α parameters corresponding to a scan of a person carrying a small revolver pistol concealed on the torso, at various frequencies (18-26 GHz).

The results for the revolver show that there remains a large number of points along the limit of the feasible region of the H- α space, but there seems to be a much larger deviation of the points away from this limit when compared to the gun at 45°. The larger deviation was also observed with the PBIED and may be related to the complexity of the shape of the concealed weapon, since the revolver and PBIED contain more seemingly random facets than the larger gun.

The H- α decomposition of measured radar data has been presented and observations have been made from the plots. It is difficult to analyse and interpret the meaning of the data presented, however certain patterns have been recorded and potential features for classifying the data have been suggested, such as the deviation of points away from the limits of the feasible region of the plot space.

5.5 Classification using Polarimetric Data

The polarimetric data that has been extracted from measurements and discussed in this chapter has shown some behaviour/patterns that could be used to classify radar scans into groups that correspond to a person carrying a concealed weapon (threat) and a person not carrying a weapon (no-threat). To test this concept an experiment has been conducted in which each method was independently tested and a measure of its suitability to an automated weapon detection algorithm was extracted from the experiment. Since the observed behaviour from the decomposed polarimetric data is complex in nature a pattern recognition based classifier was deemed most suitable to apply in such an experiment, and the application of Artificial Neural Networks (ANN) was chosen for this research. The reason for choosing ANNs in this experiment was that an ANN is adaptable and is easily trained to recognize patterns in data. The measure of suitability of each method to CWD will be taken in the form of Receiver Operator Characteristic (ROC) curves, these ROCs will then be used to statistically verify the suitability of each polarimetric decomposition.

5.5.1 Experiment

The experiment conducted in this research was a hypothesis test, with the hypothesis that each polarimetric decomposition would produce data useful for the detection of weapons. The null hypothesis being that the decompositions would not prove useful in detecting weapons. Each decomposition was tested independently of the others and was therefore considered on its own merit. The use of ROC curves in the experiment allowed for the Area Under the Curve (AUC) to be a performance metric that was used as the criteria for accepting or rejecting the null hypothesis. A straight line drawn from the bottom left of the ROC space going to the top right of the space represents the performance of a classifier with no useful capability and ‘by chance’ performance,

such a classifier would have a AUC of 0.5. Observing a ROC with an AUC greater than 0.5 would result in the rejection of the null hypothesis therefore proving that the original hypothesis was correct. For this test to have any statistical significance careful thought had to be given to the size of the data sets used in the test, Chapter 4 provided an insight into this matter and sample sizes were carefully calculated to ensure a high degree of statistical significance in this test.

5.5.2 Data sets

A set of 200 radar scans with 401 scattering matrices, one for each frequency point, were recorded per target. Each one of these datasets was processed using each of the three polarimetric decompositions resulting in three data sets for each target. This is illustrated in the diagram presented in Figure 5-20 below.

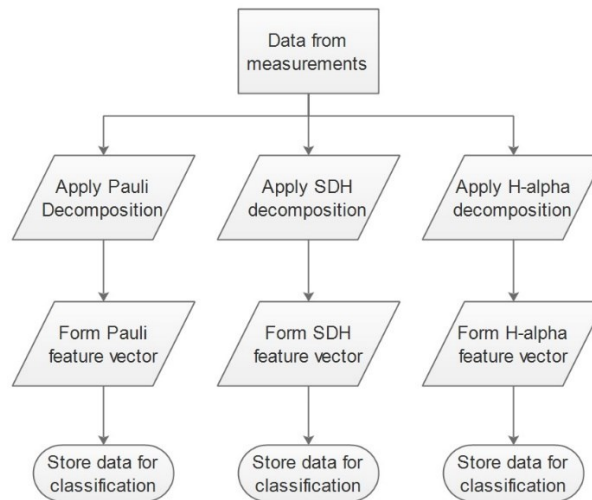


Figure 5-20 A diagram of the formation of three data sets one for each polarimetric decompositions, all taken from same measured data.

The data taken from the measurements was in the form of a scattering matrix for each point in the frequency sweep (401 points) and then 200 scans were taken per target. This results in a total

of 80,200 matrices per target set (i.e. body, gun vertical, gun 45°, revolver and PBIED). Each of the three polarimetric decompositions is then independently applied to all the matrices in each scan and at each point. The results will be three real valued parameters from each matrix for the Pauli and SDH decompositions and two real valued parameters per matrix for the H- α decomposition. In order to use this data to classify scans into the ‘threat’ and ‘no-threat’ groups, a feature vector for each scan and each decomposition was created. Essentially these feature vectors were the concatenation of each parameter, for example the feature vector for a scan processed using the Pauli decomposition would give a vector with 1,203 elements the first 401 would be the α parameter for each frequency point (ascending), the next 401 would be the β parameter for each frequency point and the final 401 would be the γ parameter from each frequency point. The same concept applies in the formation of the feature vector for the SDH and H- α decomposition. A sample of the feature vector corresponding to a single radar scan for each decomposition is formulated below. First, the Pauli feature vector is given for a single radar scan.

$$P_n = \langle \alpha_1, \alpha_2, \dots, \alpha_{401}, \beta_1, \beta_2, \dots, \beta_{401}, \gamma_1, \gamma_2, \dots, \gamma_{401} \rangle \quad (5.26)$$

Next the SDH feature vector from a single radar scan is given.

$$S_n = \langle K_{s_1}, K_{s_2}, \dots, K_{s_{401}}, K_{d_1}, K_{d_2}, \dots, K_{d_{401}}, K_{h_1}, K_{h_2}, \dots, K_{h_{401}} \rangle \quad (5.27)$$

Finally the feature vector from the H- α decomposition is given for a single radar scan.

$$H_n = \langle H_1, H_2, \dots, H_{401}, \alpha_1, \alpha_2, \dots, \alpha_{401} \rangle \quad (5.28)$$

5.5.3 Artificial Neural Network

An Artificial Neural Network (ANN) is a mathematical model designed to replicate the central nervous system of a human. In replicating this system a network of artificial neurons are created which trigger above a given threshold allowing a signal to propagate through the system in a controlled manner. The use of neural networks in solving complex problems is widespread in the literature, a few examples of the applications of an ANN to weapon detection can be found in [5], [40], and [52]. To apply an ANN to a given problem, the network must be trained; this is done by presenting examples of the input signals and adjusting weights and biases that are applied to each neuron until the output signal reaches a user specified target value. The training used in this research was based on a back propagation algorithm and the network structure used was feed-forward, an example of a three layer feed-forward ANN is given in Figure 5-21 below.

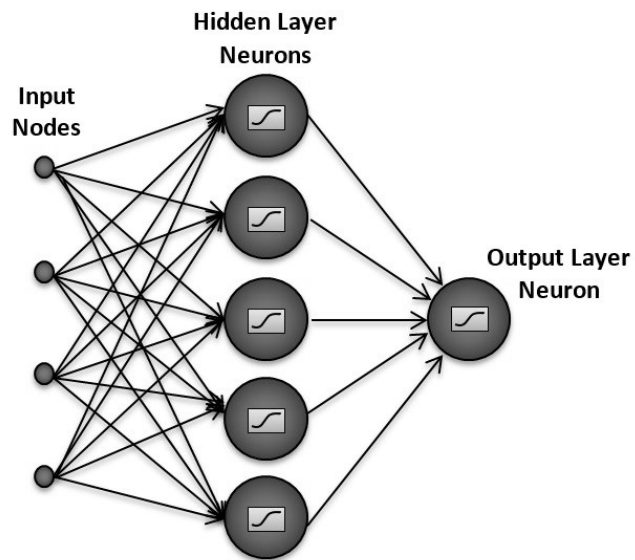


Figure 5-21 An example of the structure of a three layer feed forward Artificial Neural Network (ANN).

All three polarimetric decomposition had an individual ANN designed and trained to test the hypothesis that each one would provide information useful in the detection of weapons. A summary of the experimental design parameters for each ANN is recorded in Table 5-1 below.

<i>Parameter</i>	<i>Pauli</i>	<i>SDH</i>	<i>H-α</i>
<i>Network type</i>	Feed-forward back-propagation	Feed-forward back-propagation	Feed-forward back-propagation
<i>No. of layers</i>	3	3	3
<i>No. of neurons on hidden layer</i>	30	30	30
<i>No. input neurons</i>	1203	1203	802
<i>No. output neurons</i>	1	1	1
<i>Transfer function on neurons</i>	tansig	tansig	tansig

Table 5-1 Table encapsulating key design parameters used to form the ANNs.

A summary of the training parameters used on each of the developed ANNs for this experiment is found in Table 5-2 below, the parameters in this table have been chosen empirically.

<i>Parameter</i>	<i>Pauli</i>	<i>SDH</i>	<i>H-α</i>
<i>Training Algorithm</i>	Constant gradient descent	Constant gradient descent	Constant gradient descent
<i>Maximum no. epochs</i>	5000	5000	5000
<i>Performance function</i>	Sum Squared Error	Sum Squared Error	Sum Squared Error
<i>Performance goal</i>	0.001	0.001	0.001
<i>Minimum gradient</i>	1.0E-15	1.0E-15	1.0E-15
<i>Minimum step size</i>	1.0E-15	1.0E-15	1.0E-15

Table 5-2 Table encapsulating the key training parameters used for each of the developed ANNs.

The inputs to each network are the datasets that were outlined in the previous section. The targets for the networks were zeros for non-threat targets and ones for threat targets. The targets are plotted with the raw outputs for each data set, in the next section.

5.5.4 Methodology

The experimental methodology used to test the stated hypothesis is encapsulated in flow chart format in Figure 5-22 below. This flow chart shows the process of taking measured data, processing the data, training an ANN, testing the ANN and analysing the results. The flow chart shows the process for a single polarimetric decomposition and this process is repeated for the other two decompositions.

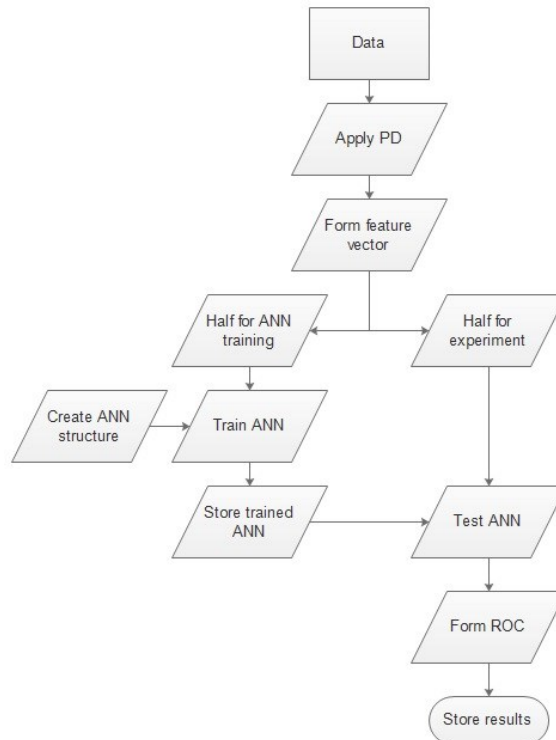


Figure 5-22 Flow chart detailing the methodology used for the proposed experiment.

The flow chart shows the separation of data after the feature vectors have been formed and shows the allocation of data for training and testing the ANN.

5.5.5 Results and Discussion

The data used to train each of the developed ANNs was run back through the relevant network post training to validate the ANNs performance. Each ANN has been trained to produce an output value of one if a threat is detected and a value of zero if no threat is detected. The value on the output will range between zero and one and can be treated like a confidence or probability that the input signal relates to the relevant classification. A trained the network would be anticipated to correctly classify all of the scans used in the training data set, that is all the data relating to the body measurements would produce an output value of zero and all of the other measurements would produce an output value of one. The output values produced when feeding the training data back through the networks are illustrated in Figure 5-23 below.

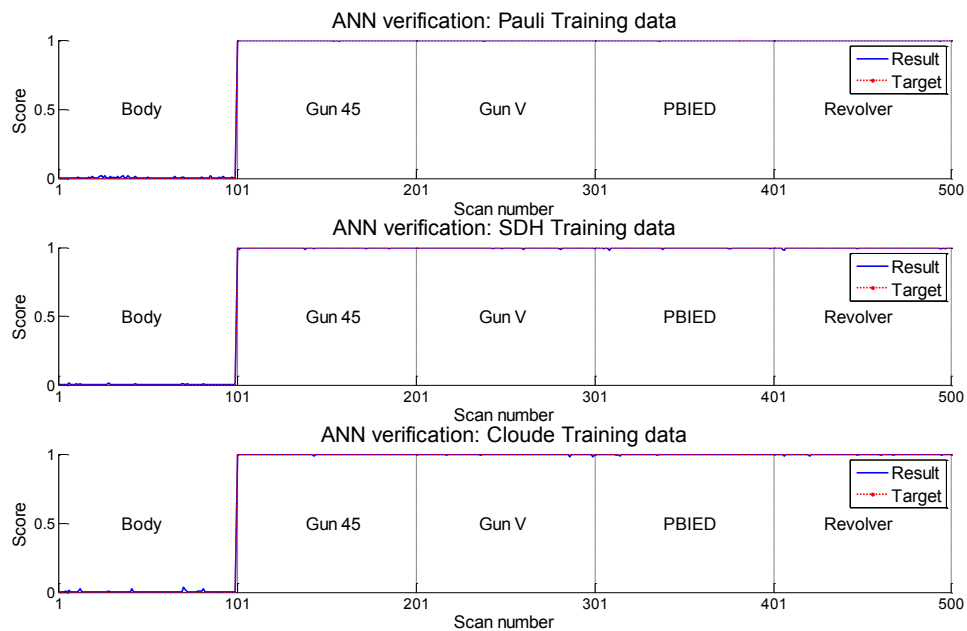


Figure 5-23 A series of plots showing the results from the validation of the developed ANNs post-training.

Figure 5-23 shows that all of the networks have been successful in classifying the training data with 100% accuracy, thus validating each of the networks performance. In each of the plots in the figure, a red line is provided, that shows the target value for the output for each scan put into the network. In each case, the blue line represents the achieved output value and it is clear to see in all of the plots that the trained network has achieved all of the target values. The results clearly validate that each network has reached its training goal and is ready to be utilized in the proposed experiment.

Now that the networks have been validated, post-training the data that was reserved for the experiment is fed into the networks. Each scan is consecutively inputted into the network and the resulting output value recorded. The plots compiling all of the resulting output values are given in Figure 5-24.

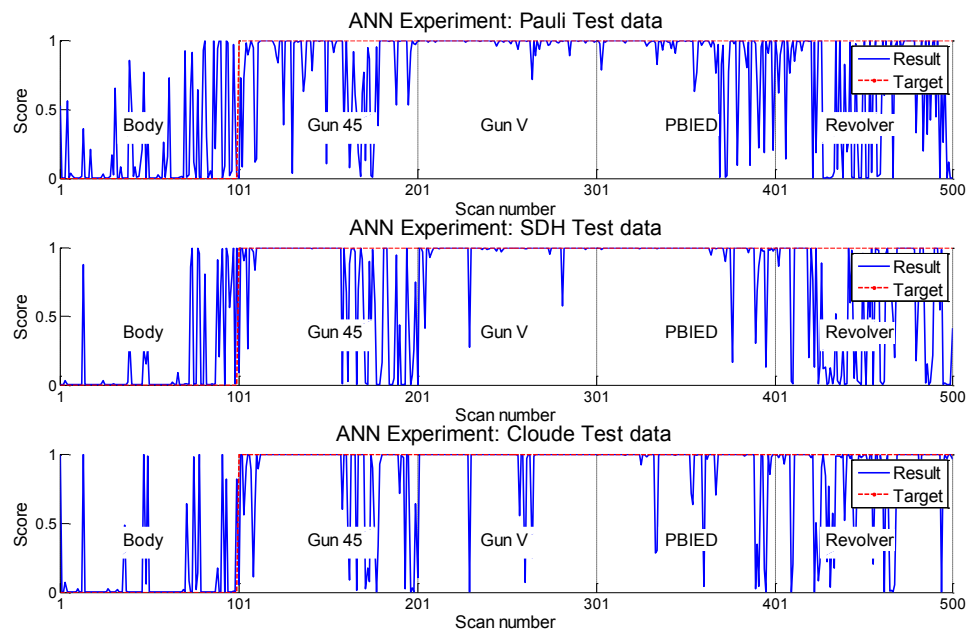


Figure 5-24 A series of plots showing the ANN output values for all of the radar scans used in the proposed experiment.

The figure shows that the output value fluctuates between zero and one for each target set. This means that there are a number of scans that are incorrectly classified; however, there remains a larger proportion of the scans that are correctly classified. This indicates that false alarms caused by the body will be present in the system. Each plot shows a different performance, which suggests that the decompositions that have been used are not equally useful in producing information that can lead to the detection of weapons. A performance metric must be extracted from the results that can be used to either prove or disprove the null hypothesis. In order to extract the chosen performance metric (AUC) the results in Figure 5-24 are used to create three ROC curves, one for each decomposition. The three ROC curves generated using these results are presented in Figure 5-25.

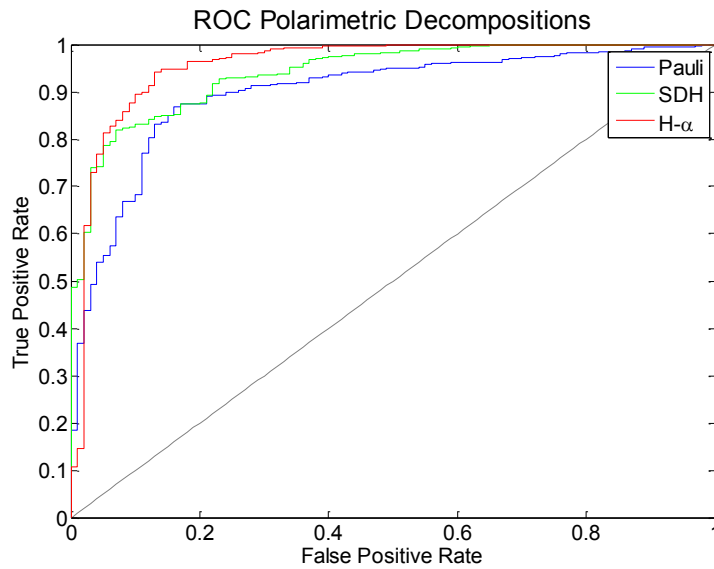


Figure 5-25 A plot showing three ROC curves each one corresponding to a different polarimetric decomposition.

The ROC curves presented in Figure 5-25 shows that there exists a trade-off between the detection rate and the false positive rate. The choice of threshold on the output neuron will determine the systems sensitivity. This should be chosen with an acceptable false alarm rate in mind, if the false alarm rate is too high then the operator will lose confidence and stop using the system.

The AUC of each of the presented ROC curves was calculated and is presented in Table 5-3.

<i>Parameter</i>	<i>Pauli</i>	<i>SDH</i>	<i>H-α</i>
<i>AUC</i>	0.9	0.93	0.95
<i>Null hypothesis rejected</i>	Yes	Yes	Yes

Table 5-3 A table showing the results of the proposed experiment with the outcome of the hypothesis test applied to each polarimetric decomposition.

In all cases, the observed AUC far exceeded the value of 0.5, which would have been observed to be the case if the null hypothesis was in fact true. This result means that in each case the null hypothesis is rejected as substantial evidence is provided which contradicts this hypothesis.

Therefore, by the process of elimination it can be said that each of the tested polarimetric decompositions provides useful information for the detection of weapons based on measurements taken with a fully polarimetric radar.

5.6 Summary

This chapter has detailed the main contribution to knowledge to arise from this thesis, which is the demonstration that selected polarimetric decomposition algorithms can be successfully applied to the detection of concealed weapons. A background into the three chosen polarimetric decompositions and their origins in Earth Observation has been provided. An introduction to the mathematical foundation of each decomposition has been presented. Data measured using the developed fully polarimetric radar was processed using the decompositions and the results were presented with detailed discussions. The design of an experiment to statistically verify the successful application of each decomposition has been presented and executed with results given and conclusions drawn based upon the results.

Chapter 6

Conclusion and Further Work

In the thesis a novel weapon detection system has been developed, this system comprises of a fully polarimetric radar implemented using a VNA. The ability to measure all of the parameters that make up a targets scattering matrix has allowed a comprehensive study of the polarimetric scattering of weapons and the human body to be conducted. The information from the polarimetric scattering properties has been identified as a viable feature for identifying the presence of a weapon concealed on a person. Furthermore, an experiment has been conducted in which conclusive proof that polarimetric decomposition algorithms can be successfully applied to weapon detection has been realized.

Key findings and contributions to knowledge taken from this thesis are:

- It has been conclusively proven that polarimetric decompositions provide information that is useful in the detection of concealed weapons.
- An investigation into the exploitation of polarization in radar based standoff weapon detection has been presented.
- An experimental fully polarimetric radar has been developed for the detection of concealed weapons.
- A calibration and signal-processing algorithm has been developed as a pre-cursor to automatic classification of radar signals based around the use of polarimetric decompositions.
- This work has resulted in an improvement in radar based standoff weapon detection by introducing new measurement capabilities and algorithms for improving classification.

- A number of artificial neural networks have been developed and trained to detect weapons automatically using data from polarimetric decompositions.

The research presented in this thesis served as a feasibility study and the aim was to test whether or not polarimetric decomposition algorithms can be successfully applied to standoff concealed weapons detection using fully polarimetric radar. The thesis has provided evidence to support the claim that these algorithms can be successfully applied to CWD; and has therefore succeeded in its aim. The instrumentation developed in this work is very much experimental and there are aspects of this system that are less than ideal. It is important that the various issues be highlighted as they set the roadmap for further development of the research presented in this thesis.

The developed radar employs a quasi-mono static antenna arrangement; this arrangement introduces systematic errors that are difficult to remove post measurement. This non-confocal arrangement also limits the use of the radar in that the illuminating beam cannot be formed into a collimated beam, this means that the beams from each antenna rapidly diverge and in slightly different directions. Chapter 3 showed that the antenna had to be angled towards one and other and that this meant the beams were only co-located at a very specific range. Ideally, the illuminating beams would be co-located across the full working range of the radar, allowing measurements to be made at any point within the radar's working range. The beam size of each of the antennas could be reduced in a confocal arrangement Figure 6-1, as this would allow the deployment of a lens. The lens should be designed such that the beam size is commensurate in size with the largest dimension of the weapons of interest.

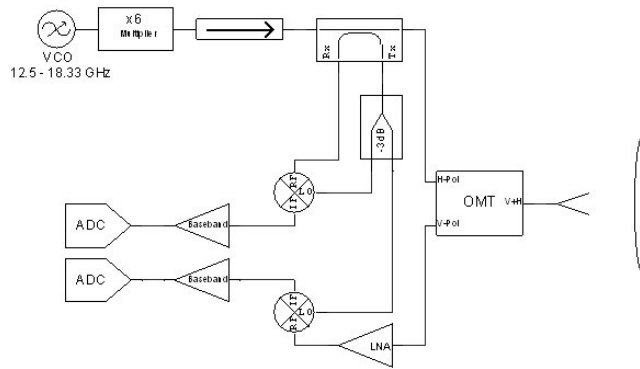


Figure 6-1 Diagram showing possible confocal radar system.

The current state of the system does not allow for easy deployment and testing of the device, given that the radar is implemented using a VNA. A portable demonstrator unit would allow the system to be put through more testing to determine the effects of weapons being presented at a wider range of orientations and to assess the level of false positives. Additionally, stringent field-testing could be conducted and would be ideal for end user application that could then be used to drive the development process.

The use of the VNA has limited the rate at which measurements can be taken to much slower than real-time. The use of a modular radar (i.e. measurement on VNA, post processing and error correction on PC) has also contributed to slowing down the process of taking a measurement, applying error correction, processing the data and then rendering a classification for the acquired data. All of these aspects need integrating into a single system that has real-time capability. This would allow more flexibility in testing the various aspects of the developed weapons detection system.

Currently the beam size is 0.9m meaning that weapon occupies a much smaller proportion of the beam than the surrounding body, this means that the systems is measuring more of the body's scattering properties and the weapon contributes much less than is desirable. Ideally, the beam

should be commensurate in size with the largest dimension of the weapon that is to be detected. This can be achieved by focussing of the beam using a lens.

The current calibration strategy involves physically disconnecting the antennas and connecting three different standards to each port sequentially followed by re-attaching the antennas and making subsequent background measurements. This process is time consuming and if not executed very carefully can lead to large measurement errors that would prevent the system from detecting weapons. If this system is to be developed and commercialized, a new calibration strategy must be outlined whereby the system does not require any dis-assembly and the process is carried out much faster.

6.1 Further Work

The developed radar has provided the ability to make the measurements required in this research. Progressing the development of the weapon detection system described in this thesis to commercialization a number of key aspects of the hardware/instrumentation will need changes. These changes are necessary if this work is to be progressed. The proposed changes are summarized as suggested future work as follows:

- To design, manufacture and test an Ortho Mode Transducer that can be used in the developed radar for making confocal (quasi optic) measurements of a targets scattering matrix across k-band.
- To design an integrated lens and antenna for focusing the illuminating waves into a collimated beam with a diameter that is commensurate with the largest dimension on the weapons presented in this research.
- To develop a portable radar capable of making a measurement of a targets scattering matrix across k-band frequencies, the design should incorporate the OMT and antenna-lens detailed in previous two recommendations.
- Design a radar capable of illuminating a target in any polarization and measuring the backscattered signal in any polarization.
- Demonstrate the real time application of the polarimetric decomposition algorithms presented in this work, for the detection of concealed weapons.
- Conduct blind trials in which the radar is deployed and used in a real world detection scenario.

Chapter 7

References

- [1] D. Anderson, "The Terrorism Acts in 2012," TSO, London, 2013.
- [2] R. Morelle, "BBC News: Working gun made with 3D printer," BBC, 6 May 2013. [Online]. Available: <http://www.bbc.co.uk/news/science-environment-22421185>. [Accessed 20 September 2014].
- [3] NABIS, "NABIS: 3D Gun Detector Trial Successful," National Ballistics Intelligence Service, 3 February 2014. [Online]. Available: <http://www.nabis.police.uk/news/3D-Gun-Dectector-Trial-Successful>. [Accessed 20 September 2014].
- [4] N. J. Bowring, J. G. Baker, N. D. Rezgui and J. F. Alder, "A sensor for the detection and measurement of thin dielectric layers using reflection of frequency scanned millimetric waves," *IOP Measurement Science and Technology*, vol. 19, no. 2, 2008.
- [5] S. W. Harmer, N. Bowring, D. Andrews, N. Rezgui and M. Southgate, "Millimetre Radar Threat Level Evaluation (MiRTLE) at Standoff Ranges," in *Proc. Of SPIE Vol.8188, Millimetre Wave and Tetrahertz Sensors and Technology IV*, Prague, 2011.
- [6] S. W. Harmer, N. J. Bowring, D. A. Andrews, N. D. Rezgui, M. Southgate and S. Smith, "A Review of Nonimaging Stand-Off Concealed Threat Detection with Millimetre-Wave Radar," *IEEE Microwave Magazine*, pp. 160-167, 2012.
- [7] A. Achanta, M. Mckenna and J. Heyman, "Nonlinear acoustic concealed weapons detection," in *Applied Imagery and Pattern Recognition Workshop, 34th Proc. Of*, Washington, DC, 2005.

- [8] J. DuChateau, "Using Ultrasound in Concealed Weapons Detection," College of William & Mary, Williamsburg, VA, 2005.
- [9] G. A. Vadakkel and S. O. Oyadiji, "Concealed Weapon Detection using Acoustic Spectral Characterisation," in *Proc. Of ASME International Design Engineering Technical Conferences & Computers and Information in Engineering Conference IDETC/CIE*, San Diego, CA, 2009.
- [10] A. Agurto, "New Proposal for the Detection of Concealed Weapons: Electromagnetic Weapon Detection for," University of Huddersfield, Huddersfield, 2009.
- [11] A. Elgwel, S. W. Harmer, N. Bowring and S. Yin, "Resolution of Multiple Concealed Threat Objects Using Electromagnetic Pulse Induction," *Progress In Electromagnetics Research M*, vol. 26, no. 1, pp. 55-68, 2012.
- [12] D. K. Kotter, L. G. Roybal and R. E. Polk, "Detection and Classification of Concealed Weapons using a Magnetometer-based Portal," in *Proc. Of SPIE Vol. 4708, Sensors and Command, Control, Communications and Intelligence Technologies for Homeland Defense and Law Enforcement*, Orlando, FL, 2002.
- [13] C. Nelson, "Wide-area metal detection system for crowd screening," in *Proc. Of SPIE Vol. 5071, Sensors and Command, Control, Communications and Intelligence Technologies for Homeland Defense and Law Enforcement*, Orlando, FL, 2003.
- [14] P. Pati and P. Mather, "Open Area Concealed Weapon Detection System," in *Proc. Of SPIE Vol. 8017, Detection and Sensing of Mines, Explosive Objects and Obscured Targets XVI*, Orlando, FL, 2011.

- [15] S. Annadurai and V. Vaithiyanathan, "Concealed Weapon Detection Using Multiresolution Additive Wavelet Decomposition," *Research Journal of Applied Sciences, Engineering and Technology*, vol. 4, no. 20, pp. 4118-4121, 2012.
- [16] S. Cho and N. Tin, "Using Infrared Imaging Technology for Concealed Weapons Detection and Visualization," in *TENCON 2010, IEEE Region 10 Conference*, Fukuoka, 2010.
- [17] S. K. Bandyopadhyay, B. Datta and S. Roy, "Identifications of concealed weapon in a Human Body," *International Journal of Scientific & Engineering Research*, vol. 3, no. 11, pp. 1-7, 2012.
- [18] R. Appleby and B. Wallace, "Standoff Detection of Weapons and Contraband in the 100GHz to 1THz Region," *IEEE Transactions on Antennas and Propagation*, vol. 55, no. 11, pp. 2944-2956, 2007.
- [19] M. C. Kemp, "Explosives Detection by Terahertz Spectroscopy- A Bridge Too Far?," *IEEE Transactions on Terahertz Science and Technology*, vol. 1, no. 1, pp. 282-292, 2011.
- [20] D. M. Sheen, D. L. McMakin and T. E. Hall, "Active Millimeter-Wave and Sub-Millimeter-Wave Imaging for Security Applications," in *Infrared, Millimeter and Terahertz Waves (IRMMW-THz), 36th International Conference on*, Houston, TX, 2011.
- [21] R. Arusi, Y. Pinhasi, B. Kapilevitch, D. Hardon, B. Litvak and M. Anisimov, "Linear FM radar operating in the Tera-Hertz regime for concealed objects detection," in *Microwaves, Communications, Antennas and Electronics Systems (COMCAS), IEEE International Conference on*, Tel Aviv, 2009.
- [22] K. B. Cooper, R. J. Dengler, N. Llombart, B. Thomas, G. Chattopadhyay and P. H. Siegel, "THz Imaging Radar for Standoff Personnel Screening," *IEEE Transactions on Terahertz Science and Technology*, vol. 1, no. 1, pp. 169-182, 2011.

- [23] S. Gu, C. Li, X. Gao, Z. Sun and G. Fang, "Terahertz Aperture Synthesized Imaging With Fan-Beam Scanning for Personnel Screening," *IEEE Transactions on Microwave Theory and Techniques*, vol. 60, no. 12, pp. 3877-3885, 2012.
- [24] A. J. Berni, "Target Identification by Natural Resonance Estimation," *IEEE Transaction on Aerospace and Electronic Systems*, vol. 11, no. 2, pp. 147-154, 1975.
- [25] S. W. Harmer, D. A. Andrews, N. D. Rezgui and N. J. Bowring, "Detection of handguns by their complex natural resonant frequencies," *IET Microwave, Antennas and Propagation*, vol. 4, no. 9, pp. 1182-1190, 2010.
- [26] M. Gashinova, M. Cherniakov and A. Vasalos, "UWB signature analysis for detection of body worn weapons," in *International Conference on Radar (CIE)*, Shanghai, 2006.
- [27] S. Harmer, A. Andrews, N. Bowring, N. Rezgui and M. Southgate, "Ultra wide band detection of on body concealed weapons using the out of plane polarized late time response," in *Proc. Of SPIE Vol.7485, Millimetre Wave and Terahertz Sensors and Technology II*, Berlin, 2009.
- [28] S. W. Harmer, S. E. Cole, N. Bowring, N. D. Rezgui and D. Andrews, "On Body Concealed Weapon Detection Using A Phased Antenna Array," *Progress In Electromagnetics Research*, vol. 124, no. 1, pp. 187-220, 2012.
- [29] A. Vasalos and H. Ryu, "Fast Concealed Weapon Detection via LTR Analysis," in *IEEE Radar Conference (RADAR)*, Kansas City, MO, 2011.
- [30] L. Zhang, Y. Hao and C. G. Parini, "Natural Resonant Frequency Extraction for Concealed Weapon Detection at Millimeter Wave Frequencies," in *Second European Conference on Antennas and Propagation (EuCAP)*, Edinburgh, 2007.

- [31] W. Lee, T. K. Sarkar, H. Moon and S.-P. M., "Identification of Multiple Objects Using Their Natural Resonant Frequencies," *IEEE Antennas and Wireless Propagation Letters*, vol. 12, no. 1, pp. 54-57, 2013.
- [32] S. S. Ahmed, A. Schiessl, F. Gumbmann, M. Tiebout, S. Methfessel and L. Schmidt, "Advanced Microwave Imaging," *IEEE Microwave Magazine*, pp. 26-43, September/October 2012.
- [33] B. E. Bernacki, J. F. Kelly, D. M. Sheen, D. L. Mckakin, J. R. Tedeschi, R. V. Harris, A. Mendoza, T. E. Hall, B. K. Hatchell and P. L. J. Valdez, "Passive fully polarimetric W-band millimeter-wave imaging," in *Proc. Of SPIE Vol.8259, RF and Millimeter-Wave Photonics II*, San Francisco, 2012.
- [34] A. Schiessl and S. S. Ahmed, "W-Band Imaging of Explosive Substances," Proc. Of the 6th European Radar Conference, Rome, 2009.
- [35] B. Elias, "Airport Body Scanners: The Role of Advanced Imaging Technology in Airline Passenger Screening," Congressional Research Service, Library of Congress, Washington D.C., 2012.
- [36] S. Bertl and J. Detlefsen, "Effects of a Reflecting Background on the Results of Active MMW SAR Imaging of Concealed Objects," *IEEE Transactions on Geoscience and Remote Sensing*, vol. 49, no. 10, pp. 3745-3752, 2011.
- [37] T. Allett, "ProVision: EU Approved," *Airport International*, pp. 28-29, March 2013.
- [38] D. A. Andrews, S. Smith, N. D. Rezgui, N. J. Bowring, M. Southgate and S. W. Harmer, "A swept millimeter-wave technique for the detection of concealed weapons and thin dielectric material with and without fragmentation," in *Proc. Of SPIE Vol.7309, Passive Millimeter-Wave Imaging Technology XII*, Orlando, FL, 2009.

- [39] S. Harmer, J. Bowring, N. Rezgui and A. Andrews, "A Comparison of Ultra Wide Band Conventional and Direct Detection Radar for Concealed Human Carried Explosives Detection," *Progress In Electromagnetics Research Letters*, vol. 39, no. 1, pp. 37-47, 2013.
- [40] D. O'Reilly, N. Bowring and S. Harmer, "Signal Processing Techniques For Concealed Weapon Detection By Use Of Neural Networks," in *IEEE 27th Convention of Electrical and Electronic Engineers*, Eilat, 2012.
- [41] N. Rezgui, D. Andrews, N. Bowring, S. Harmer and M. Southgate, "Standoff Detection of Concealed Handguns," in *Proc. Of SPIE Vol.6948, Passive Millimetre-Wave Imaging*, Orlando, FL, 2008.
- [42] B. Kapilevich and M. Einat, "Detecting Hidden Objects on Human Body Using Active Millimeter Wave Sensor," *IEEE Sensors Journal*, vol. 10, no. 11, pp. 1746-1752, 2010.
- [43] R. J. Douglass, J. D. Gorman and T. J. Burns, "System and method for standoff detection of human carried explosives". US Patent U.S. Patent 7800 527, 11 October 2005.
- [44] P. Peachey and C. Milmo, "How British technology could keep world cup fans safe from gunmen," 29 May 2014. [Online]. Available: <http://www.independent.co.uk/news/science/how-british-technology-could-keep-world-cup-fans-safe-from-gunmen-9456608.html>. [Accessed 20 September 2014].
- [45] D. O'Reilly, N. Bowring, N. Rezgui, D. Andrews and S. Harmer, "Remote concealed threat detection by novel classification algorithms applied to multi-polarimetric UWB radar," in *Proc. of SPIE Radar Sensor Technology XVII*, Baltimore, 2013.
- [46] M. Skolnik, *Introduction to Radar Systems*, 3rd Edition, New York: McGraw-Hill, 2001.
- [47] D. K. Rytting, "Network Analyzer Accuracy Overview," in *58th ARFTG Conference Digest-Fall*, San Diego, CA, 2001.

- [48] K. Sarabandi and F. Ulaby, "A convenient technique for polarimetric calibration of single antenna radar systems," *IEEE Transactions of Geoscience and Remote Sensing*, vol. 28, no. 6, pp. 1022-1033, 1990.
- [49] A. Technologies, "Agilent Network Analyzer Basics," [Online]. Available: <http://cp.literature.agilent.com/litweb/pdf/5965-7917E.pdf>. [Accessed 12 August 2015].
- [50] M. Grace, "Measurement of Radar Cross Section Using the VNA Master Handheld VNA Application Note," 31 August 2011. [Online]. Available: <http://www.anritsu.com/en-GB/Downloads/Application-Notes/Application-Note/DWL8848.aspx>. [Accessed 20 September 2014].
- [51] J. A. Hanley and B. J. McNeil, "The Meaning and Use of the Area under a Receiver Operating Characteristic (ROC) Curve," *Radiology*, vol. 143, no. 1, pp. 29-36, 1982.
- [52] D. Andrews, S. W. Harmer, N. J. Bowring, N. D. Rezgui and M. J. Sothgate, "Active Millimeter Wave Sensor for Standoff Concealed Threat Detection," *IEEE Sensors Journal*, vol. 13, no. 12, pp. 4948-4954, 2013.
- [53] W. M. Boerner, "Recent advances in extra-wide-band polarimetry, interferometry and polarimetric interferometry in synthetic aperture remote sensing and its applications," *IEE Proc. Radar sonar navigation, Special issue of the EUSAR-02*, vol. 150, no. 3, pp. 113-125, 2003.
- [54] J. R. Huynen, "Phenomenological Theory of Radar Targets, Ph.D. thesis," University of Technology, Delft, The Netherlands, 1970.
- [55] E. Krogager and Z. H. Czyz, "Properties of the Sphere, Di-plane and Helix decomposition," in *Proc. of 3rd International Workshop on Radar Polarimetry, IRESTE*, Nantes, 1995.

- [56] S. R. Cloude and E. Pottier, "A review of target decomposition theorems in radar polarimetry," *IEEE Trans. GRS*, vol. 34, no. 2, pp. 498-518, 1996.
- [57] V. Alberga, E. Krogager, M. Chandra and G. Wanielik, "Potential of coherent decompositions in SAR polarimetry and interferometry," in *Geoscience and Remote Sensing Symposium, 2004. IGARSS '04. Proceedings. 2004 IEEE International*, Anchorage, Alaska, 2004.
- [58] .. European Space Agency, "Polarimetric Decompositions," 23 December 2011. [Online]. Available: http://earth.eo.esa.int/polsarpro/Manuals/4_Polarimetric_Decompositions.pdf. [Accessed 20 September 2014].